 AFRL-RZ-ED-TR-2009-0020

Experimental Study of the Mini-Helicon Thruster

Oleg Batishchev
Massachusetts Institute of Technology
77 Massachusetts Avenue, 37-351
Cambridge, MA 02139

Jean-Luc Cambier
AFRL/RZSA
10 E. Saturn Blvd.
Edwards AFB CA 93524-7680

February 2008

Special Report

AIR FORCE RESEARCH LABORATORY
AIR FORCE MATERIEL COMMAND
EDWARDS AIR FORCE BASE CA 93524-7048

REPORT DOCUMENTATION PAGE

Form Approved
OMB No. 0704-0188

1. REPORT DATE *(DD-MM-YYYY)*	**2. REPORT TYPE**	**3. DATES COVERED** *(From - To)*
04-02-2009	Special Report	01 Jan 2005 – 29 Feb 2008

4. TITLE AND SUBTITLE
Experimental Study of the Mini-Helicon Thruster

5a. CONTRACT NUMBER

5b. GRANT NUMBER

5c. PROGRAM ELEMENT NUMBER
62203F

6. AUTHOR(S)
Oleg Batishchev

5d. PROJECT NUMBER

5e. TASK NUMBER

5f. WORK UNIT NUMBER
50260542

7. PERFORMING ORGANIZATION NAME(S) AND ADDRESS(ES)

Massachusetts Institute of Technology
77 Massachusetts Avenue, 37-351
Cambridge, MA 02139

8. PERFORMING ORGANIZATION REPORT NO.

9. SPONSORING / MONITORING AGENCY NAME(S) AND ADDRESS(ES)

Air Force Research Laboratory (AFMC)
AFRL/RZSA
10 E. Saturn Blvd.
Edwards AFB CA 93524-7680

10. SPONSOR/MONITOR'S ACRONYM(S)

11. SPONSOR/MONITOR'S REPORT NUMBER(S)
AFRL-RZ-ED-TR-2009-0020

12. DISTRIBUTION / AVAILABILITY STATEMENT

Approved for public release; distribution unlimited. Public Affairs No. 09358 (4 Aug 09).

13. SUPPLEMENTARY NOTES

14. ABSTRACT

An experimental program to develop and test a mini-helicon thruster is described. The helicon discharge was designed and built in several different configurations using low- and high-current electromagnets. The program was designed to address several objectives: (i) to achieve a high coupling of RF-power to plasma and efficient acceleration to >20km/sec; (ii) to evaluate the scaling relations between power density, flow rates and B-field strength; (iii) to demonstrate operation with common molecular and atomic gases, and mixtures; (iv) to provide detailed characterization of the performance using spectroscopic and invasive techniques; (v) to experimentally demonstrate variable specific impulse capability. These objectives were successfully achieved. Stable discharges with well-collimated plume exhaust were achieved for argon (Ar), nitrogen (N_2), mixtures of Ar and N_2, and air. The parameters of the plasmas were measured using high-resolution spectroscopic and in-situ diagnostics, including super-fine emission line structure and isotopic shift of a seeded impurity. Plasma plume flow velocities in the 10-40km/sec interval were measured, and plume acceleration could be easily varied by altering applied RF-power or propellant flow rate. Very high ~4MW/m^2 power density throughput has been achieved in a steady-state regime. Operation with permanent magnets was attempted as well, including a magnetic nozzle and the possibility of a double layer formation. The experimental program thus demonstrated the potential of the mini-helicon discharge as an excellent space thruster design, given its high throughput, absence of internal electrodes and cathodes, potentially long life time, very low divergence of the plasma plume, flexible choice of propellants, and variable specific impulse.

15. SUBJECT TERMS
electric propulsion; helicon discharge; atmospheric gases; emission spectroscopy; plasma probes; variable specific impulse

16. SECURITY CLASSIFICATION OF:			**17. LIMITATION OF ABSTRACT**	**18. NUMBER OF PAGES**	**19a. NAME OF RESPONSIBLE PERSON**
					Dr. Jean-Luc Cambier
a. REPORT	**b. ABSTRACT**	**c. THIS PAGE**			**19b. TELEPHONE NO** *(include area code)*
Unclassified	**Unclassified**	**Unclassified**	SAR	81	N/A

STINFO COPY
NOTICE AND SIGNATURE PAGE

Using Government drawings, specifications, or other data included in this document for any purpose other than Government procurement does not in any way obligate the U.S. Government. The fact that the Government formulated or supplied the drawings, specifications, or other data does not license the holder or any other person or corporation; or convey any rights or permission to manufacture, use, or sell any patented invention that may relate to them.

Qualified requestors may obtain copies of this report from the Defense Technical Information Center (DTIC) (http://www.dtic.mil).

AFRL-RZ-ED-TR-2009-0020 HAS BEEN REVIEWED AND IS APPROVED FOR PUBLICATION IN ACCORDANCE WITH ASSIGNED DISTRIBUTION STATEMENT.

FOR THE DIRECTOR:

/ signed /
JEAN-LUC J. CAMBIER
Project Manager

/ signed /
INGRID J. WYSONG
Chief, Aerophysics Branch

/ signed /
PHILIP A. KESSEL
Technical Advisor
Space & Missile Propulsion Division

This report is published in the interest of scientific and technical information exchange, and its publication does not constitute the Government's approval or disapproval of its ideas or findings.

This Page Intentionally Left Blank

TABLE OF CONTENTS

LIST OF FIGURES

Figure **Page**

GLOSSARY

AFOSR	Air Force Office of Scientific Research
AFRL	Air Force Research Laboratory
Ar, Ar I	argon, argon I
ArII,Ar^+,ArIII	argon II, argon ion, argon III
B, BI, BII,B^+	boron, boron I, boron II, boron ion
BN	boron nitride
CAD	Computer Aided Design
CCD	Charged Coupled Device
CRM	Collisional-Radiative Model1
Cu	copper
D	deuterium
DURIP	Defense University Research Instrumentation Program
EM	Electromagnetic
EP	Electric Propulsion
FRC	Field Reversed Configuration
H	hydrogen
He	helium
Hg	mercury
I	current, *A*
I_{sp}	specific impulse, *sec*
ICP	Inductively Coupled Plasma
IDF, IEDF	Ion Distribution Function, Ion Energy Distribution Function
Kr	krypton
LH	Lower Hybrid
mHTX	mini-Helicon Thruster Experiment
MHT	Mini Helicon Thruster
MIT	Massachusetts Institute of Technology
MRI	Magnetic Resonance Imaging
MW	Mega Watt
N, N_2, N^+,N_2^+	nitrogen, molecular nitrogen, atomic ion, molecular ion
NdFeB	neodymium-iron-boron [strong ferromagnetic]
Ne	neon
O_2	molecular oxygen
P	power, *W*
PIC	Particle-in-Cell [method]
PPT	Pulsed Plasma Thrusters
RF	Radio Frequency
RPA	Retarding Potential Analyzer
SPL	Space Propulsion Laboratory
T	thrust force, *mN*
UROP	Undergraduate Research Opportunity Program
UV	Ultra-Violet [radiation]
VIS	Visible [light]
Xe	xenon

This Page Intentionally Left Blank

SUMMARY

An experimental study of a mini-helicon thruster (mHTX) for space propulsion was performed during the period 01/2005-02/2008 at the Massachusetts Institute of Technology (MIT) Space Propulsion Laboratory (SPL), under a contract from Air Force Research Laboratory (AFRL) at Edwards Air Force Base (Program Manager: Dr. J.-L. Cambier). With Dr. O. Batishchev as a Principal Investigator, twelve MIT students from three MIT departments were involved into this project, resulting in one Ph.D. and five M.S. theses.

The initial step of the experimental program consisted of developing a working device capable of operating in a small vacuum facility with a limited pumping capacity. Several configurations of the radio-frequency (RF)-delivery sub-system were tried prior to achieving the first inductively coupled discharge. Low-current electromagnets were built to excite the helicon mode in Argon. The efforts were made to gain required controllability of the discharge parameters. Various RF-antenna designs, materials and connections were tested. Preliminary gas and plasma characterization was performed using borrowed instruments from AFRL/Hanscom.

The second step included detailed characterization of the mini-helicon operation. A high-resolution UV-VIS system for spectral analysis was designed and built using Air Force Office of Scientific Research (AFOSR) support (Program Manager: Dr. M. Birkan) via Defense University Research Instrumentation Program (DURIP) grants. A new, fully computerized system to control RF-power, magnetic field strength and gas flow was implemented. The spectral sub-system was separated from the rest to improve stability. Stable operation with Argon and N_2 gases was achieved in double- and single-magnet configurations. Invasive Mach probes were machined and used to measure the plasma exhaust.

The third step included system optimization and development of the refined diagnostics to quantify energy balance, heat fluxes, plume detachment and divergence, thrust force, etc. A half-year delay due to serial failure of the SPL's vacuum system components forced a correction to the schedule. The RF-delivery and matching networks were re-designed to minimize losses and gain control. Compact high-current electromagnets were built. Seeding light impurity was attempted to facilitate diagnostics. In-situ retarding potential analyzer (RPA) probing and non-invasive Doppler shift measurements have indicated high plasma acceleration in the mHTX with a collimated plume formation. Variability of the specific impulse by controlling power density was demonstrated.

All major steps are reflected in this report in chronological order. Key experimental data and their analyses are presented, along with theoretical estimates of plasma conditions and thruster performance.

1. MOTIVATION AND OBJECTIVES

There is a need for efficient thrusters operating in the ~10-1000W power range producing 0.1-100mN thrust at 1-2$Ksec$ I_{sp}. There is also a general need, arising from the fact that commonly used xenon gas is rare and pricey, and, therefore, has to be replaced with readily available propellants. Ideally one should use gases common to the Earth's atmosphere such as nitrogen (79%) and argon (1%). Using of liquid (water) and other molecular propellants (ammonia) is also feasible as a future development. There is another critical requirement for the low-power system – long lifetime. Present plasma systems as Ion Engines and Hall Thrusters suffer from notorious erosion of extracting electrodes and ceramic walls, respectively. They also require an external cathode for charge compensation that limits the overall life time of the system, as well as the efficiency of operation at start-up and at low operational powers.

As a possible solution we have proposed development of an RF-driven mini-helicon thruster. The original reason was that the helicon plasma sources were broadly used by industry [1] due to their robustness and efficient plasma production, ~200eV per ion [2-4]. Industrial helicon sources operate predominantly with heavy gases as Ar in the 10-1000kW power ranges. The light gases operation was scarce until a breakthrough was made by VASIMR [4-5] 3-50kW H/D/He/Ar helicon source experiments [6,7]: i) near 100% gas ionization – experimental proof of the theoretical result predicted by MIT [8,9] gas burn-out regime, ii) sharp T_e rise at the high mode threshold to ~10eV, iii) strong axial acceleration of plasma, with measured specific impulse I_{sp} in the excess of 4000sec and ambipolar potential at ~40V, iv) no erosion of RF antenna and inner quartz walls – there are no internal electrodes, RF antenna is evacuated from gas and plasma, the inner wall of the discharge tube is magnetically insulated. Thus, the helicon has a potential for the unlimited operational life time. Accordingly, we propose an RF-driven helicon plasma thruster utilizing inexpensive light dia- and monoatomic gases, mixtures, air, and compounds to be used in the 10-1000W operational range. The beam efficiency is expected to be in 30-50% range, with 100% propellant utilization, I_{sp} in the 1000-5000sec range. These numbers come from the analysis, which is based on the energy balance relation:

$$\mu\left(\frac{I}{M}+\frac{I_{sp}^2 g^2}{2}\right)=P \tag{1}$$

where μ is the propellant mass flow rate, I – ionization cost, M-atomic (molecular) mass, g – acceleration of free fall, P – applied RF-power. By using the definitions of reaction force:

$$T=\mu I_{sp} g \tag{2}$$

and the definition of beam efficiency

$$\eta=\frac{E_{beam}}{P}=\frac{T^2}{2\mu P} \tag{3}$$

thrust can be expressed in terms of P and μ as:

$$T=\sqrt{2\mu\left(P-\frac{\mu I}{M}\right)} \tag{4}$$

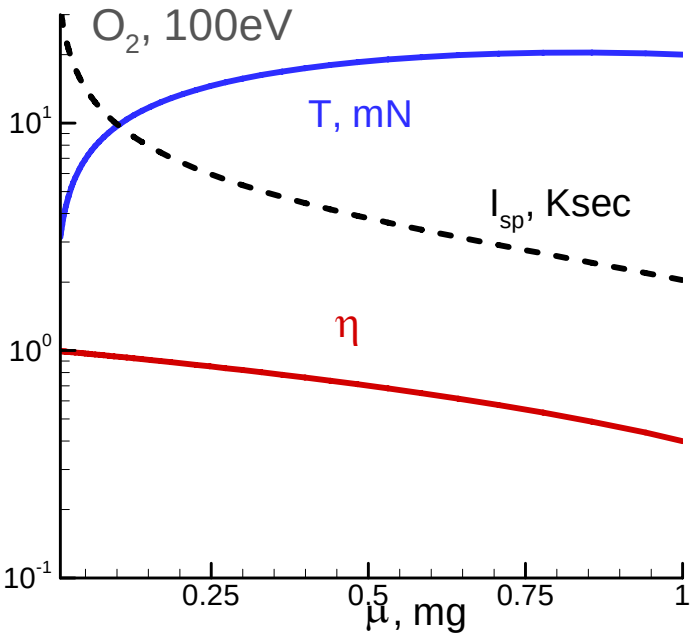

Figure 1: Specific impulse, I_{sp}, thrust, T, and efficiency, η, vs flow rate for O_2 at *P=500W*

An illustration of achievable parameters for *P=500W*, and *I=100eV* per O_2 molecule are given in Fig. 1. Efficiency of 50%, with I_{sp}*~3-10Ksec*, and thrust *T~5-20mN* appear to be achievable. The overall performance of the helicon strongly depends on the ionization cost. The latter is assumed to be constant for the sake of analysis. The ionization cost does depend in a non-linear way on the mass flow rate, as well as RF-to-plasma coupling and other key parameters, which have to be studied.

Thus, the major objectives can be summarized as follows:

i) achieving high coupling of RF-power to plasma and its acceleration to >20km/sec;
ii) scaling-up the power density by altering flow rates and B-field strength;
iii) operation with common molecular and atomic gases, and gas mixtures;
iv) characterization of the performance using spectroscopic and invasive techniques;
v) experimental demonstration of variable specific impulse capability.

2. MAIN RESEARCH ISSUES

There is growing interest in particular in the experimental use of Helicon plasma generators, either for direct electro-thermal propulsion [12-14] or as first stages for other devices, as in VASIMR [4-8], FRC-based, and other concepts. Most ongoing experimental works in this area involve kW-level devices operating at 13.56 to 50 *MHz*, with applied magnetic fields in the 300-2000 *Gs* range. Available pumping capability would not allow us to operate at these power levels. Instead, we propose to develop the capability to operate mini-helicon devices that are designed according to known scaling laws listed below, so as to reproduce the non-dimensional parameters, and hence the performance, of the larger devices. This will establish an independent, low cost alternative for verification of results from larger facilities, while at the same time allowing the development of low-power Helicon thrusters.

2.1 Low-power operation

Instead of going towards high operational powers we plan to accept the low-power restriction and optimize its use to obtain valid data of general value as well as design information for mini-Helicon class thrusters. This is possible through implementation of known [2,3] scaling laws:

- Plasma density scales inversely with power;
- Discharge dimensions scale as the power;
- Magnetic field strength scales inversely with power;
- RF-frequency scales inversely with power;
- Propellant flow rate and thrust force increase with power.

These laws preserve the essential non-dimensional microscopic ratios, including the electron collisional mean-free-path and gyro-radius to the gas tube ratio. They also keep the excitation frequency in the desired range, just above the Lower Hybrid frequency for the gas used. In turn, they should guarantee constancy of the important non-dimensional performance factors, including beam efficiency - the key parameter for the targeted space application.

2.2 Use of common mono- and diatomic gases

Our second concern is economics. Ion Engines and Hall Thrusters tend to operate with Xe, the scarcest non-radioactive noble gas. Those devices have to operate with xenon due to high ionization loses. Helicon discharge is more efficient, and, therefore can operate with a range of propellants. The list of feasible propellants is collected in Table 1, assuming μ=1mg/sec flow. Clearly, Xe has the lowest I/M ratio.

Table 1. Characteristic parameters of various propellants

	H_2	He	B	N_2	Ne	Ar	Kr	Xe
***M**, AU*	1.008×2	4.003	10.8	14.007×2	20.18	39.95	83.8	131.3
***μ**, sccm*	740	370	136	52	74	37	17.6	11.3
***I**, eV*	2.8	5.5	15	39	28	55	116	181
I_1, *eV*	13.598	24.587	8.298	14.534	21.564	15.759	13.999	12.13
I_2, *eV*	-	54.416	25.154	29.601	40.962	27.629	24.359	21.21
I_3, *eV*	-	-	37.93	47.448	63.45	40.74	36.95	32.1
$B_{LH}^{13.56}, Gs$	208.5 (**295**)	415.5	682.4	777.2 (**1099**)	932.9	1312	1901	2379.5

Use of light gases (H-He) is only feasible from the energy efficiency standpoint for very high specific impulses I_{sp}>5000s, while we are targeting 1-3Ks range. Heavy gases are a composition of several stable isotopes (4-5 in Xe&Kr) that makes difficult, for instance, refined spectroscopic measurements, such as of the Doppler shift. Of all gases with moderate atomic numbers of interest only nitrogen and argon (oxygen is excluded) are readily found in the atmosphere with a single stable isotope, ^{14}N and ^{40}Ar, respectively.

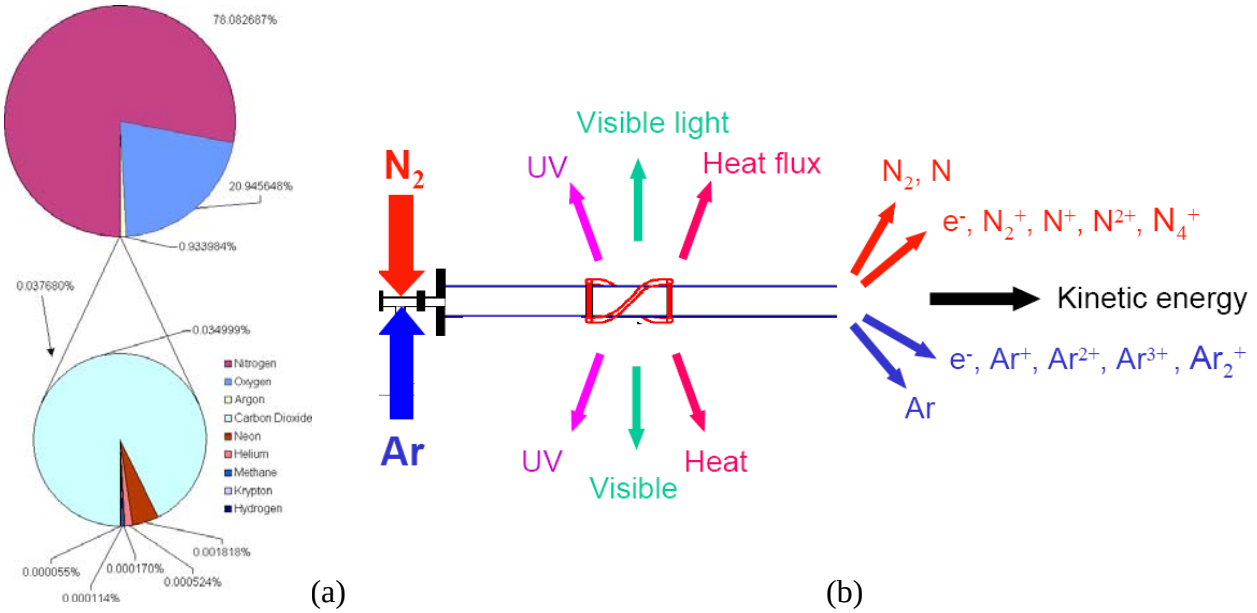

Figure 2: (a) - Earth's atmosphere composition, with ~78% N and ~1% Ar fractions, while Ne ~0.002%, Kr ~0.0001%, Xe ~0.000009%; (b) – expected products of the helicon discharge operation on diatomic and atomic gases

N and Ar elements are among the most abundant in Earth's atmosphere (see Fig.2a); however, plasma chemistry of the discharges using these gases is made complicated by to possible formation on multi-charged ions and molecular ions as shown in Fig.2b. A spectrum of charge/mass ratios for a single species brings about a possibility for multi-mode operation using just one gas as a propellant.

2.3 Vacuum facility limitations

We used existing SPL's $3m^3$ vacuum tank General parameters of the AstroVac facility are as follows: 1.5x1.6 m bakeable vacuum tank, with a pumping speed of 7000 liters/sec of Xenon, capable of reaching pressures under 10^{-8} torr without gas puff. At ~20-30sccm flow rates quasi-stationary background gas pressure is about $5\text{-}7\times10^{-5}$ torr. It has a roughing mechanical pump and two liquid helium-cooled cryopumps, with operational T~11K. Therefore, use of the lightest gases is prohibited.

Figure 3: SPL's AstroVac

2.4 Use of passively cooled copper electromagnets and permanent rare-earth magnets

Following older helicon designs, our first intent was to have water-cooled system, which includes magnets and helicon antenna. To accomplish this task, two undergraduate students built a water-cooled magnet (Fig.4) as a part of UROP project. However, there were problems with non-uniform heating of the layered design, and the magnet did not deliver the required field

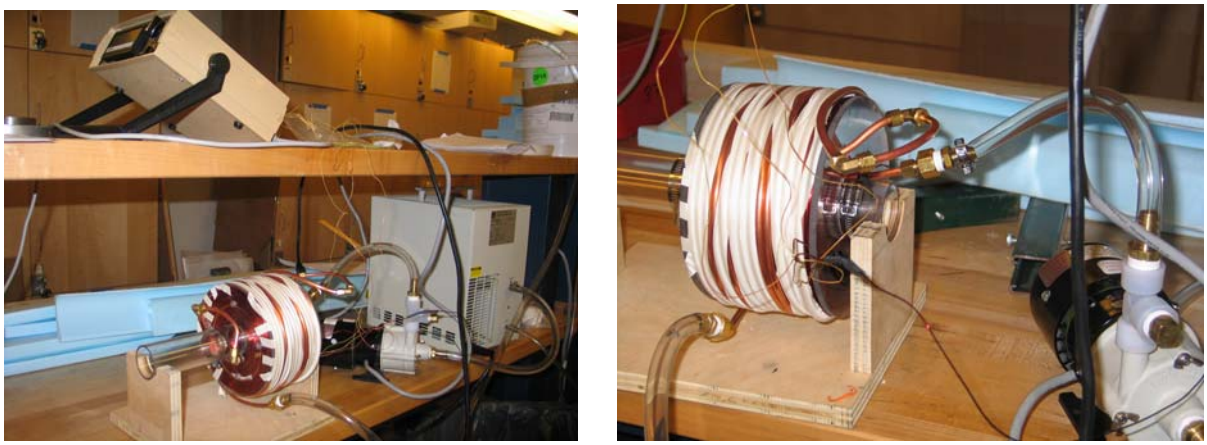

(a) (b)

Figure 4: Student-built water-cooled magnets: shown are copper coils, water pump, heat exchanger and power supply

Our second path was to reuse existing magnet system. The one shown in Fig. 5 delivers continuous 0.5T. The entire 2-ton assembly was brought to the shop. However, detaching 200kg coils from the solid ion core became an impossible task. Moreover, only external use of these meter-sized coils was feasible, while in-tank system gives more flexibility. It became clear that actively cooled conventional copper wire and superconducting electromagnets create a major problem if used in a vacuum tank which is susceptible to water leaks, in particular cryopumps. Thus, we were left with single option of using passively cooled electro- or permanent magnets.

Figure 5: Existing 2-magnet MRI system by Varian was too bulky

2.5 Non-invasive diagnostics and plasma probes

The ability to diagnose Electric Propulsion (EP) systems and the associated plasmas through the measurement of radiation emission is an attractive alternative to the more traditional plasma diagnostics methods that employ intrusive probes. Invasive probes do not allow measuring certain things as plasma composition, rate of erosion, etc. Most importantly they distort the object they are trying to characterize.

Investigating the use of emission spectroscopy to deduce important plasma parameters such as plasma temperature, density, flow velocity, etc, as well as to identify regimes of operation that minimize thruster erosion rate thus allowing increased thruster lifetime seems quite attractive. Specifically, conducting spectral measurements in the plume region of the thrusters and measuring bulk ion velocities through the measurement of line Doppler shift may yield important missing information.

However, for helicon source characterization we planed to also use available invasive instruments, as well as to build new Mach probes, Faraday caps, Retarding Potential Analyzers (RPA), Langmuir probes, thermocouples. Those data should be correlated with spectroscopic measurements.

2.6 Operational frequency, RF source, matching network

MIT's laboratory is located in a densely populated urban area. Thus, we had to limit operational frequency to an open RF band. Bounded by achievable magnetic field, B~0.2T, and desire to be in reach of LH resonance, we have chosen operation at fixed $f_{RF} \approx 13.56 MHz$. Ideally we would like operating at variable frequencies, but tunable sources are more expensive, and there is an option to vary magnetic field instead. Thus, used rack-mountable 1.2KW RF Power Products RF-10S/PWT generator was acquired. It has a standard RG10 connector attached via coaxial cable to a vacuum feed-trough, which transmits RF power to the antenna.

Such setup was not readily available, as well as matching network, which has to nullify imaginary part of the antenna's impedance. Due to change of plasma load the network has to be tunable in a broad range.

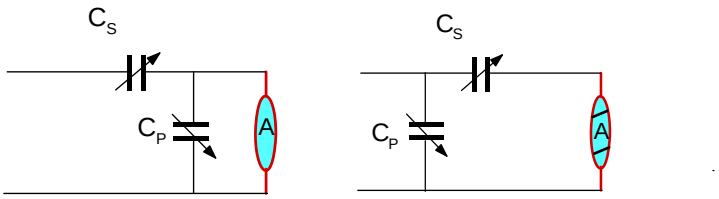

(a) (b)

Figure 6: Two possible arrangements of the serial, C_S, and parallel, C_P, variable capacitors and the helicon antenna, A, in a matching network

In addition, good surface contact inside entire air-to-vacuum RF network has to be maintained because at MHz frequencies current travels in the ~20 μm-thin skin layer:

$$\delta = \left(\lambda / \pi\sigma_{Cu}\mu c\right)^{1/2} \qquad (5)$$

of the copper conductor. Thermal expansion due to antenna heating and joule heat dissipation within matching network and RF-delivery system had to be taken into consideration as well.

3. INITIAL DESIGN (2005)

The first half of 2005 was devoted to the preliminary design of the mini-helicon thruster experiment, aka mHTX@MIT. It included calculation of the magnetic field, gas flows, dimensions of the quartz tube, supporting system, designing of the matching network, RF-delivery system, and helicon antenna. The physical construction of the 1st design took place in the summer and finished in the Fall of 2005. The assembled inside vacuum tank device is shown in Fig.7.

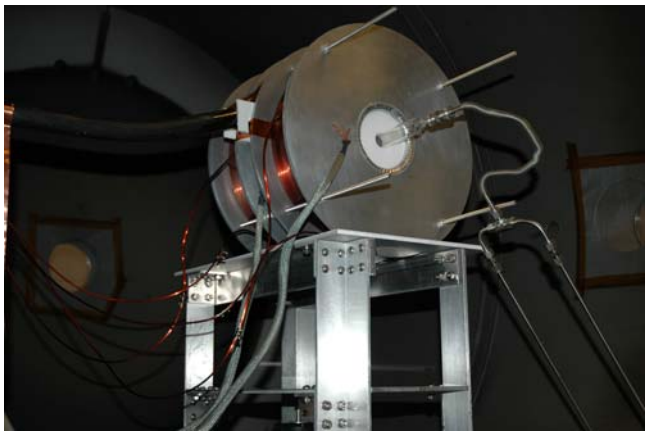

Figure 7: First mHTX configuration, finished in November 2005. Shown are 2 electro-magnets in a Helmholtz pair setup on a stand, Teflon™ inserts in the magnet bores to support quartz tube, gas feeding manifold, thick RF cable, thin wires for T-couple and magnet current

We briefly describe various systems as they were originally designed and constructed.

3.1 Low-current electromagnets

Three electromagnets (Fig. 8) wound from 10 AWG square high-T, insulated magnet wire. Two were near-identical while the third one not as densely packed due to initial trial. The following magnets were wound on a professional lathe at MIT Bitter Magnet Laboratory (Fig. 8 insert). The magnets are powered by 35-A, 350-V power supplies and are controlled via the main SPL computer system. Two or three magnets are held in place via four tie rods which have removable spacers, allowing the spacing between the magnets to be varied if field shaping is desired. The two main magnets are capable of producing a continuous B of 1800G at the axis at maximum 35A current per each coil, roughly 50G per 1A of current. The current and the magnetic field could be controlled in the 0-35A, corresponding to the 0-0.18T range.

Because of operation at high vacuum each of the magnets has been equipped with two thermocouples to monitor heating, allowed to ~200°C. During single ~10-15sec shot magnets were heated by several degrees. The passive cooling allowed them to cool to the operational (~100°C) temperature in several minutes. However, complete cooling to the room temperature required over-night stay in vacuum, or ~one hour in the vacuum tank vented to 1atm.

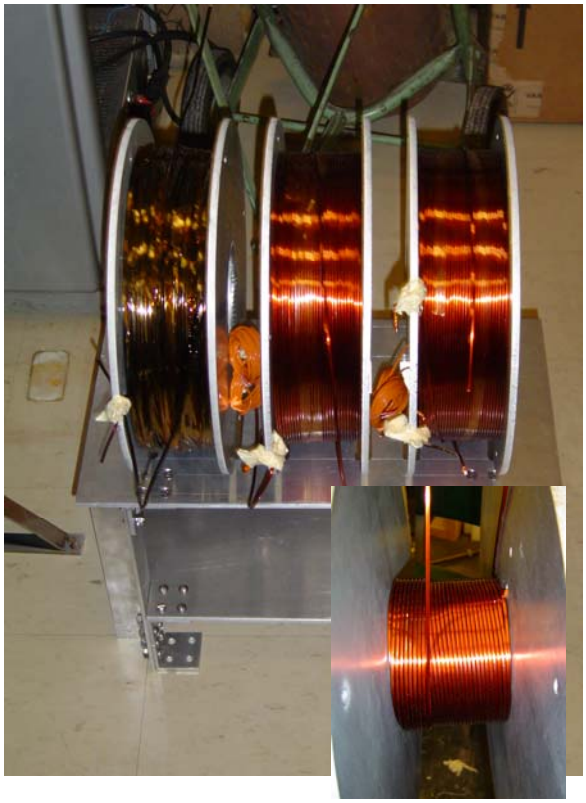

Figure 8: Three low-I electromagnets on the stand; (insert) – 10-gaude square wire is perfectly packed

3.2 Gas and current vacuum feeds and controls

Gaseous propellant was fed through existing manual flow controller with maximum dialed flow of 10sccm Xe (Fig. 9a). Thus, at first the flow was limited, as well as the magnet current. Multi-pin vacuum current feedthrough was rated to ~50A (Fig. 9b).

(a) (b)

Figure 9: (a) – manual gas feed, (b) – vacuum current feedthrough to supply 0-35A current to maximum of 3 electromagnets (white spacers are machined of Teflon™ insulation)

3.3 RF delivery system, matching network and helicon antenna

RF generator (1.2KW 13.56 MHz) was connected via 50 ohm coaxial cable to the matching box as shown in Fig.10a. The box was firmly mounted on top of 8" window port. The matching network had configuration given in Fig. 6a. A 1.5KW-rated vacuum RF-feedthrough was screwed into the flange covering window port as one piece with the aluminum box. Entire assembly was grounded through the chamber ground. High-voltage tunable vacuum capacitors have been used, as to ~10KV potential jumps were expected at the breakdown.

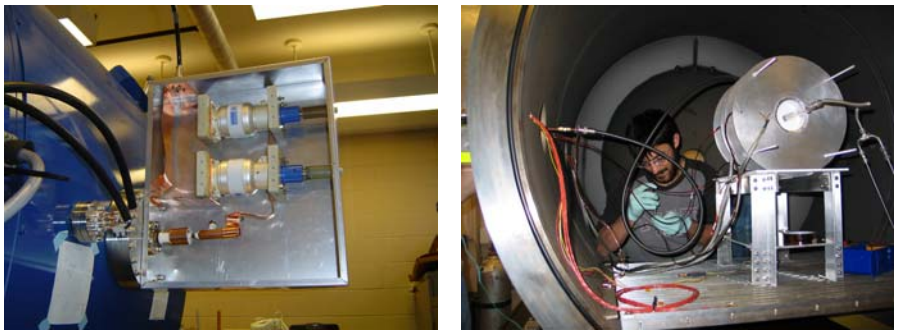

(a) (b)

Figure 10: (a) – matching box attached to the window 8" port; (b) – vacuum feedthrough is connected to antenna via coax cable

Vacuum side of the RF feedthrough was connected with helicon antenna using MW-rated coaxial cable. The stripped end of the cable (Fig. 11a) was screwed together with helicon antenna (Fig. 11b) cut from a piece of copper utility pipe of 1" ID. Type: M=1 double half-twist.

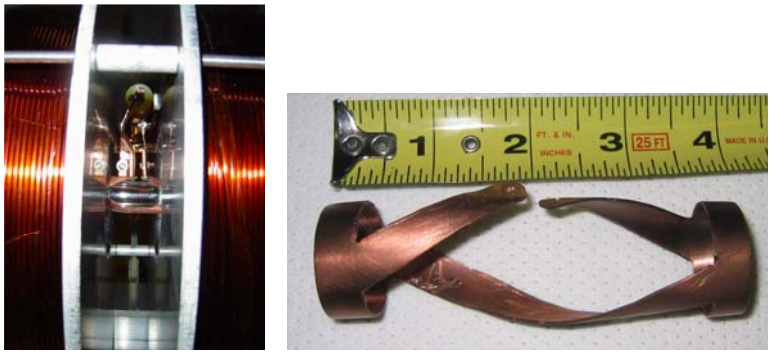

(a) (b)

Figure 11: (a) – antenna attachment to the coax cable; (b) – M=1 symmetrical helicon antenna, ~10 cm long and ~2.5cm ID.

4. FIRST PLASMA FOLLOWED BY QUICK REDESIGN

First plasma was obtained on 11.23.05 with nitrogen gas, ~8sccm flow rate. At low power inductively coupled discharge plasma (ICP mode) was achieved (Fig. 12a). But as the power was increased to ~700W it was clearly flowing towards the gas feed side. This end was visibly much brighter (Fig. 12b). Upon inspection it became obvious that plasma indeed flows towards the grounded metal manifold burning thin insulation installed in the swage lock.

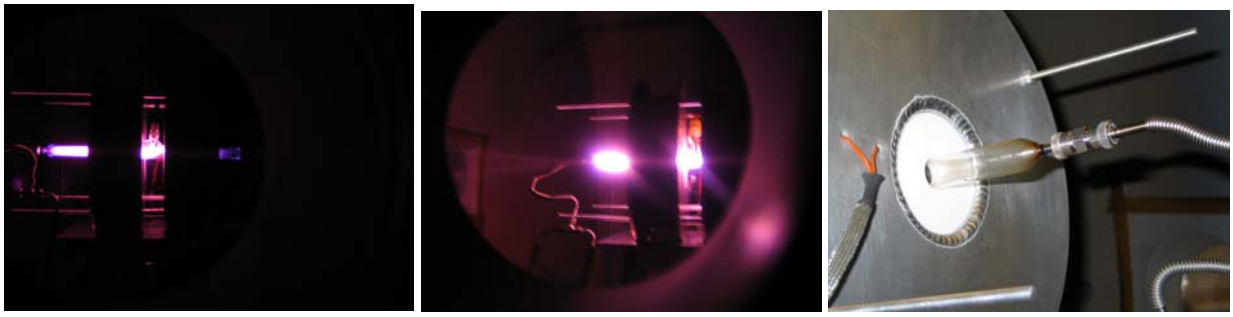

(a) (b) (c)

Figure 12: (a) – ICP discharge in nitrogen; (b) – plasma rushes towards grounded manifold; (c) – burned insulation at the gas intake.

Another important outcome of initial experimentation was that the MW-class coaxial RF-cable experienced substantial damage to the insulation. Apparently, the axial heat conduction was not high enough to prevent overheating. Therefore, three important modifications were made:

- plastic manifold for gas puff was installed instead of grounded metal;
- RF-cable was replaced with two coaxial utility pipes;
- sliding continuous connector for helicon antenna was introduced

These “obvious” modifications are shown in Fig.13.

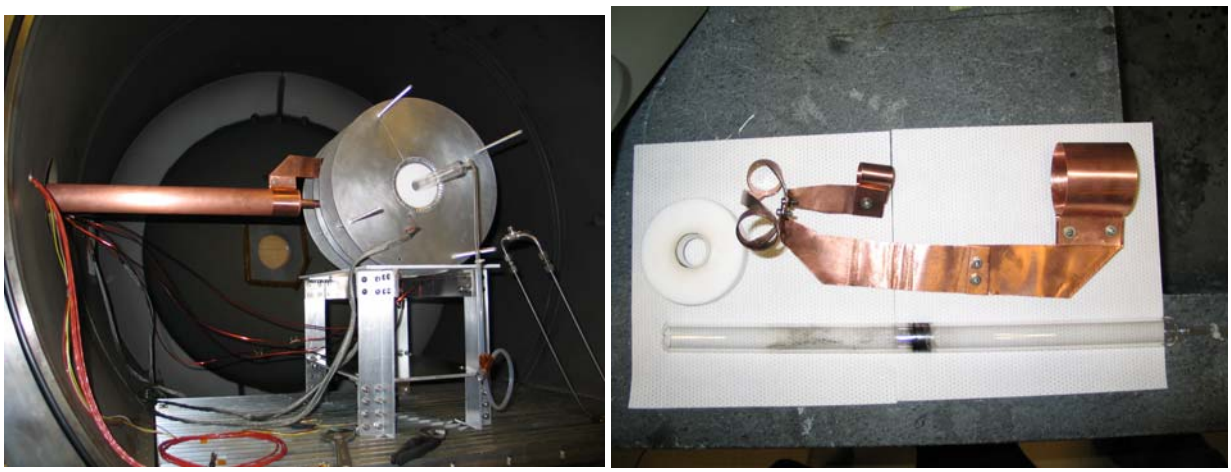

(a) (b)

Figure 13: (a) – 3rd design of the mHTX; (b) – flat metal copper connector with attached antenna. Also shown is a used 2cmID×40cm quartz tube.

At the end of 2005 automation of the experiment was initiated. First design allowed controlling gas flow rate, output RF power, and magnet temperature, but not currents due to the limitations of the older power supplies.

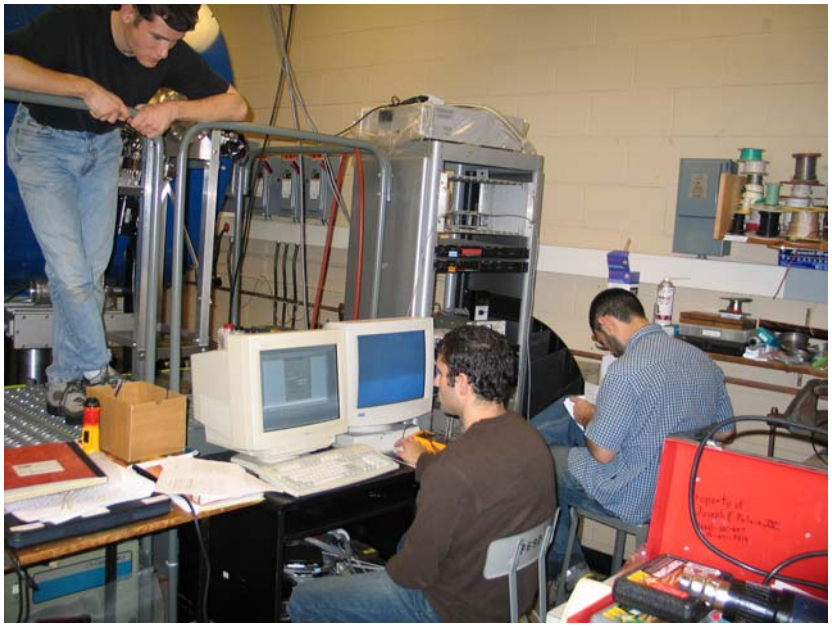

Figure 14: First design of the mHTX control system

5. HELICON DISCHARGE WITH INITIAL SPECTRAL CHARACTERIZATION

As the result of the improvements described in the previous section, on December 9th 2005 first stable truly helicon mode discharge was achieved with argon operation, the so-called "blue argon" mode, at ~20sccm flow rate and 1kW RF-power delivered to the helicon antenna in two-magnet configuration with I~30A in each, delivering B~1500 G (Fig.15)

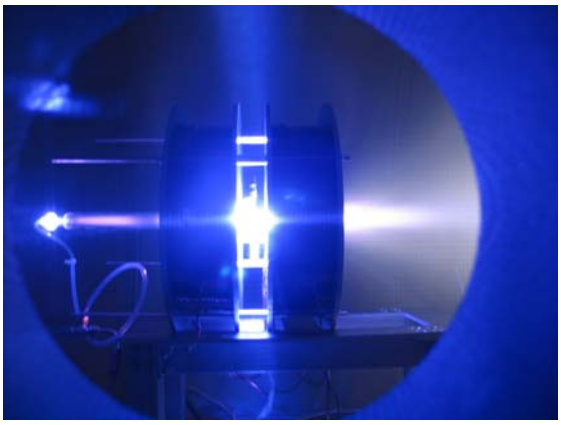

Figure 15: Stable helicon mode discharge operating on argon

The only quantitative characterization of the discharge at that time was visible spectrometry. We had on lease from AFRL/Hanscom AFB a spectrograph Jarrell Ash MonoSpec 18, a 0.156 m (F/3.7) Czerny-Turner type. The CCD detector is a cooled type (Andor iDus DU420A). The dimension of the whole system is compact, about 14"x10"x 5". A laptop computer is used to interface with the CCD detector. There are four available gratings with 300 (blazed at 300 and 500 nm), 600 and 1200 grooves/mm. We used an Oriel- 6035 Hg-Ar spectral calibration lamp to calibrate the wavelength.

A set of collimating (1000mm focal length) and focusing (100mm focal length) lenses and a fiber optic bundle collect the emission to the spectrograph. The optical setup is located on a platform attached to the one of the windows of the vacuum chamber (Fig. 16b). The portable platform can easily be moved and located on another window for alternative viewing of the inside of the vacuum chamber, for instance at the downstream window. Setup could be rotated at an angle to allow view across the plume.

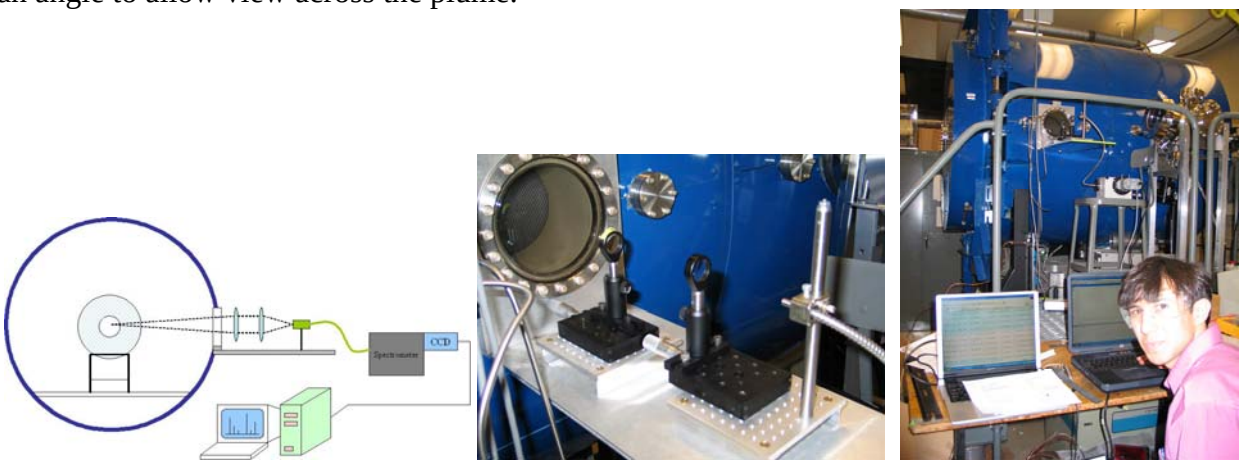

(a) (b) (c)

Figure 16: Visual spectroscopic data acquisition on mHTX: (a) – general scheme, (b) – two-lens system collecting light through the window port onto an optical fiber; (c) – general view of the optical shelve, spectrometer with attached CCD, which is in turn connected to the PC

The first calibration spectra and ICP-to-Helicon discharge comparison were taken 12.10.05.

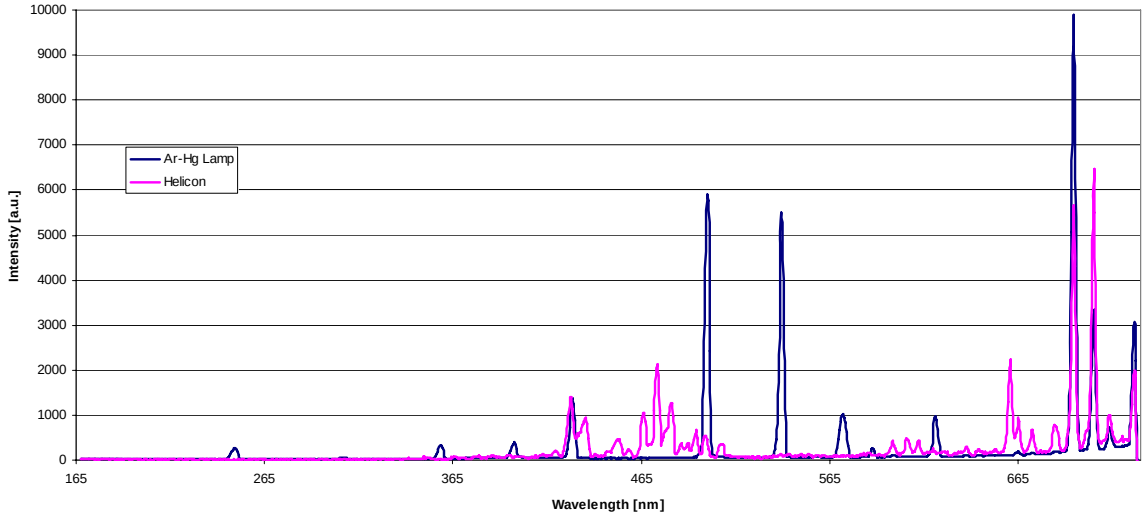

(a)

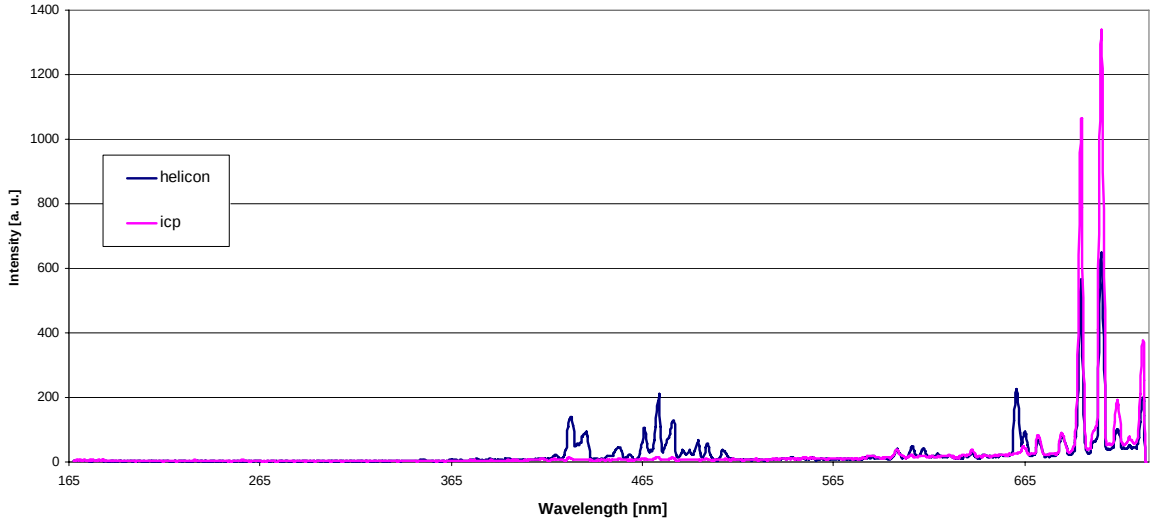

(b)

Figure 17: First coarse VIS spectra: (a) – calibration Ar-Hg lamp spectrum vs Helicon discharge spectrum; (b) – helicon vs ICP discharge spectrum

From comparative spectra presented in Fig. 17a, one can conclude that ArI lines do match well with a standard source. From the second Fig. 17b one concludes that

- neutral gas is at least 50% ionized, and
- ion lines, invisible in ICP regime, are significantly present in the helicon mode.

Some additional details of the initial mHTX design and construction could be obtained in Joseph Palaia's MIT MS thesis in Nuclear Engineering [19], submitted in January ’06, accepted in April ’06. He was the first MIT student supported by the mHTX Project.

In summary, the first year work yielded an operational mini-helicon system.

6. FIRST EXPERIMENTAL CAMPAIN (2006)

After a robust operation was achieved, a broad study of various operational regimes was undertaken. The main varied parameters were:

- RF-power, magnetic field and mass flow rates;
- different antenna designs and antenna materials;
- dual- and single-magnet operations;
- operation with different propellants – Ar, N_2, Ne, Xe
- operation with mixtures as Ar-N_2 and air;
- operation with permanent magnets;

In parallel some main sub-systems were upgraded. Also more accurate spectral characterization of discharge area and plume was performed.

6.1 Spectroscopic system upgrade

At some point, a better demo spectrometer was loaned to us by Acton Research, namely SpectraPro-500i spectrometer. This fully automated, 500mm focal length, f/6.5 aperture Czerny-Turner type spectrometer provided a resolution of ~0.1A/pixel at 435nm using a 1200 g/mm grating for the CCD detector attached to it. The inlet port was equipped with an adjustable slit. The spectrometer has a triple-grating turret, and was equipped with three different diffraction gratings. A grating with 300 grooves/mm blazed at 500nm was used to obtain broader range spectra. The second grating at 1200 grooves/mm blazed at 500nm was widely used due to its better wavelength range at relatively good resolution. The high resolution grating at 1800 grooves/mm blazed again at 500nm provided high resolution spectra with small wavelength range. A photo of the spectrometer with old visible emission collection system is shown in Fig.18.

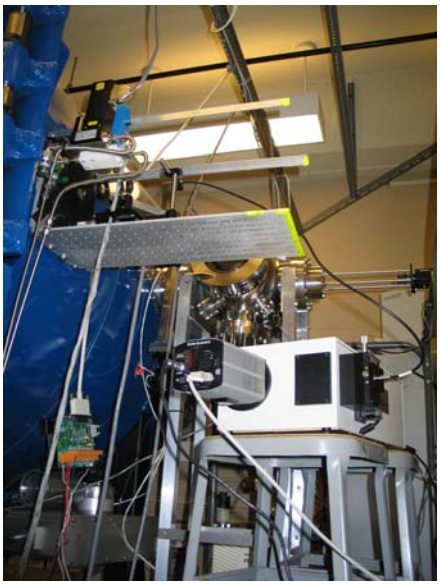

Figure 18: 50cm spectrometer with attached -40°C cooled CCD camera

We hoped to use this new instrument for Doppler shift and other advanced spectroscopic measurements, but the spectral resolution was one order short from required. Thus most of the data that were taken with Jarrell Ash were not retaken with new instrument later in 2006.

Attempts were made to take spectral data for Ar and N_2 discharges. Nitrogen data were heavily populated with molecular lines. In some regimes strong atomic lines were diagnosed, but overall N_2 data were inconclusive.

Despite many attempts in 2006 to characterize plume with integral measurements, Mach and other probes, the majority of information was collected in the form of visual observations, recorded movies, running power and flow scans, and also as low-medium-resolution spectra for regimes with various operational parameters and different equipment, e.g. helical antennae.

6.2 Spectral study of mHTX operation on Ar

6.2.1 Low resolution ICP and Helicon modes comparison

More (1800g/mm) and less detailed (300g/mm) spectra of Helicon (B>1400G) and ICP modes (B~0) were taken and compared. In Fig. 19 below we present data for ICP (no current) and bright helicon mode (30A current ~ 1500Gs magnetic field). One can immediately conclude that

- there are no sizable ion lines in the ICP mode;
- neutral lines are depleted by at least half in the helicon mode compared to ICP.

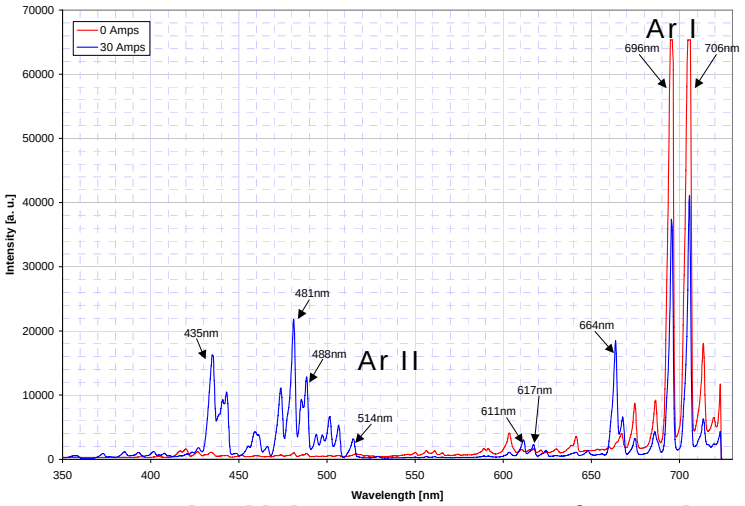

Figure 19: Measured visible line emission spectra of MHT plasma: (red line) – ICP mode with no ion (ArII) lines, and (blue) – Helicon mode with depleted ArI

From these measurements we can draw a conclusion that the neutral density had dropped by at least in half in the discharge volume. This means that we ionize at least 10sccm of argon. This value is very pessimistic, because i) electron temperature went up, and ii) plasma flows axially at a much faster pace than neutrals. More probably we do ionize >95% of the gas.

The ionization efficiency looks very promising. Indeed, from the power balance of input RF power and efficient flow ionization power, assuming 50% efficiency of RF power coupling to plasma column:

$$300W \approx P = I\dot{N} = I \times 30sccm \times 4.5. \cdot 10^{17}\, sccm^{-1} \times 1.6 \cdot 10^{-19}\, J/eV \qquad (6)$$

we obtain an effective "ionization cost" $I = 140eV$! This result is close to VASIMR data [14] for argon $I \approx 60eV$ at 20kW operation, and is very encouraging if true. We are planning to further diagnose helicon plasma and obtain direct measurements of plasma and gas density, temperature [9,10] and velocity. We are also planning to assess role of charge-exchange [12] and wall effects [16] on the plasma flow. Using current data, and assuming sub-sonic plasma flow [11] we can estimate plasma density from the known plasma production rate and source cross-section:

$$\dot{N} = 30sccm \times 4.5 \cdot 10^{17}\, sccm^{-1} \approx 0.1 C_s \pi R^2 n_p \qquad (7)$$

where $C_S = \sqrt{kT_e / M}$ is the ion speed of sound. If one assumes a high electron temperature, $T_e = 10eV$, for $R = 1cm$ one can still obtain a relatively high plasma density $n_p \approx 10^{14} cm^{-3}$.

6.2.2 Medium resolution ICP and Helicon modes comparison

Spectral comparison of Helicon and ICP discharges were repeated using higher 1800g/mm grating. Spectral interval per CCD reduced due to higher dispersion. Therefore, data were collected in continuous sections of the wavelengths. In Fig. 20 below we present data from the far red region, representig only ArI atomic lines, and "blue region" centered around the most prominent ArII ionic lines. Two spectral lines correspond to I=0 inductively coupled and I=30A helicon modes. The mass flow rate was the same for both runs at 20sccm, the same delivered to antenna RF power of 1kW, and the same experimental configuration was used.

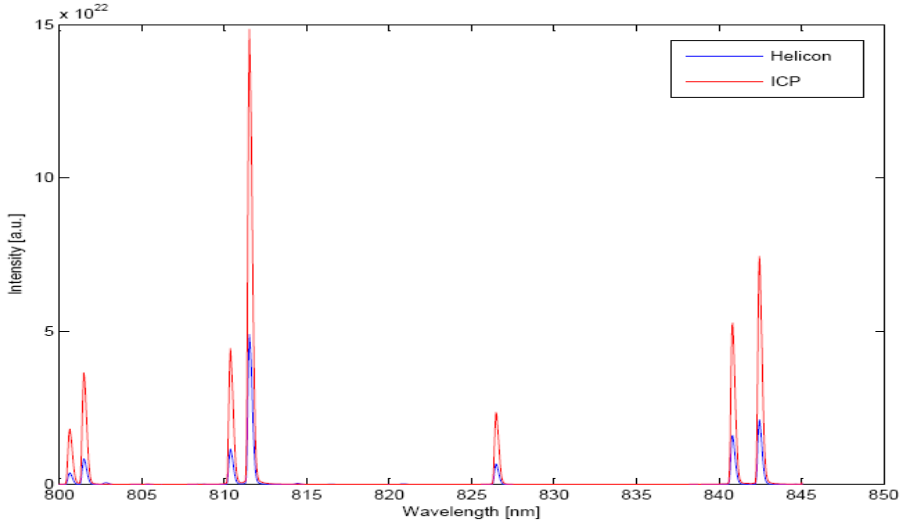

(a)

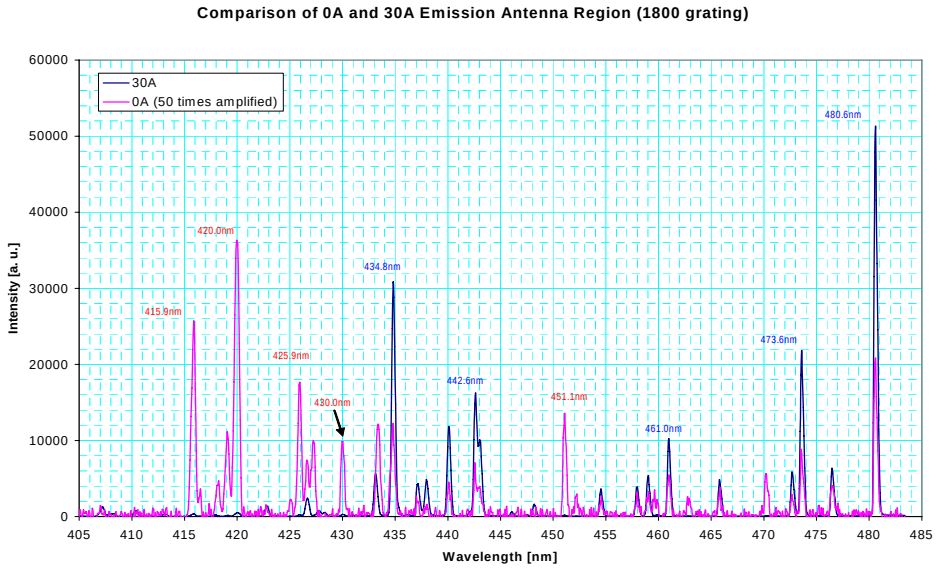

(b)

Figure 20: (a) – spectra of Helicon vs ICP mid-resolution spectra in the far-red region dominated with ArI atomic lines; (b) - the same for blue ArII ion-dominated part

It can be deduced from Fig. 20a that the degree of gas ionization fraction (static) exceeds 60-70%, which assuming sonic flow with room 0.025eV temperature for neutrals and ~25eV energy for ions translates into >99% ionization flow-wise.

Spectral data for the intervals of spectrum were stitched together using WinSpec option, which is not perfect. It may produce artificial spikes at the boundaries. Nethertheless the ICP and Helicon spectra for the visible 400-850nm range were compiled and are presented in Fig. 21 separately for the two modes. It is clear that in ICP mode plasma is very weekly ionized, while in the Helicon mode the outflow is predominantly ionic.

(a)

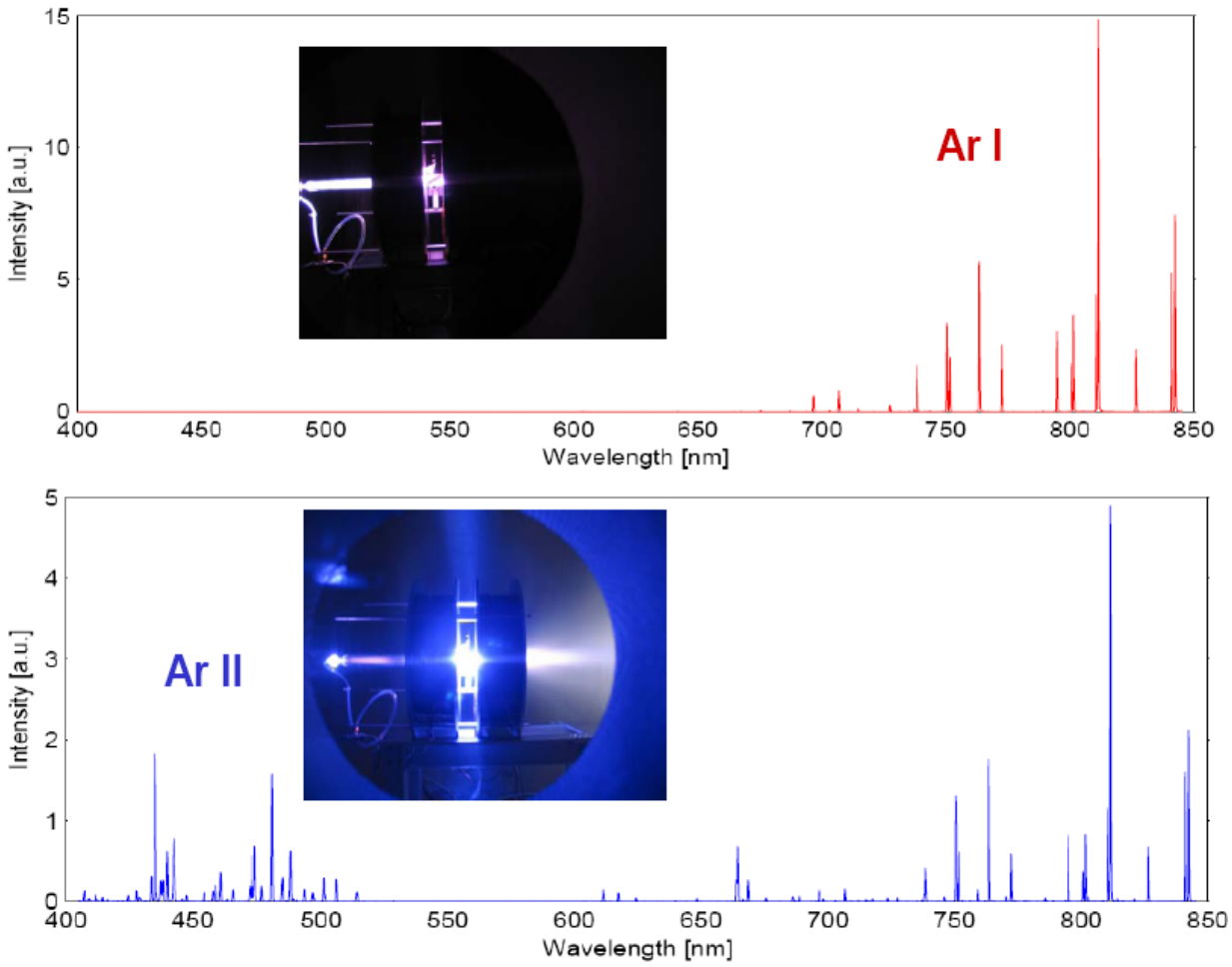

(b)

Figure 21: Broad 400-850nm mid-resolution spectrum: (a) – ICP discharge dominated with "red" atomic ArI lines; (b) – Helicon discharge populated with "blue" ionic ArII lines

Note that ICP spectra in the 450nm region (Fig. 20b) has to be magnified by ~two orders to make ion lines visible. Therefore, these lines are completely invisible in Fig. 21a. This is an indication of much higher electron temperature (or energy in the helicon wave) in the helicon regime compared to the inductively coupled regime.

6.2.3 Analysis of the experimental parameters scans

Direct spectroscopic measurements of the flow scans, magnetic field scans, different antenna lengths and materials, magnetic field and antenna variations, allowed discovery of optimum performance spots in each studied configuration. Best operation corresponded to maximum ratio of ion to neutral line radiation ratio in visible 400-900nm spectrum range. It could be also judged by the shape and dimension of the exhaust plume as produced by the discharge.

6.2.4 Mass flow scan

Taken through side port pictures of the mHTX operation in two-magnet configuration at ~30A per magnet (B~1500G) and ~650W applied RF power are shown in Fig. 22. The RF-to-plasma matching was continuously adjusted to approximately preserve the discharge parameters. One can see the ionization region being pushed progressively towards the exhaust as the flow rate is increased between 10-100sccm (and becomes hidden by the first electromagnet). At the same time a progressively brighter visible plume is formed, reaching maximum at ~30sccm.

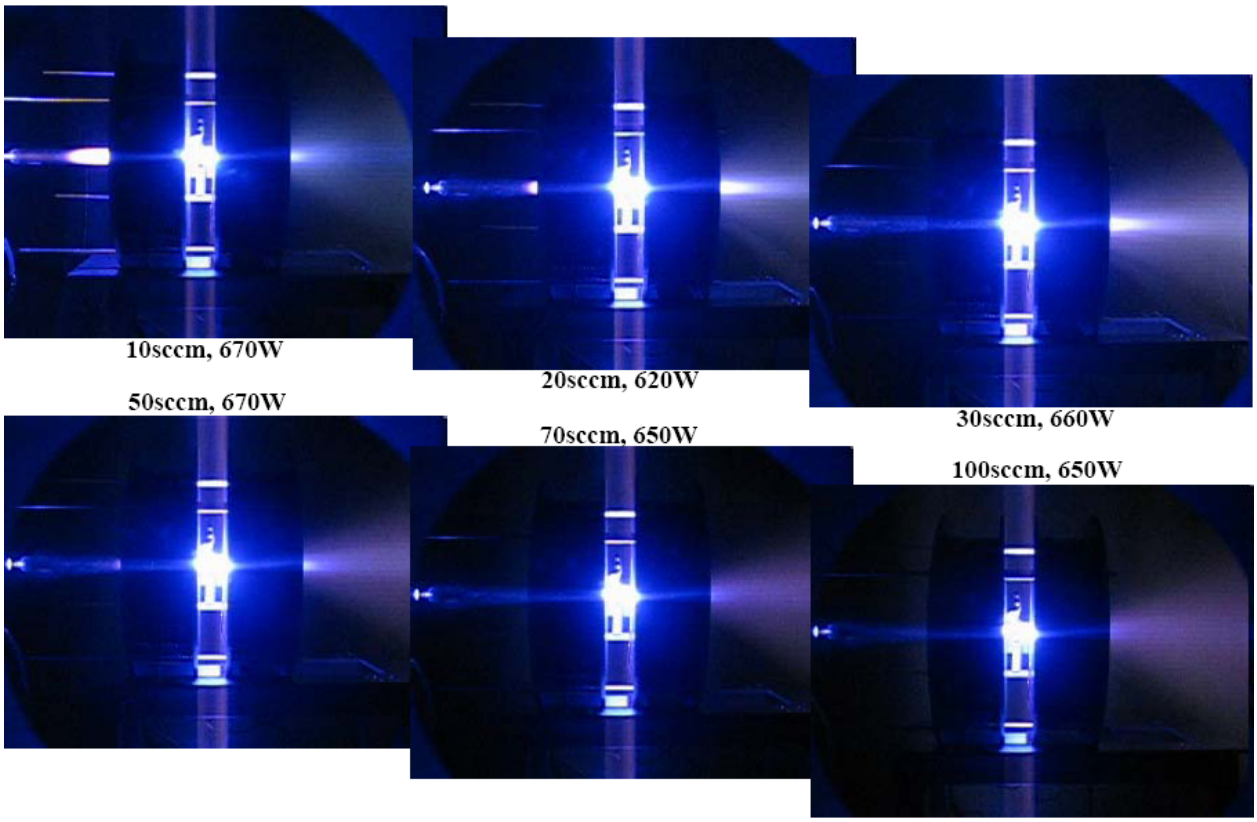

Figure 22: Consecutive photos of a steady-state helicon discharge with different flow rates of argon, but approximately similar conditions otherwise

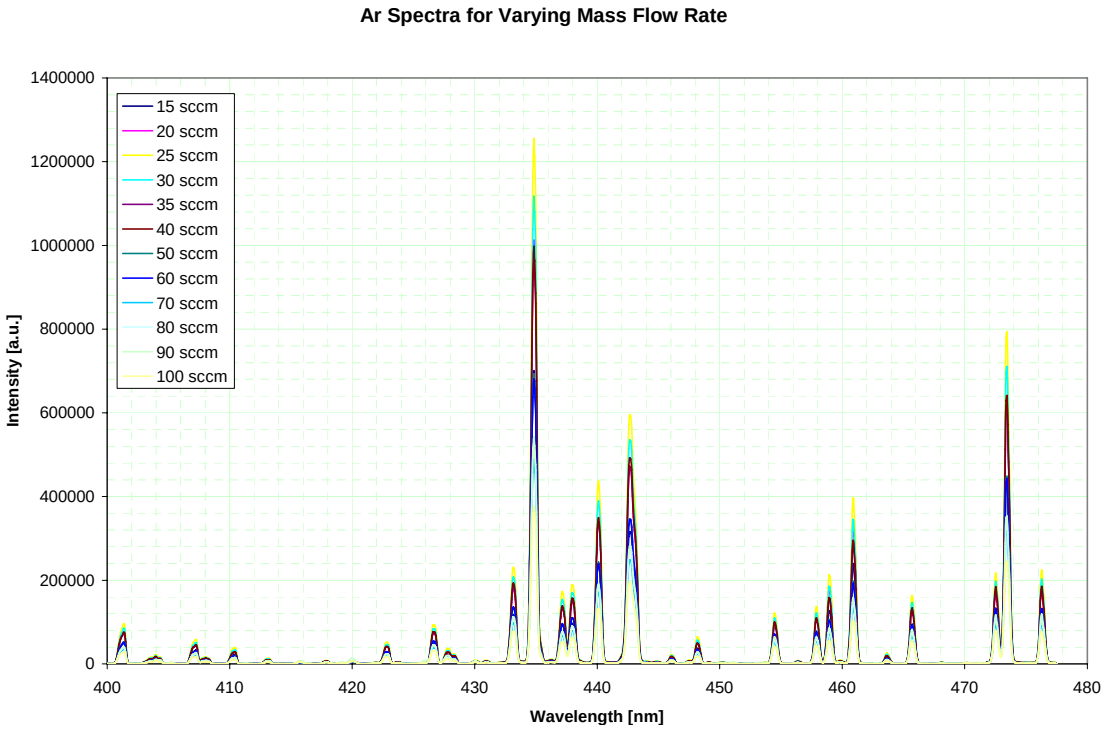

Figure 23: Ionic spectra for 10-100sccm mass flow scan

Visual observation is confirmed with spectroscopic measurements given in Fig. 23. The ionic line intensity goes up and then down for the same temporal exposure. Because no neutral lines appear, we may say that most of the puffed gas is ionized. The intensity must scale roughly as:

$$I \sim R(T_e)n_p^2 \sim K(T_e)\dot{\mu}^2 \qquad (8)$$

Since the flow rate is monotonic, the non-monotonic emission behavior indicates that the electron temperature (or mean energy in the RF-wave) is changing drastically. To quantify spectral measurements it is sufficient to look at one single ionic line. In Fig. 24a the prominent 434.8nm line is zoomed. The second pane, Fig. 24b, presents maximum of the line intensity for different gas flows. Note that width of the line is purely instrumental in this case, the same for all flow rates.

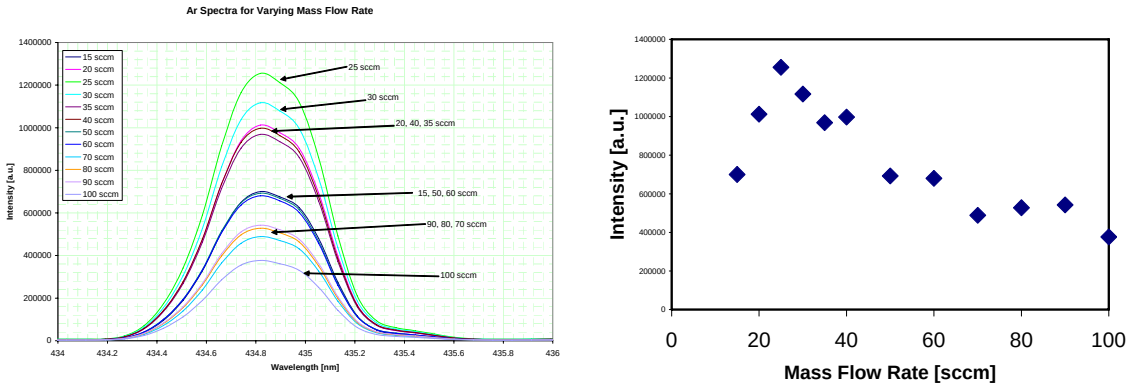

(a) (b)

Figure 24: (a) – zoomed 434nm region, (b) – peak intensity vs flow rate

It is possible to try extracting more data from the peak intensity dependence on flow rate, but with temperature and flow velocity variations this becomes speculative. What one can only affirm that the mean electron temperate drops after maximum emission is reached at $\dot{\mu} \approx 25 sccm$.

Due to the observed fact of complete gas ionization at the highest $\dot{\mu} = 100 sccm$ with $P_{RF} = 650W$ RF-power applied, one gets the cost of ionization to be $I \approx 90eV$. Assuming ~25eV exhaust ion velocity, beam efficiency is roughly $\eta \approx 25 - 30\%$.

6.2.5 Power and magnetic field scans

Scans of varied applied power and magnetic field were made as well. A similar simple spectroscopic analysis was performed by looking into a single ionic line emission. In these scans gas flow was fixed at 25sccm. In the first scan power was varied in the 400-1200W range with fixed I=30A in both electromagnets. In the second scan, the current was varied in the 10-35A range. For the low currents and powers helicon mode was impossible to achieve.

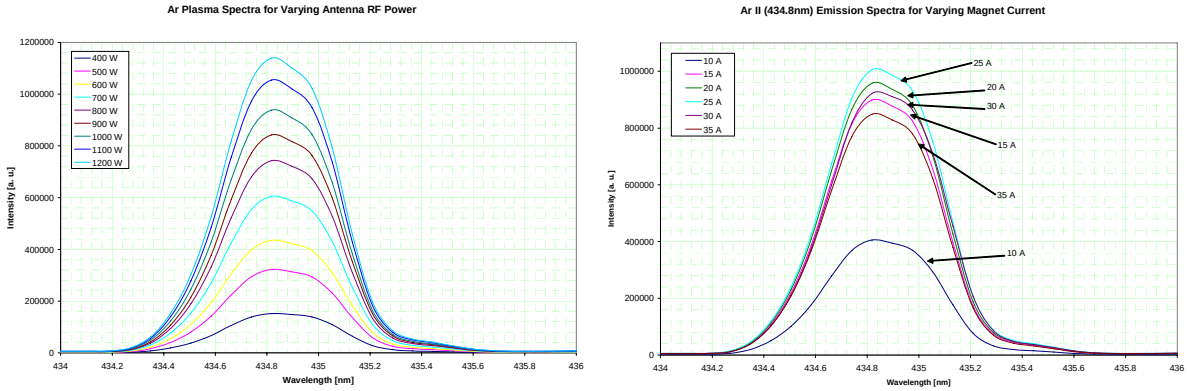

(a) (b)

Figure 25: (a) – ionic line for the power scan;
(b) – the same for magnetic field (electric current) scan

Similarly, the mass flow scan peak of the spectral line is used to quantify the discharge dependence on parameter, as summarized in Fig. 26 for both scans. Power scan gives near-linear dependence without saturation. For the complete gas ionization this indicates that electron temperature is monotonically increasing with power. Part of the energy is being converted into the exhaust beam. Magnetic field scan shows a wide peak of efficient helicon mode excitation with maximum at ~1300G which is remarkably close to the lower-hybrid resonance of single Ar^+ ions at 13.56MHz frequency (see Table 1).

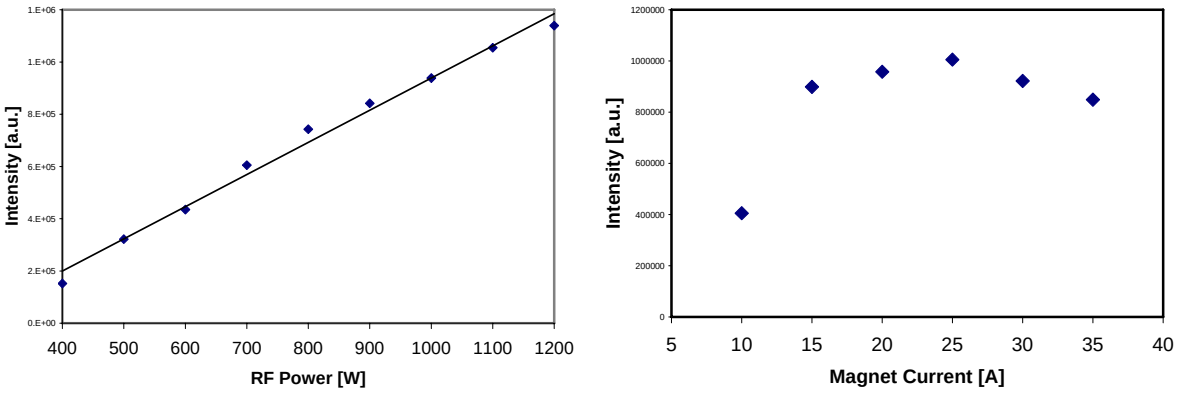

(a) (b)

Figure 26: (a) – ionic line for the power scan;
(b) – the same for magnetic field (electric current) scan

6.2.6 Different observation window ports and views

Portable spectroscopic system allows viewing from the side window (Fig.27a) at different discharge regions, even at an angle across the plume (Fig.27b). Back window (also 8") allows collecting emitted light by looking upstream, directly into the accelerated plasma beam (Fig. 27c) including/excluding discharge region.

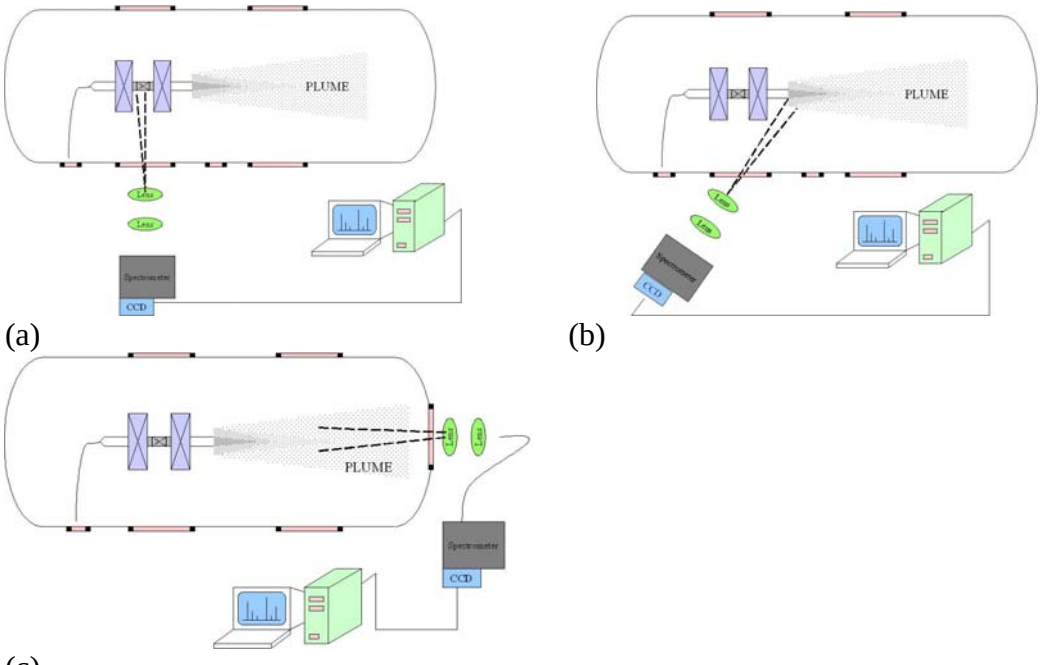

(a) (b)

(c)

Figure 27: (a) – side window mount of the portable optical table allowing looking into the discharge region; or by tilting (b) – across the plume exhaust;
(c) – back window mount allows looking directly into the accelerated plasma beam

6.2.7 Plume vs. discharge region

In the helicon mode there is a bright plume formed. Side window mount allows collecting light from the plume region at longer (seconds) exposures and comparing them to the antenna - discharge region spectra. The discharge region is very bright, and millisecond exposures are required to saturate the CCD. In Fig. 28 calibrated spectra for two regions are presented for comparison. All significant lines are ionic ArII emissions. No neutral lines are detectable. This means that most of the gas is ionized before reaching antenna (and plume). Another very important outcome is that the relative ratio of different lines is preserved within each spectrum and between the two. This fact suggests that the exciting electron energies are roughly the same in both of these regions.

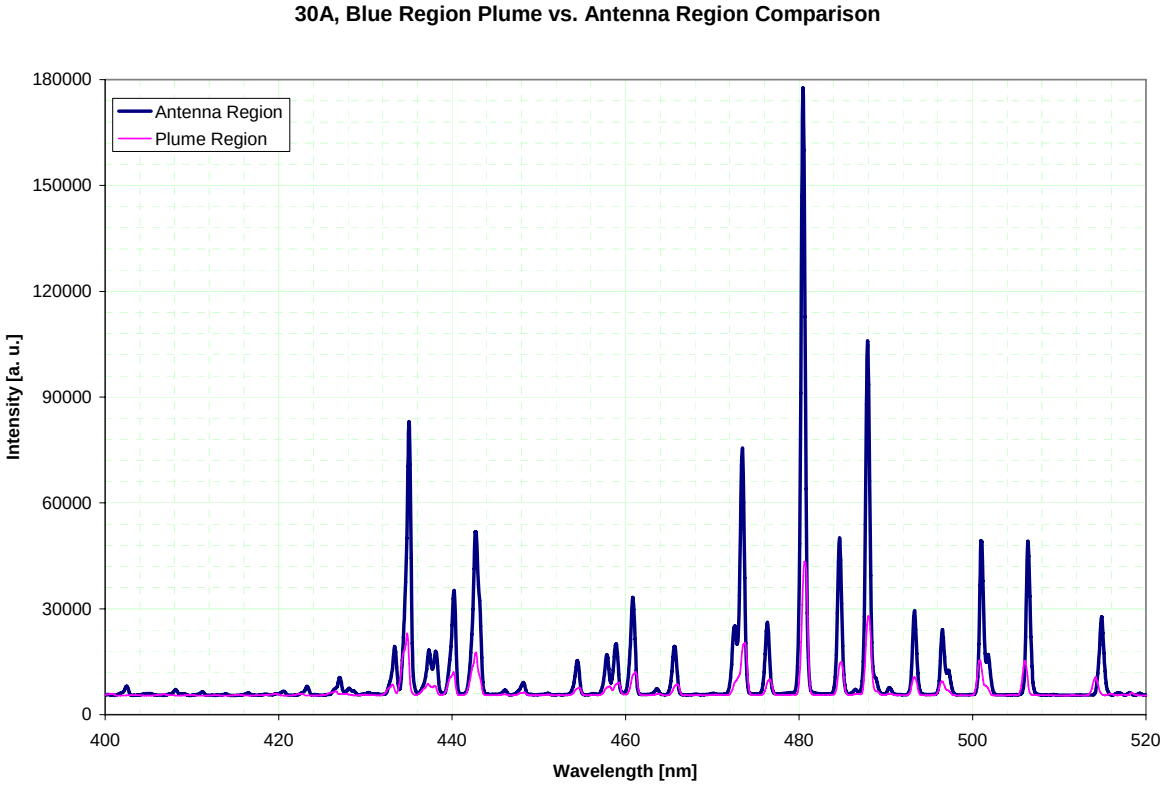

Figure 28: 400-520nm ionic spectrum of the discharge vs plume region is showing the same lines and the same line-to-line peak ratio

6.2.8 Discharge region: side vs. back ports

Next we compare side and back port mounts, namely Fig. 27a and Fig. 27b setups. The most striking observation is that the back window captures bright neutral ArI lines: 415.859, 420.9674, 419.8317, 425.9362, 430.0101nm and some others, while they are almost undetectable in the spectrum taken from the side window (Fig. 29). This strongly confirms the fact that all gas ionization happens in the region upstream from the antenna. Combining this with the observation of a very dark region near the gas inlet and also visible sharp boundary of shining plasma one may conclude that the ionization region is probably a couple of centimeters wide.

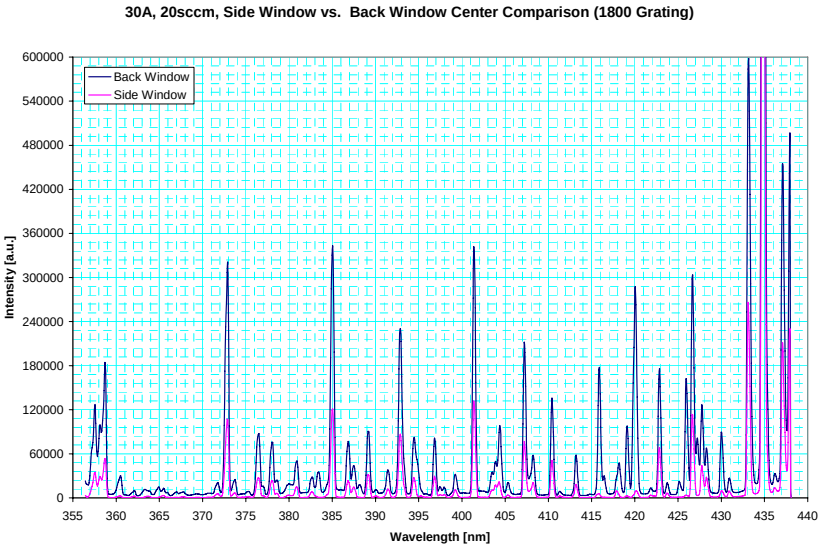

Figure 29: 355-440nm spectra of the discharge region taken from the side and back window ports

6.2.9 Antenna length and material

The original M=1 symmetrical helicon antenna was ~10cm long. It was designed to excite electrons to ~20eV energies for optimum ionization. A second antenna was built of the same exact copper tube, but was ~14cm long, accordingly driving electrons to ~40eV. Another antenna was similar to the original, but made of stainless steel. Both new antennas are shown in Fig. 30 side-by-side.

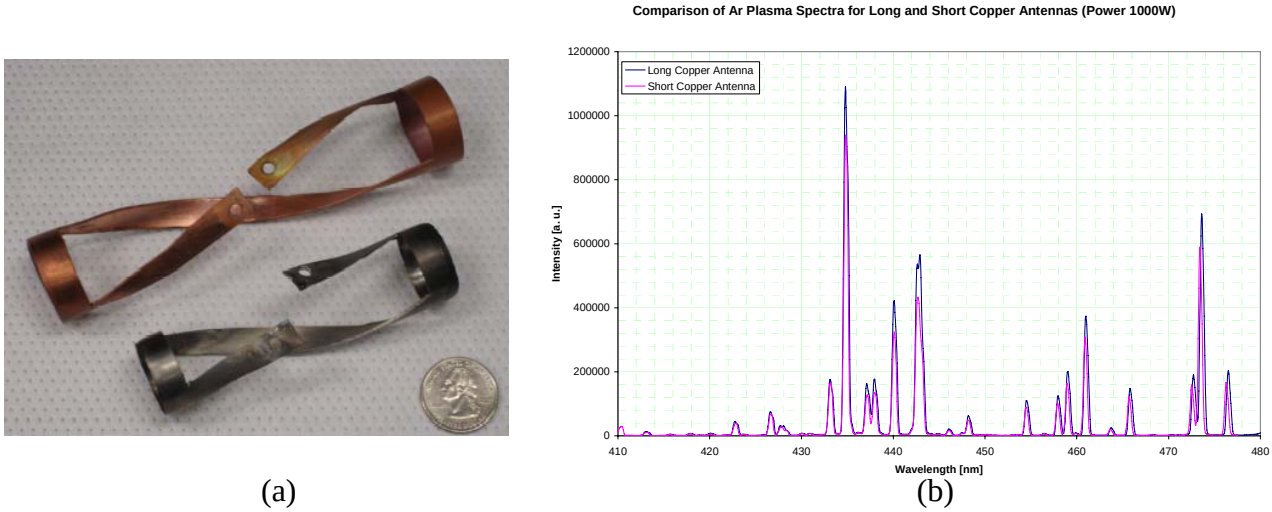

Figure 30: (a) – 14cm copper and 10cm stainless antennae;
(b) – 450nm spectra of the discharges operating with short and long Cu antennas

Longer Cu antenna delivers brighter emission vs short Cu for the same discharge parameters – fields, input powers and gas mass flows. It may deliver a slightly better ~20% coupling of RF to plasma. Short Fe antenna delivered ~30% less power into discharge compared to the short Cu

antenna, which might be due to poor electrical contact between the two metals at the bolted junction and/or due to differential expansion at the joints during operation when the antennae normally heat to high temperatures, >200C.

6.3 Different antenna designs

In addition to the classical double-twist antenna we tried two other antenna designs during 2006 campaign: “Flat” and “Braided.” They are shown in Fig. 31 as installed between the magnets.

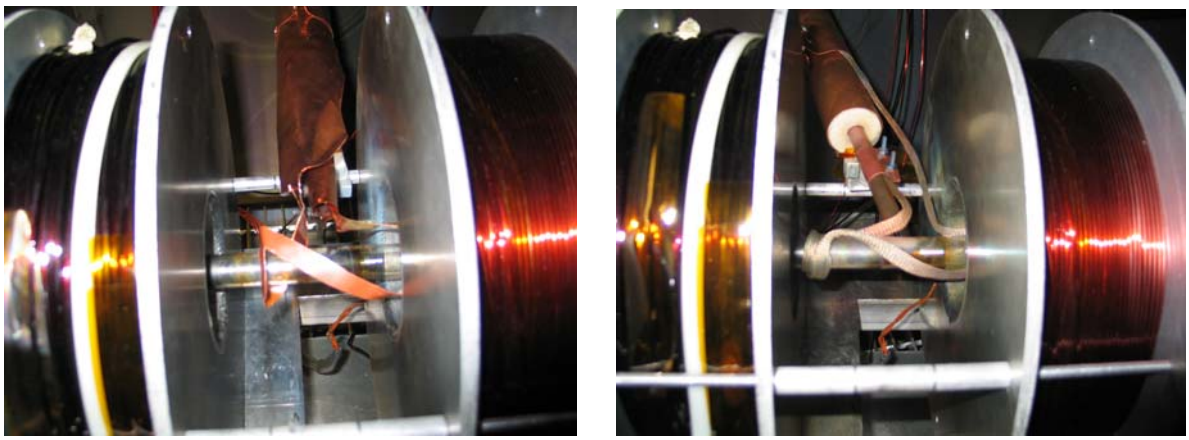

(a) (b)

Figure 31: (a) MIT flat type antenna, and (b) – MIT braided type helicon antenna

Both these antennas are very inexpensive and utilize the fact that current flows in the skin layer. Braided antenna allows easy optimization study.

Examples of operation using three types of antennas are presented in Fig. 32. We have selected the discharges with the most developed plumes. There is no other way of comparing discharges other than by the plume’s length to the diameter, which is the same 2cm for all cases. In all discharges maximal 1.2kW RF power was delivered to the antenna and the flow rate was optimal at ~25sccm of argon gas. Plasma beam appears to be more collimated with new flat and braided antennas.

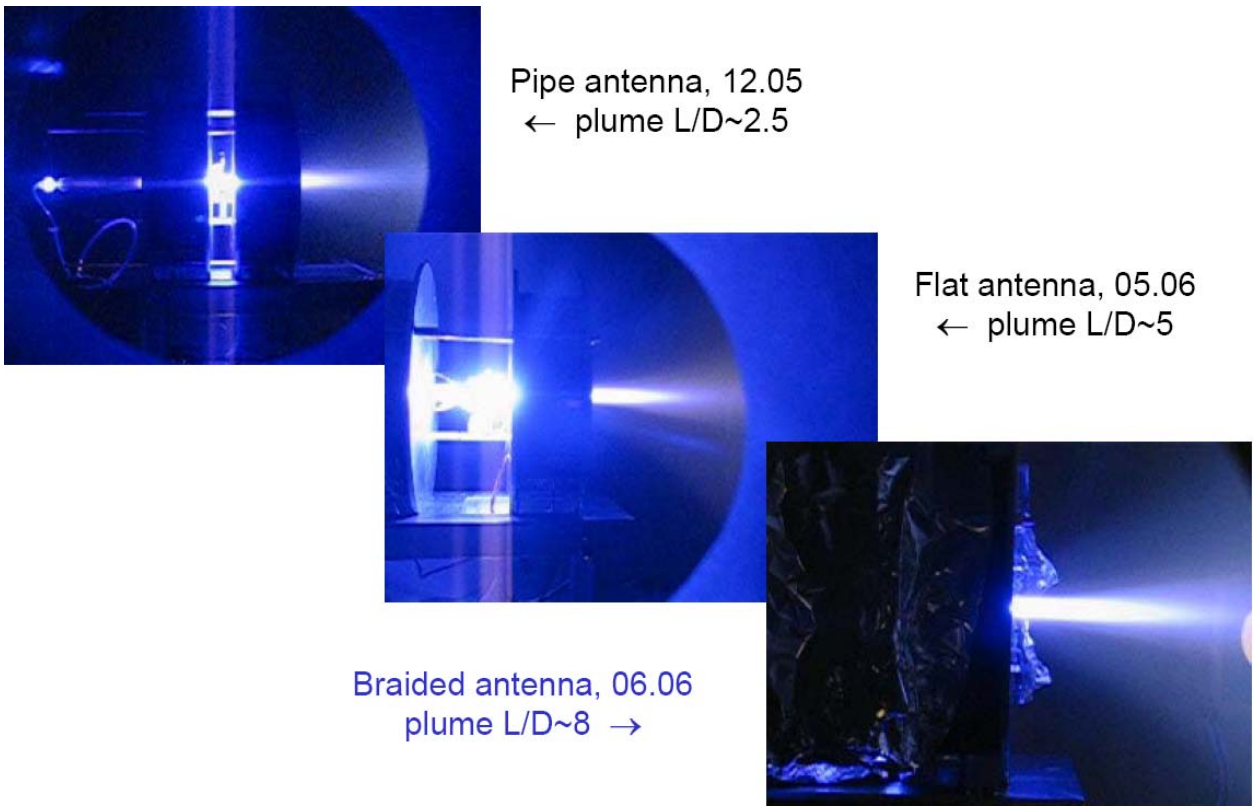

Figure 32: Helicon discharge as obtained with 3 different antennas, left-to-right: M=1 pipe, flat and braided. Plume's length to diameter ratio is shown for each

6.4 Single magnet operation with different propellants

At some point during 2006 campaign of measurements we realized that single magnet operation looks more interesting both from the engineering-propulsion and physics points of view. It is not only simpler, but also demonstrated better performance.

Another venue was to study a range of propellants: different noble gases as neon, argon, krypton, xenon, diatomic nitrogen gas, and different mixtures. We performed test runs using argon-nitrogen mixture, continuous from 100:0% to 0:100%. The same was done for Xe-Ar mixture, and for pure gases we used: Ar, N_2, Ne, Xe

6.5 Operation with N_2

The configuration was: MIT type-F antenna, single magnet #1, nitrogen puffed at 25sccm into the standard ID 2cm×40cm long quartz tube. During the magnetic field scan we increased current in the 0-30A range with 5A increments. The system did not require much matching. Full ~1200W of RF power was delivered to the antenna for each field.

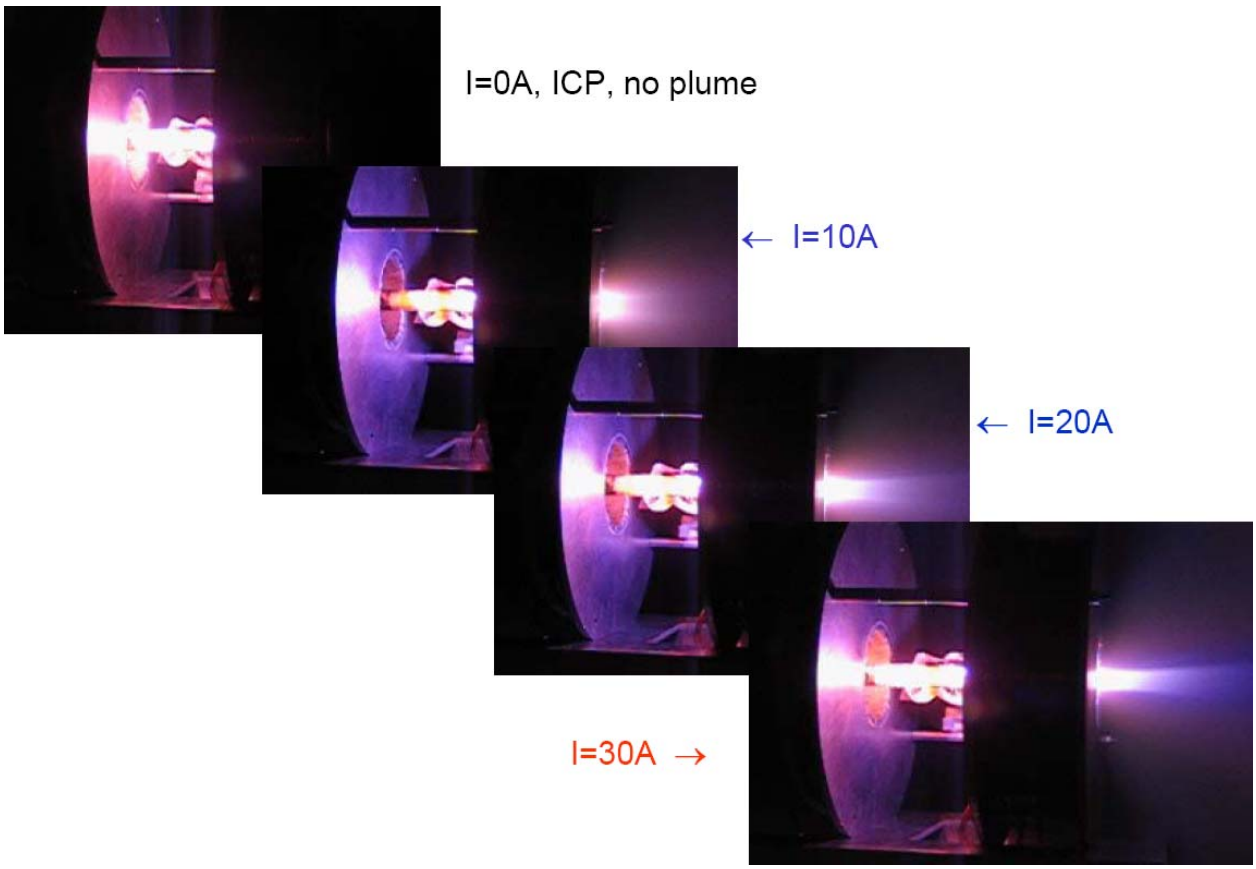

Figure 33: Stable helicon discharge in Nitrogen with different magnetic field strengths

A side window view of the experiment for different electromagnet currents is shown in Fig. 33. As one can see, a progressively larger well-defined plasma plume was formed. As the magnetic field was cranked up, the color of discharge changed from reddish (ICP mode) to more bluish (Helicon mode), which is presumably more ionic. The bright ionized region moves to the right, towards the orifice, forming eventually a plume. It is difficult to say what the composition of the plasma products was, as we saw both molecular bands and atomic/ionic lines, which were difficult to identify.

One suggestion comes from the fact that it was easier to sustain discharge at low B~500-800G than at higher fields. At I~25-35A it was impossible to start discharge at all. We had to initiate it at I~5-10A then raise the current to higher values. At I>30A it was impossible to sustain the discharge at all. Table 1 gives ~777G as a LH frequency for atomic nitrogen N^+. A molecular ion N_2^+ would have resonance at ~1100Gs. It would more probably immediately dissociate in the electron plasma with 10-20eV electrons. Thus, it is very likely that the plume in Fig. 33 is composed of predominantly NII ionic species

6.6 Operation with Ne, Ar and Xe

We performed episodic operation with neon and xenon gases. It was possible to couple ~1kW of RF power to plasma in different configurations, in both ICP and Helicon modes. Some of the examples are shown in Fig. 34. The mass flow rates were 15 seem (Ne), 25 sccm (Ar), 30 sccm (Xe) and 20 sccm (Ne).

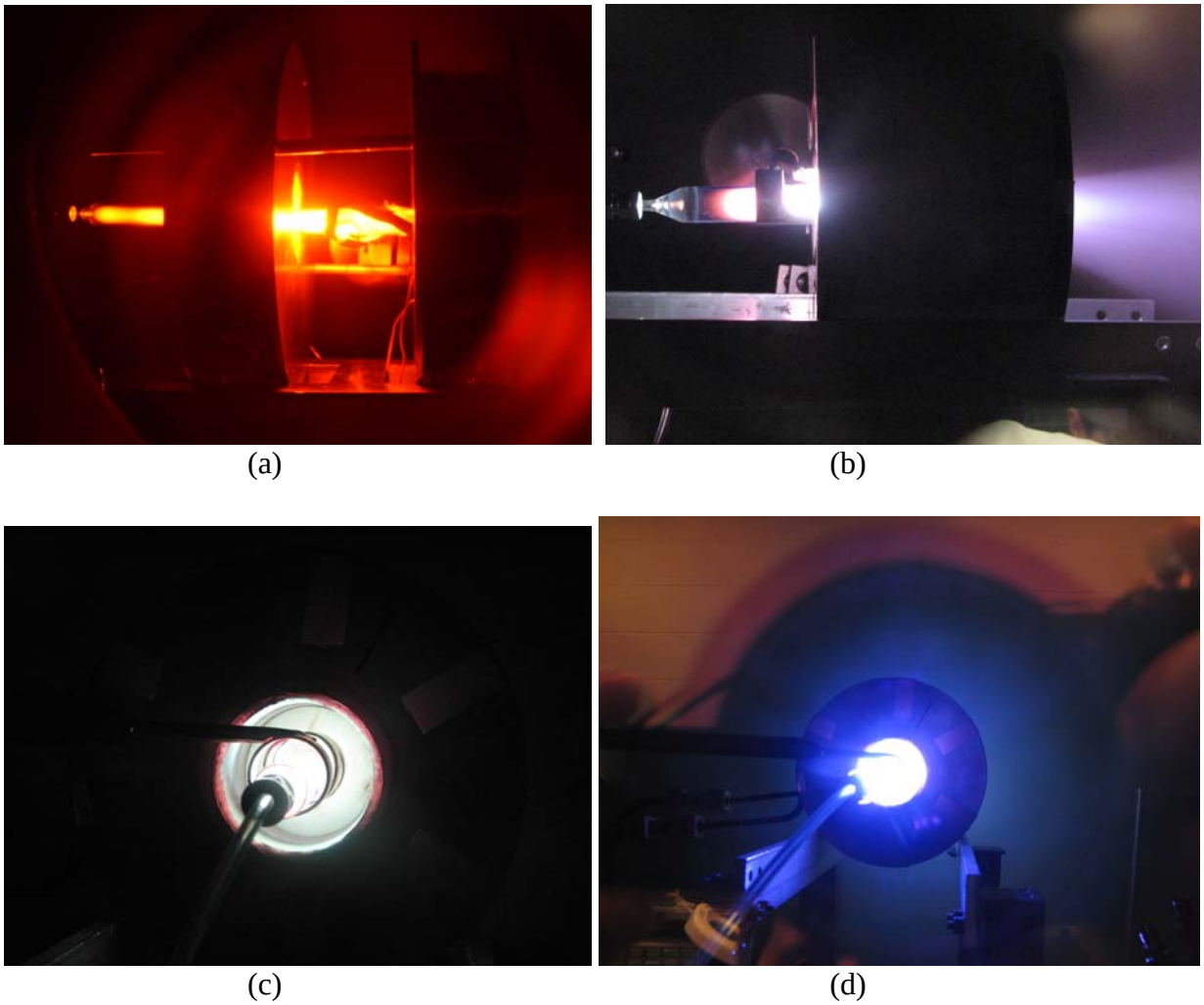

(a) (b)

(c) (d)

Figure 34: (a,b) - ICP discharge with neon and helicon mode with xenon, (c,d) - back view of the xenon and argon discharges

6.7 Operation with gas mixtures

We run helicon on air, on Ar-N_2 and Ar-Xe mixture as a transient. It was always possible to deliver 1kW of RF power with 0W reflected to the RF-source in each case and for any ratio of gases in the mix. A continuous matching network tuning was required to minimize the reflected power. Some of the illustrations for operation with mixtures are presented in Fig.35.

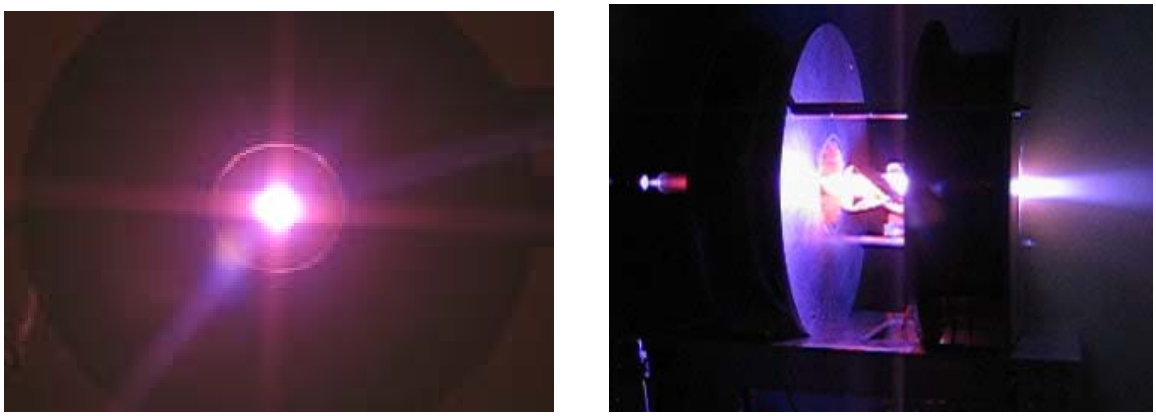

(a) (b)

Figure 35: (a) back window view of the helicon mode on air; (b) – helicon mode running on the 70%N_2 : 30%Ar mixture

7. USE OF PERMANENT MAGNETS

Permanent rare-earth magnets can deliver B~1T near the surface, which is sufficient for helicon studies. High-T SaCo magnets can operate at higher temperatures to ~500°C. We are using cheaper NdFeB magnets for initial studies; the maximum operational T for sh38h material is 150°C, which is sufficient. One of the first uses was to form a magnetic cusp to prevent plasma from flowing back to the gas inlet, Fig. 36.

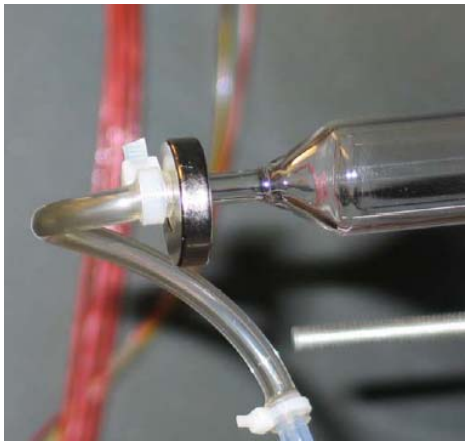

Figure 36: Small NdFeB magnet forming a cusp

7.1 All-permanent magnet setup

As a proof of principle two permanent ring n42 magnets were installed at two sides of the helical antenna, see Fig. 37a. The magnets were under 1cm thick. We were able to deliver ~800W of RF power for the ~20sccm argon gas flow. A hybrid mode was formed with a plume. We also ran a 3-magnet configuration shown in Fig. 37c. After running for ~10 minus we lost permanent magnet #2. It lost magnetization completely. The maximum working T for n42 material is 80°C. The other magnets did not lose their magnetization.

(a) (b) (c)

Figure 37: (a) – two small ring magnets installed in parallel and attached to the quartz tube; (b) – back view of the discharge, (c) – 3-magnet system running on 20sccm Ar flow

7.2 Magnetic nozzle experiment

As a matter of fact we have tested a magnetic nozzle configuration, which was created by a permanent magnet attached to the very end of the quartz tube in the 3-magnet configuration.

The effect on the flow is very profound, as can be seen from Fig. 38. Possibly, a double layer is formed, and plasma flow experiences additional acceleration, which is potentially beneficial for space propulsion applications.

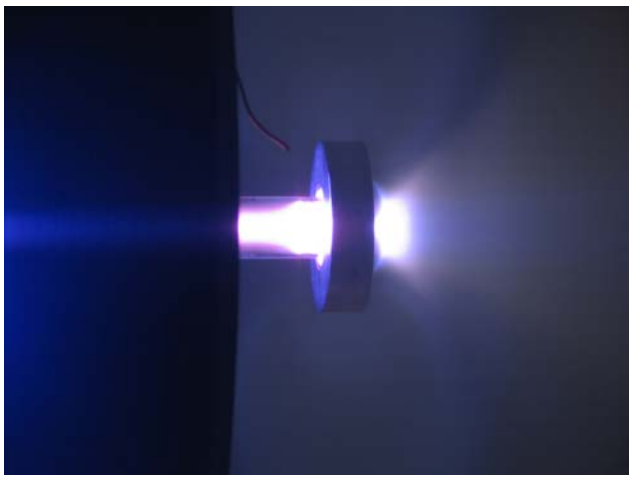

Figure 38: Magnetic nozzle formed in the mHTX all-permanent magnet experimental setup

8. MECHANISM OF PLASMA ACCELERATION

A simple analysis of ambipolar acceleration can be done by assuming that the electrons in the discharge are isothermal, with $T_e \approx 6-10eV$ in the helicon mode. In the steady-state regime pressure gradient of the electrons is balanced by electrostatic pull:

$$en_p E_A = \nabla P \approx kT_e \nabla n_p \tag{8}$$

Axial drop in the electrostatic potential can be easily integrated:

$$\Delta\Phi = \int_A^B E_A dz \propto T_e \ln \frac{n_p^A}{n_p^B} \tag{9}$$

If plasma expands and density drops by 1-2 orders of magnitude, one may expect a sizable ambipolar potential built-up to $\Delta\Phi \approx 3-5T \approx 20-50V$. This will accelerate plasma flow to a significant $I_{sp} \approx 1-4K\sec$. Increase of T_e and density variation by proper discharge tuning and magnetic field shaping is very possible. Double and triple ionization states presence (Table 1) may further increase flow velocity.

9. RESULTS FROM THE FIRST HALF OF 2007

During reported period mini-Helicon Thruster Experiment (mHTX) at MIT was redesigned to achieve more flexibility, gain performance and better discharge characterization. Improvements are based on experimental data accumulated during previous campaign.

9.1 Hardware development

9.1.1 Magnets

Two new high-current (>200A) compact 2-gauge square-cross-section high temperature (>200C) coated copper wire magnets were designed, built and tested.

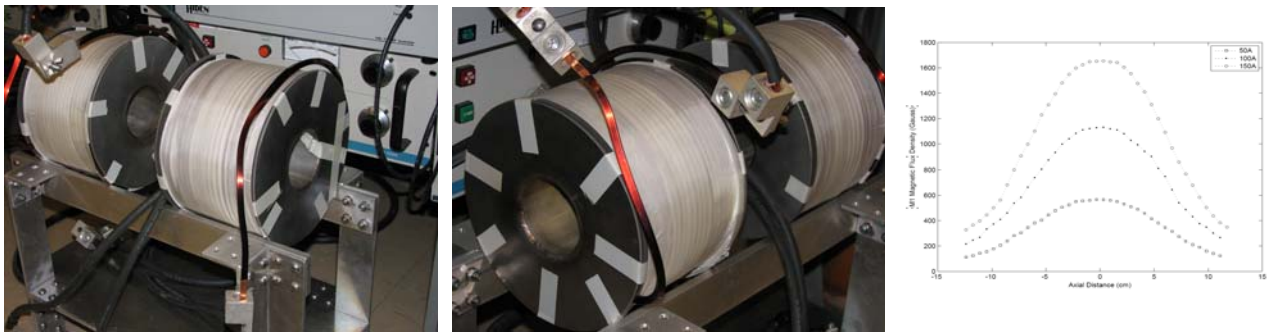

(a) (b)

Fig. 39: (a) new high-current compact copper magnets assembled on the stand; (b) B-profile

A magnetic field scan was performed using borrowed gauss-meter, and B-I curves documented. Magnets deliver continuous B~0.2T for ~15 minutes inside vacuum tank with passive cooling, which is a sizable improvement. Power consumption is reduced by ~40% compared to old high-voltage thin wire magnets.

9.1.2 High-current power supplies and high-current vacuum feedthrough

Two economical, rack-mountable, high current (~200A) low voltage (0-6V) power supplies by Agilent were acquired and integrated into mHTX control system. A 4-pole high-current (~200A steady) vacuum feedthrough was installed and leak-tested.

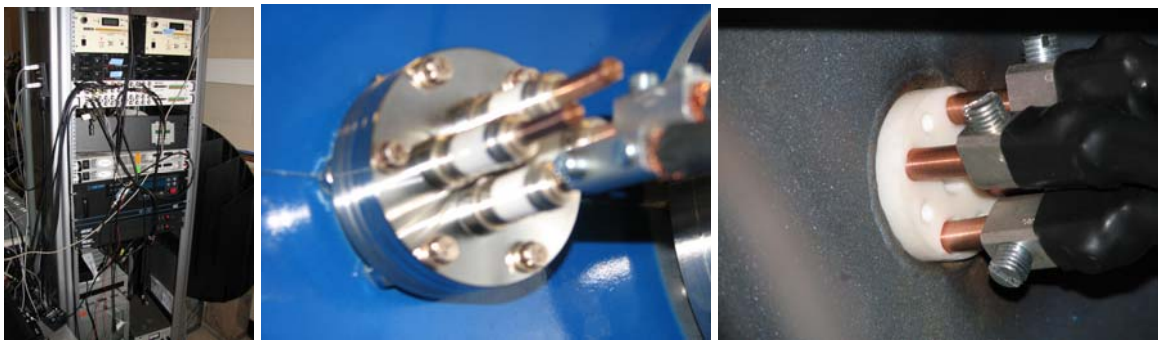

(a) (b) (c)

Fig. 40: (a) - high-current power supplies on a system rack, (b) – lab side of the high-current feed through, (c) – vacuum side of the feed-through

9.1.3 RF-delivery system

This system was redesigned completely based on our Year-2006 experimental campaign. The CAD drawing of the new design showing external connector, vacuum connector, vacuum coaxial feed and antenna are given in Fig. 41a. The same elements machined are shown in Fig. 41b.

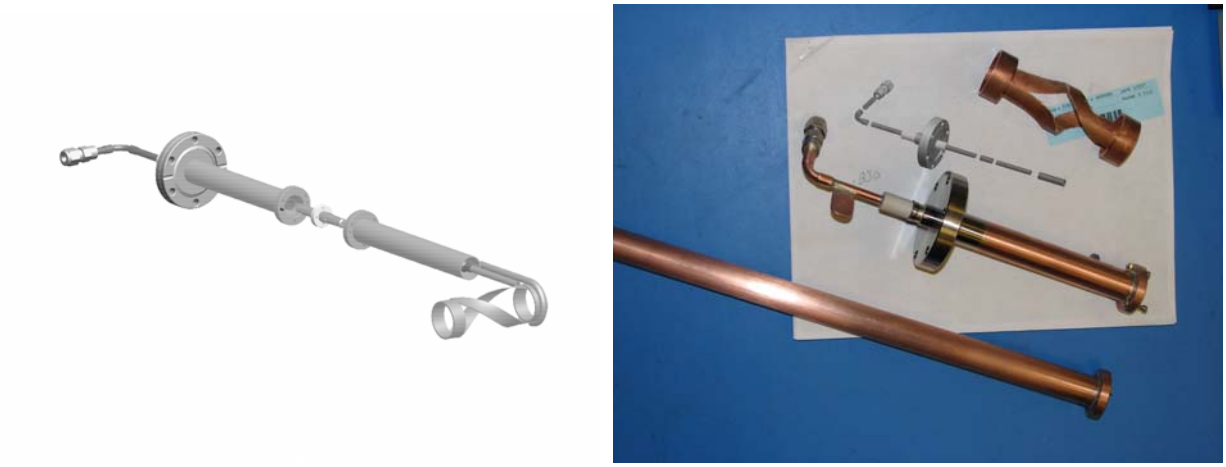

(a) (b)

Fig. 41: (a) - CAD rendering of RF-delivery network, and (b) – machined pieces

9.1.4 RF-matching network

Matching network was redesigned and rebuilt using last-year experience. Matching network is essential for RF-power delivery to the helicon antenna, not to multiple elements of the RF-delivery system. Plasma impedance changes in a wide range during discharge initiation and operation, and fine tuning is required to gain efficiency. A new vacuum 10kW RF feedthrough and a new vacuum capacitor have been installed, along with RF current sensor (green coil in Fig. 42), allowing network characterization. The entire box was rebuilt using non-electroplated aluminum to eliminate surface leaks. The box attachment to the vacuum tank was redesigned as shown in Fig. 42.

Fig. 42: Re-designed matching network box mounted to the 8-inch window vacuum port next to new high-I feedthrough. New 2.75" RF- vacuum feedthrough is attached to the window flange together with the box to eliminate leaks

The matching network box with attached RF-delivery system and antenna was characterized using MIT EED's 0-100MHz network analyzer, confirming improved (~5x) tuning ability.

9.2 Advanced *0.01A* spectroscopy system

A new 750mm spectrometer was equipped with three sensors shown in Fig. 43:

- UV-rated photo-multiplier tube (PMT);
- UV-rated, super-sensitive CoolSNAP$_{K4}$ camera (one in existence) with very small 7.4μm square unmasked pixel of the 2K×2K CCD array;
- 255-1000nm CoolSNAP$_{cf2}$ camera with super-small 4.65μm square pixel size, 1320x1040 imaging array.

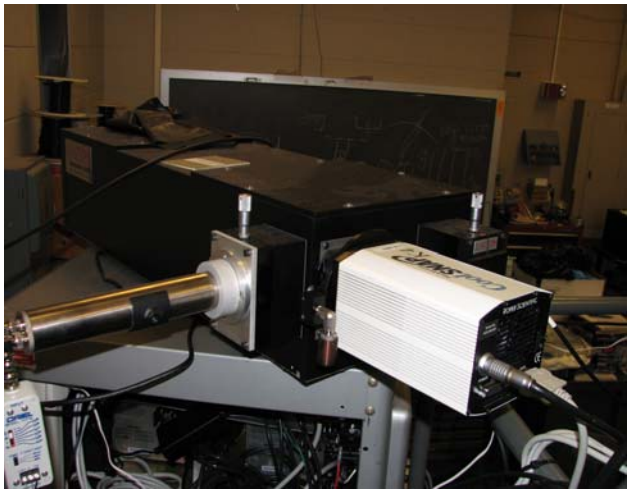

(a)

(b)

Fig. 43: Nitrogen-purged 75cm Acton 750i spectrometer with PMT attached to the side exit port and UV-rated CCD camera attached to the frontal exit port. Behind CCD a frontal exit port with tunable 1μm input slit and a multi-fiber barrel-ended 180nm-rated optical cable are shown. A separate picture presents imaging camera with ultra-small pixel size and good quantum efficiency

In the absence of plasma in January-May we have tested spectrometer using Hg-Ar OceanOptics calibration source. The results for prominent 313.1555nm and 313.1844nm UVA HgI lines are shown in Fig. 44. Using finest holographic 3600g/mm grating, the observed pixel-to-pixel resolution was ~0.0013nm and ~0.002nm, respectively for imaging and spectral CCD, respectively. This translates into ~0.01A/pixel resolution at the highest ~450nm wavelength allowed for 3600g/mm, and ~0.02A/pixel for the 1800g/mm at its maximum λ~850nm.

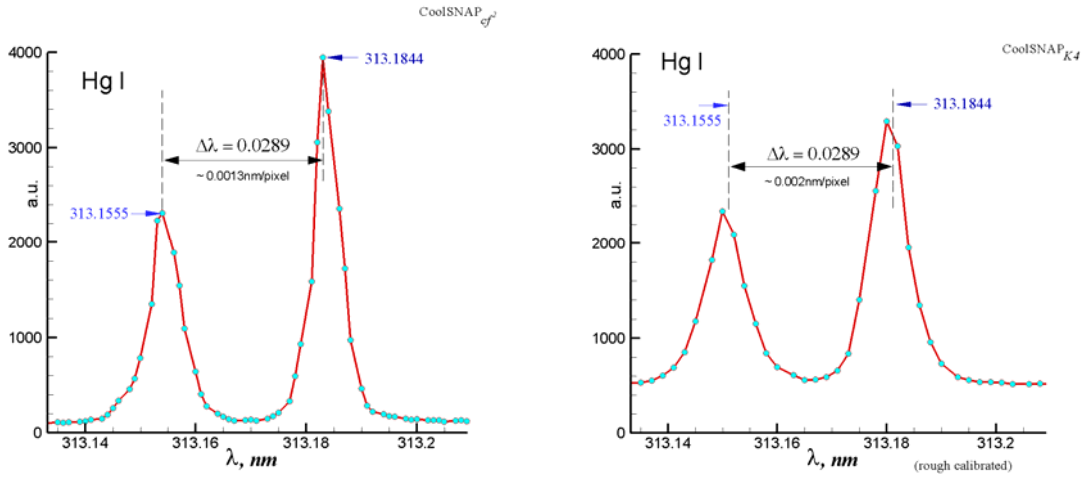

(a) (b)

Fig. 44: Atomic Hg spectrum at 313nm. Left pane (a) is taken by CoolSNAP$_{cf2}$ with 4.65μm square pixel and micro-lens installed; (b) by CoolSNAP$_{K4}$ with 7.4μm pixel size and removed micro-lens (unmasked)

9.2.1 Portable spectroscopic system

Originally, the Acton 750i spectrometer through USB connector and CCD camera – through PCI card were connected to the main mHTX control PC. This did not allow controlling experiment and collecting spectroscopic data at the same time, not to mention frequent conflicts of proprietary software supplied by different digital controller manufacturers.

As a solution we installed spectroscopic WinSpec software on existing Lab notebook. The 2-port Magma CardBus-to-PCI port extension was acquired and the CCD controller cards installed within port extension box. This setup (Fig. 45) together with calibration source and spectrometer are placed on a wheeled table and can be easily moved to any location.

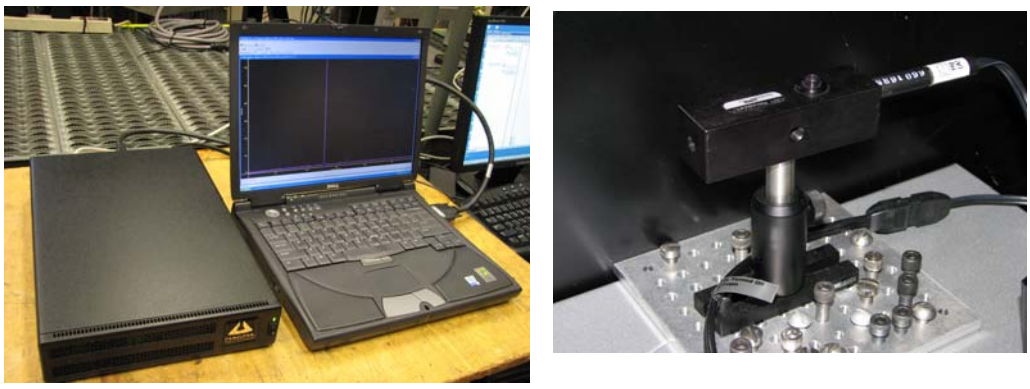

(a) (b)

Fig. 45: (a) PCMCIA-to-PCI extension system by Magma connected to a designated spectroscopy notebook - its screen is showing measured prominent 434.8064nm ionic ArII line of the new mHTX experiment. (b) Shown separately is a portable calibration Hg-Ar light source

9.2.2 Multi-channel UV-rated vacuum light collection system

So far we used mini-optical table that collected light coming from the vacuum tank through the optical window ports. The windows are made of glass that blocks all UV and distorts VIS lines. Moreover, we can collect only directly visible light, which is quite limited due to experimental equipment – magnets, pipes, cables, support structures, etc. To solve this problem new 4-channel UV-rated optical vacuum feed-through was designed and installed at the tank 2.75" port. Four 3m and four 4m-long optical fibers, also UV-rated to 180nm, have been connected at both vacuum and atmospheric ends of the optical feedthrough.

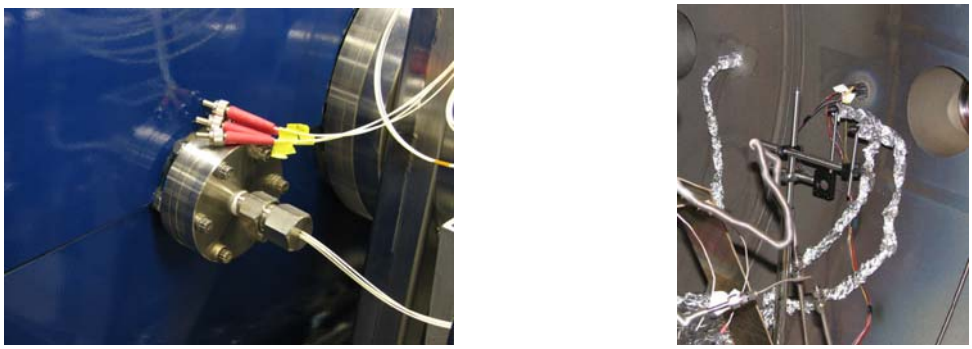

(a) (b)

Fig. 46: Vacuum optical feed-through with 4 UV-rated fibers at the outside, and (right pane) – four 3m optical fibers shielded by foil inside the vacuum tank. Two of the fibers are attached to the mini-focusing lenses (collimators) mounted at the adjustable mechanical arms for accurate light collection

This vacuum UV-VIS collection system was tested using portable light source that produces 253nm Hg I line while installed inside the vacuum tank.

9.2.3 Thermocouple array

Thermocouples were acquired and an array of them was attached to the quartz tube (Fig. 47a). A highly-conductive adhesive epoxy was identified as well as the proper baking procedure. A similar procedure is planned for alumina tubes. A set of different sizes and non-standard tubes have been designed and requested from different vendors.

(a) **(b)**

Fig. 47: (a) - standard 40-cm 2cm ID quartz tube with 5 thermocouples attached using high-conductive high-T (~600C) epoxy, (b) – various non-standard quartz and non-transparent alumina tubes were built for different mHTX experiments

Different size, shape and material tubes are required for power balance and light emission studies, discharge optimization, gas flow investigation, plasma probing and thrust force measurements.

9.2.4 Thrust balance upgrade

Existing old SPL's thrust balance was reequipped with new controller/amplifier given by Draper Labs. The previous setup was tested in early 2007 and showed poor performance. New configuration with x10 enhanced sensor feedback is being tested. It is now equipped with an aluminum platform and a bracket that serves two important goals:

- holds gas tube in place (Fig. 48);
- improves thermal drift by adding extra resistance points.

This is our second attempt to make this old balance useful. If unsuccessful once again, we will switch to a pendulum design: suspending the tube on thin nylon fibers inside the tank.

Fig. 48: Old SPL's 0.1-10mN thrust balance with new controller and a connection platform. Quartz tube is attached to bracket that holds a fused glass flange

9.2.5 Gas flow control

Gas flow controller was affected by RF signal coming from helicon antenna when mounted on the tank, and failed. It was serviced and mounted (Fig. 49) seprately using insulated lines to eliminate electrical contact.

Fig. 49: 0-100sccm gas flow controller is insulated from the electrical ground to eliminate RF-interference

9.2.6 Plasma probes and Retarding Potential Analyzer (RPA)

Several plasma sensors – two-pin Mach probe to measure plasma parameters and flow along magnetic lines, Faraday cup and Langmuir probe have been built. An RPA was designed and assembled as well, but was not tested due to absence of vacuum in January-May. After good vacuum was achieved later in the summer, several measurements using Mach and also Langmuir probes were performed.

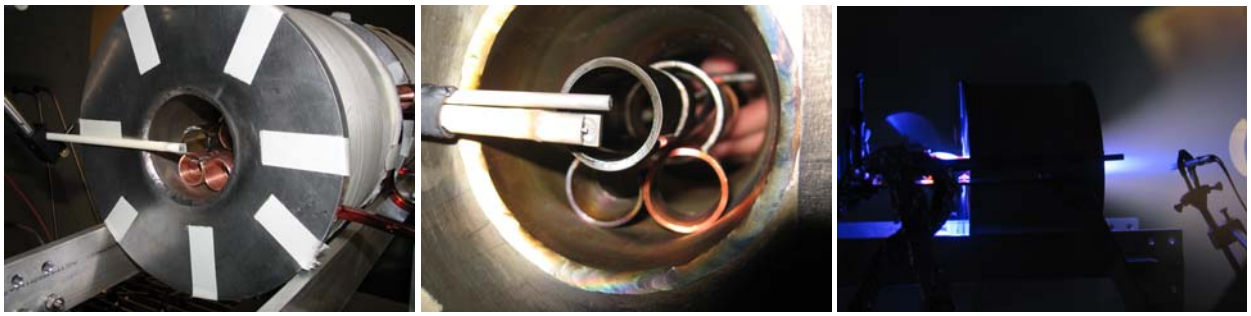

(a) (b) (c)

Fig. 50: (a) – Mach probe installed to intersect the exhaust, (b) – Mach and flat Langmuir probes in parallel, (c) – Mach probe in the plasma plume

After several attempts retarding potential analyzer was completed and used to measure ion energy distributions in the plume ~30-50cm away from the orifice (Fig. 51)

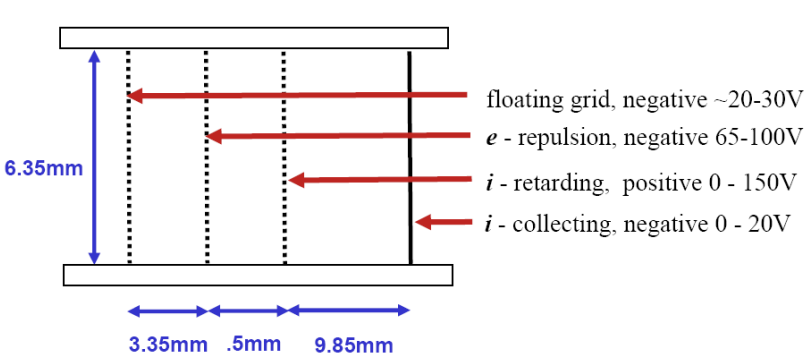

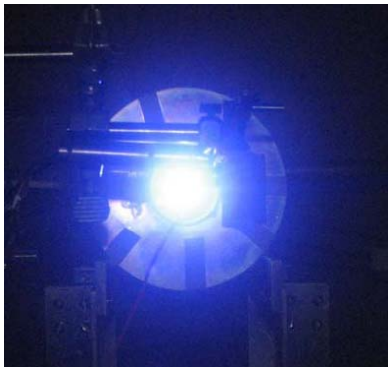

(a) (b)

Fig. 51: (a) - RPA design showing mutual grids position and dimensions,
(b) - RPA installed on an arm inside the vacuum tank and intersecting plasma exhaust plume as seen from the back port window

9.3 Software Development

9.3.1 Control system

The control system was re-coded using LabView software. All major characteristics – gas flow, RF-power in and out, pulse duration, RF-system parameters, magnet currents – magnetic fields, temperatures, etc. are automated, controlled and saved for analysis. Systems – RF, propellant, magnetic - status is displayed in the efficient way as shown in Fig. 52.

Fig. 52: center – mHTX control panel allowing real-time correction of experimental parameters, left & right sides – diagrams of the different sub-systems reflecting their status.

9.3.2 CRM model for Ar

Collisional-radiative model (CRM) for Ar gas discharge was developed to facilitate analysis of spectroscopic measurements. CRM gives a very good agreement for neutral ArI lines, and reasonable for ionic ArII spectrum. [More details are given in Ph.D. Thesis by M.Celik [23].]

9.3.3 Thermal analysis

Heat transport model and code for analysis of the gas tube thermal conditions, required for power balance studies of the mHTX was developed [More details are given in M.S. Thesis by J.Pucci [28].]

9.4 Vacuum System Failure

Vacuum system by Varian consisting of $3m^3$ tank, leak detector, one mechanical and two cryo-pumps, two vacuum gates had a major failure in early 2007. All elements have been serviced, re-installed, re-generated, and tested. Larger OB-400 cryo-pump failed upon 1^{st} rebuilt by MassVac in mid-April and again after 2^{nd} return in mid-May. It was sent back to service for the 3^{rd} time.

We were trying to run pulsed helicon discharged using single operational CT-10 cryo-pump.

9.5 Pulsed Experiments

Because of limited (<1/3 of nominal) pumping capacity we can run steady helicon discharge at low <10sccm Ar flow rates, with uncomfortable high background pressure $\sim 3-4\times10^{-5} torr$. At these conditions RF-power coupled to the plasma is limited to ~500W.

Therefore, we are running pulsed 2-10 sec discharges at 15-20sccm flow rates. We can deliver up to 800-1000W, depending on configuration, but data collection is difficult. The stability of discharge is a problem too as the background pressure builds up in the excess of $10^{-4} torr$ causing direct ionization of ambient gas by the helicon antenna, volume glow and spark discharges inside the vacuum tank.

10. NEW EXPERIMENTAL SETUP

The upgraded experiment was assembled inside $3m^3$ SPL vacuum tank as shown in Fig. 53 for a single-magnet configuration. The same old stand was used, but the top part with slits for larger low-current magnets was removed. New features, visible in photos include:

a) thick high-current magnet cables, attached to new high-current 4-pole feedthrough;
b) new port for the propellant flow with all-insulated gas feed;
c) RF-vacuum feedthrough, which is ending with a flat flange;
d) long attachable coaxial vacuum feed with solid antenna at the end;
e) multi-fiber optical feedthrough with fibers (at the right wall) wrapped in protective foil.

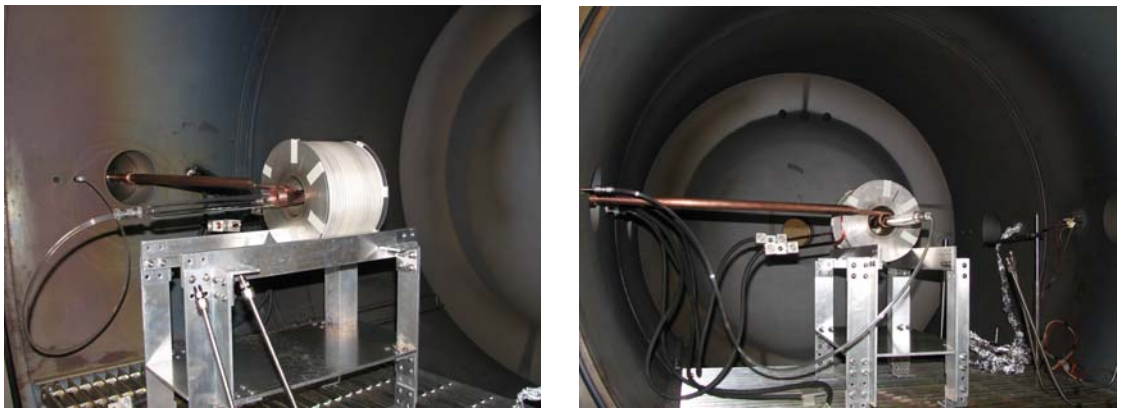

(a) (b)

Fig. 53: (a) – gas, RF and high-current feedthroughs at the left wall of the vacuum tank; (b) – electrical cables and gas feeds, optical vacuum feedthrough with Al shielded fibers coming from the right wall. The quartz tube and helicon antenna are inside the magnet bore, which sits on a stand

The closer look to the helicon antenna region is given in Fig. 54. The most important new features of the RF-delivery system are that i) solid copper is used across, and ii) all connections

are either solid flange or brazed. For instance helicon antenna is solidly brazed to the copper pipe coax vacuum RF transmitting line using silver alloy to eliminate contact loses.

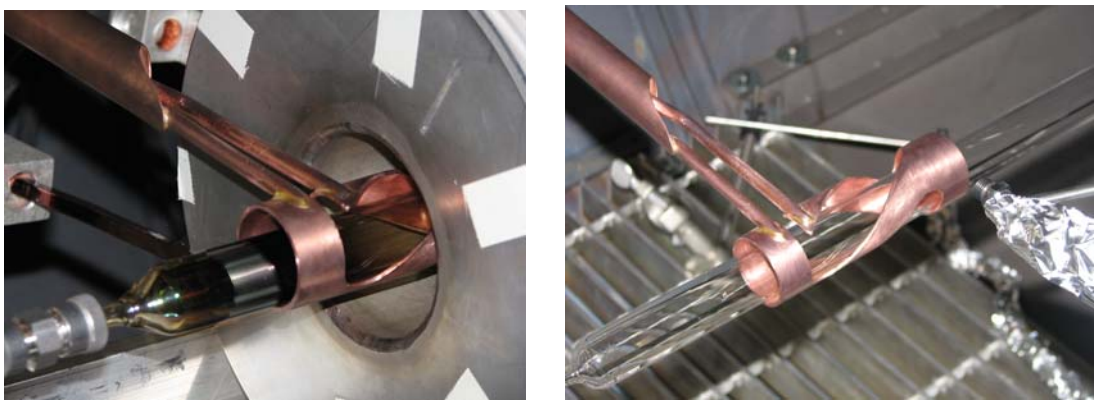

(a) (b)

Fig. 54: (a) – closer look to the helicon antenna – short quartz tube (20cm) region. Golden tone metal at the connecting copper poles - helicon antenna interface is the silver alloy used for solid brazing. Antenna is half-submerged into magnet's bore for optimal coupling. (b) – wider view with electromagnet removed and longer (40cm) gas tube installed. Also visible are two optical fiber ends shielded with foil and equipped at the ends with mini-lenses for precise light collection.

We present below several illustrations of the pulsed Ar gas helicon discharges, which we began running since May 31st, 2007.

10.1 Inductively Coupled Mode

Inductively coupled plasma (ICP) was obtained in configuration shown in Fig. 54b – longer tube and no magnetic field. Gas flow varied in the 10-20sccm range and power in the 200-900W interval. Reflected RF power was small, <10W. The ICP discharge was very bright and stable. As the RF power went up, the color of the discharge switched from purple to blue-purple (Fig. 55), and a diffuse plume formed near the orifice.

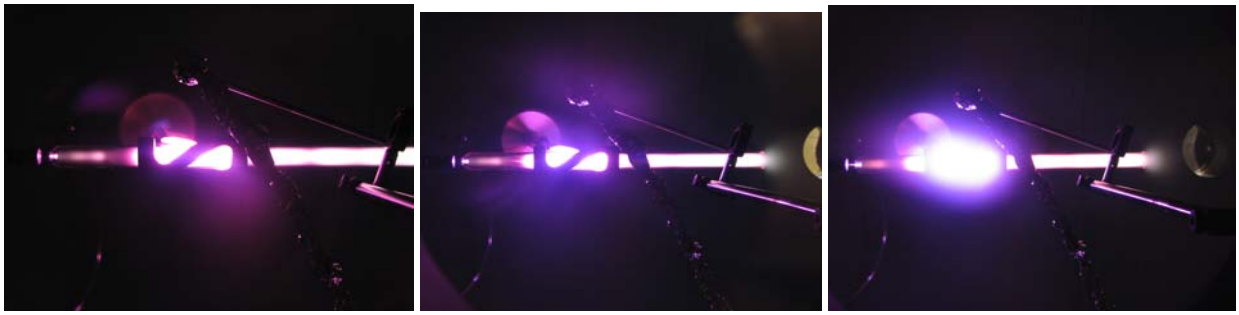

(a) (b) (c)

Fig. 55: Inductively coupled Ar plasma at 15sccm flow rate, applied 13.56MHz RF power Left-to-right: P=300W, P=500W and P=800W

10.2 Helicon Mode

Helicon mode was achieved in two configurations presented in Fig. 56. Both setups are basically the same, but use different - longer and shorter - quartz tubes.

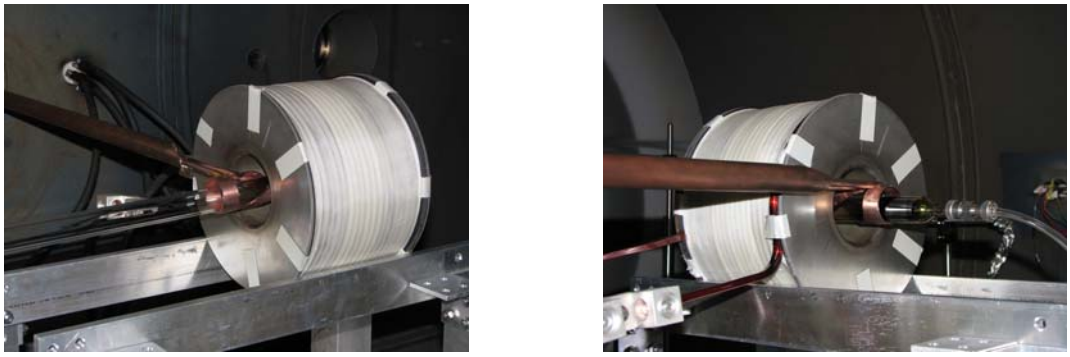

a) b)

Fig. 56: Two single-magnet setups used to achieve helicon mode in Ar: (a) – long 40cm, (b) – short 20cm quartz tube

Several photos presented below in Figs. 57-58 give an impression of the Helicon Ar discharges obtained for different operational conditions with longer (40cm, ID 2cm) quartz tube.

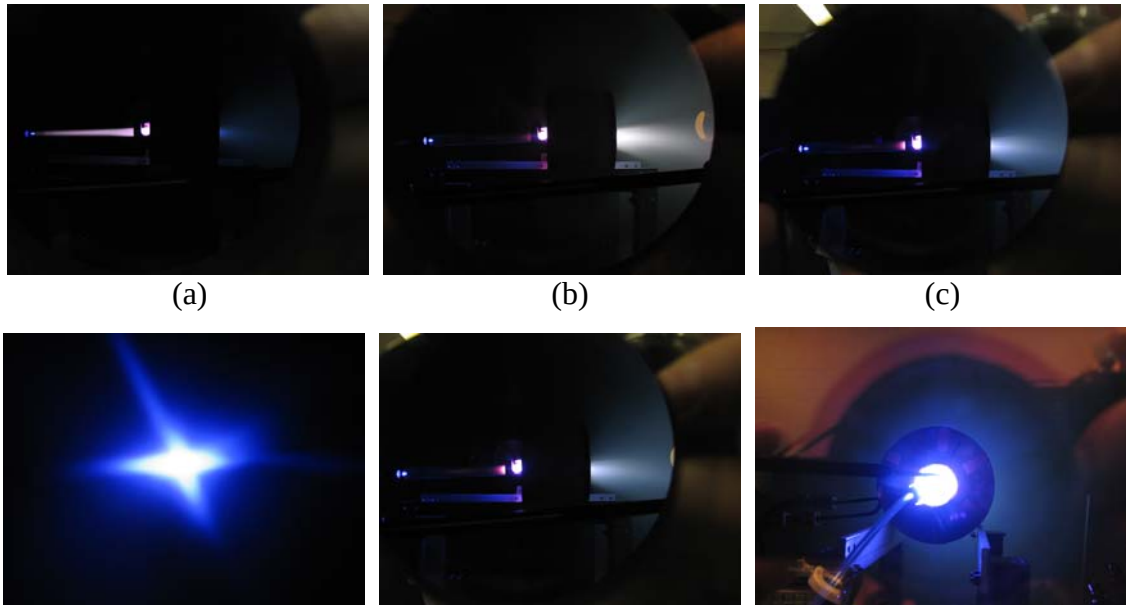

(a) (b) (c)

(d) (e) (f)

Fig. 57: Helicon mode with long tube, P=300-500-800W, side views (obstructed by the magnet), and frontal views into the plume (star) and upstream (bright magnet bore)

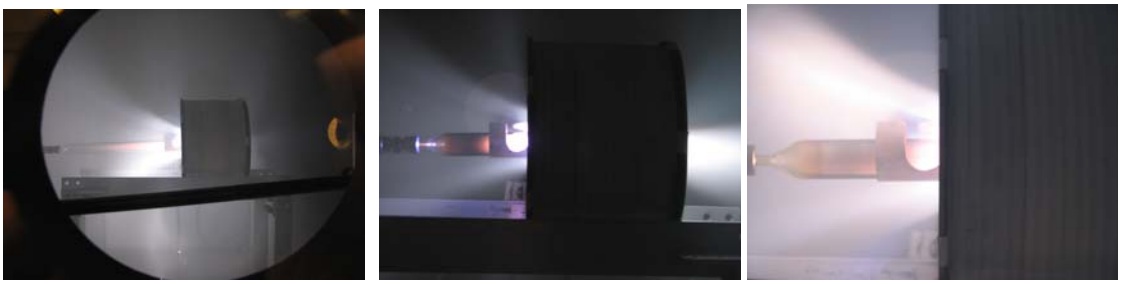

(a) (b) (c)

Fig. 58: Pressure buildup in the vacuum tank causes ambient gas ionization by the antenna and consequent helicon discharge termination in both configurations

Photos in Figs. 59-60 illustrate modified mHTX operation with short (20cm, ID 2cm) quartz tube under varied gas flow rate and applied 13.56MHz RF-power.

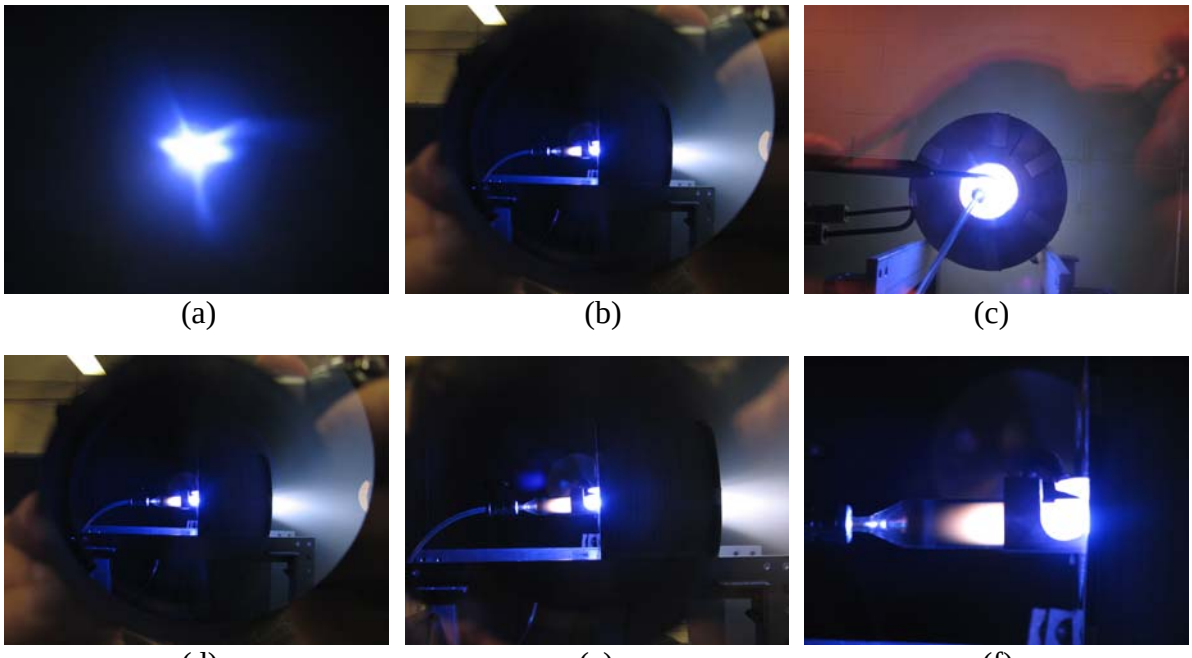

(a) (b) (c)

(d) (e) (f)

Fig. 59: Helicon discharge in a short tube configuration with 15sccm Ar flow, magnetic field ~1500Gs, RF power ~500W. Shown are frontal views and side views with different magnification to highlight the structure of the gas-plasma flow

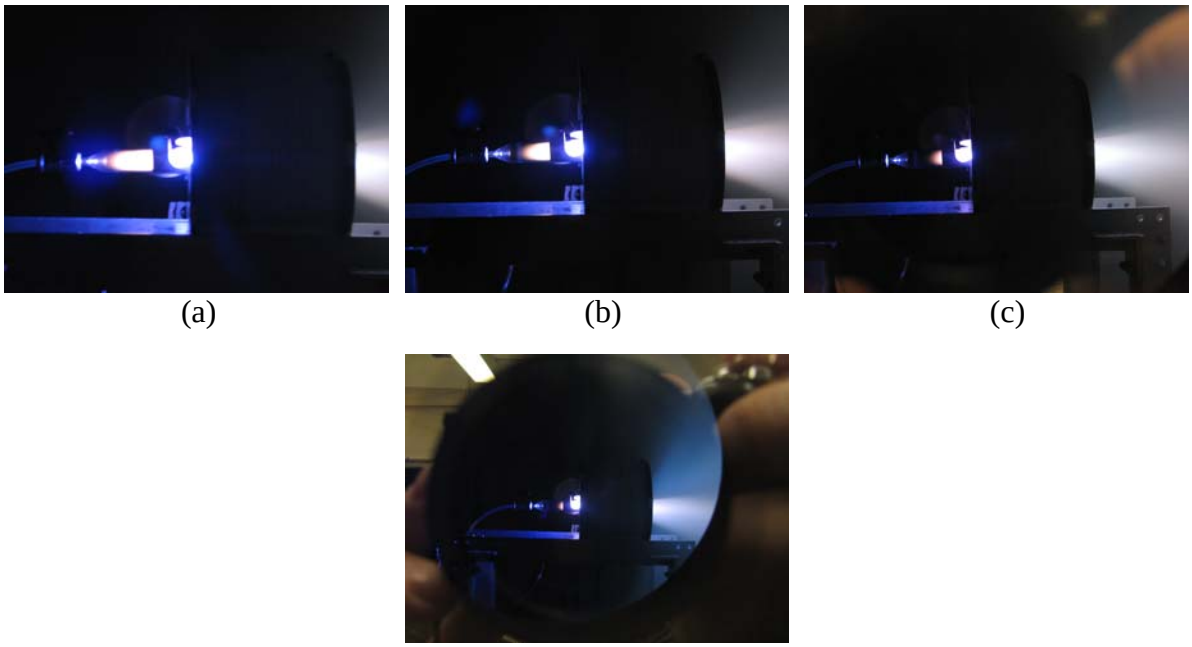

(a) (b) (c)

(d)

Fig. 60: Scan of the applied RF power. Delivered power was gradually increased (with continuous tuning of the matching network) from P=300W to P=600W. The flow rate was fixed at 10sccm of Ar. It is clear that the ionization region steadily moves away from the gas inlet towards the tube's exit. The exhausted plume becomes progressively more collimated and its color turns more bluish, indicating higher degree of gas ionization.

Running in the pulsed mode is not as productive, because extra time has to be allocated to evacuate background gas from the tank between shots. Discharges themselves last 2-10sec, during which matching network has to be tuned and the experimental data collected.

11. RESULTS FROM THE SECOND HALF OF 2007

In the second half of 2007 campaign we were trying to obtain the following mHTX data:

i) Accurate spectroscopic characterization of ArI and ArII lines in the Helicon & ICP modes of operation using UV-VIS rated CCD and both highest 1800g/mm ruled and 3600g/mm holographic gratings. Light will be collected by UV-rated multi-channel vacuum fiber system from different regions of the discharge, hopefully in 200-850nm and 180-450nm wave-length intervals allowed by Acton 750i spectrometer.

ii) Characterize plasma outflow by measuring:
- plasma density and velocity near the orifice using Mach probe;
- thermal force exerted on the quartz tube using thrust balance;
- ion energy distribution in the plume using RPA;
- Doppler shift of ionic lines coming from the plume region.

Certain measurements (like RPA) are complicated by high vacuum tank backpressure.

11.1 Full-power helicon mode with Ar

Helicon mode was achieved in two- and single-magnet configurations. Up to 1200W of RF power was delivered to the antenna with 25-50sccm of Ar gas flow. At 10-20sccm 800-1100W were deliverable. The discharge was stable for 5-10 minutes. However, we could run on full 160A of current only for 1-2 minutes due to magnet heating and 6V power supply limitations. Most of the scans were performed at 140A.

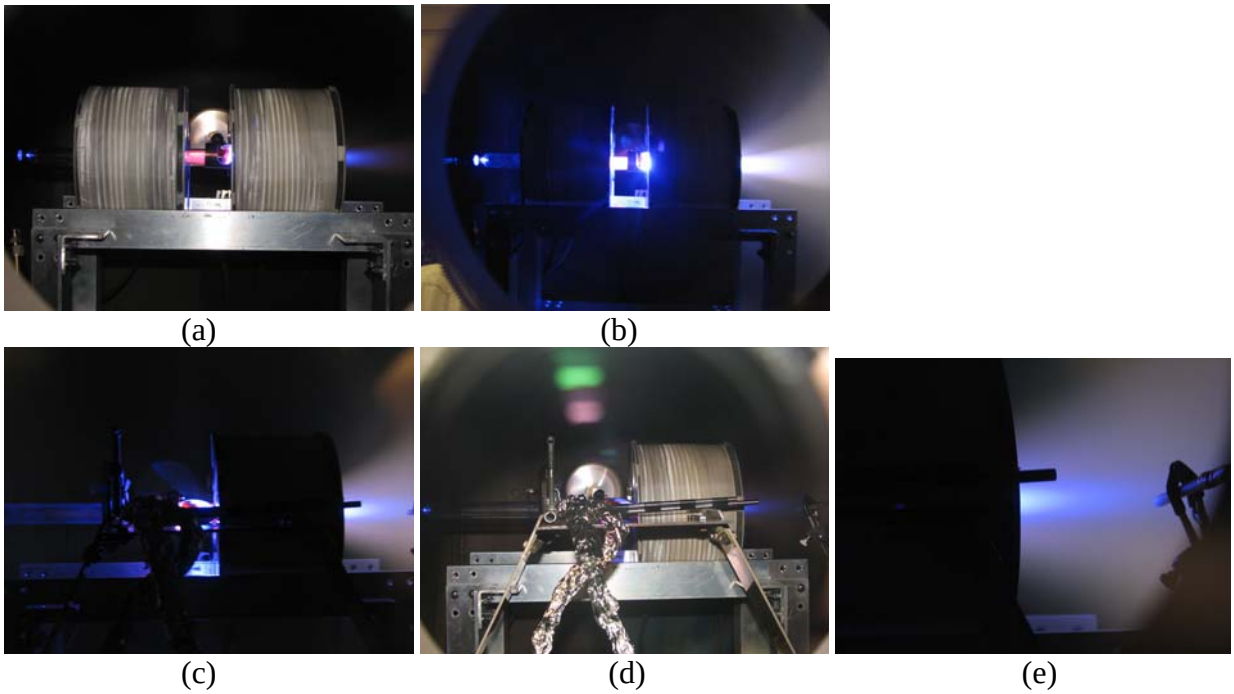

Fig. 61: Helicon mode in (top) the 2-magnet setup; (bottom) – single magnet configuration. Photos of Ar running mHTX were taken with and without camera flush.

To allow running at 180A deliverable by the high-I supplies, we constructed a pair of shorter magnets, 8cm coil (present coils are 12cm wide) 2-gauge 250°C rated wires with a smaller bore to allow continuous operation up to ~2000G.

11.2 High-resolution UV-VIS spectroscopic measurements

In-tank emission collection together with high-resolution acquisition system was applied for UV-VIS spectral characterization of the Ar discharge. Due to very high dispersion and small CCD's sensor pixel & overall sizes a narrow region can be measured and calibrated at a time, usually 3-10nm at a time. Because the spectrometer mechanical system is ~0.5nm accurate, precise calibration has to be done for each measurement range, or every time the gratings bearing turret is moved. Therefore, taking broad spectra using segmented spectra and built-in spectral software function is not very accurate in the first place, also adds artifacts at the boundaries.

Using 1800g/mm we studied several regions of interest in deep detail. One of the interesting regions is around 377nm. There are two the closest Ar neutral and Ar^+ single ion lines, namely, 377.0369 and 377.0519nm, with just 0.15A separation. Fig. 62 insert gives a good feel of the kind of resolution we were able to obtain with updated system. The two lines are well defined.

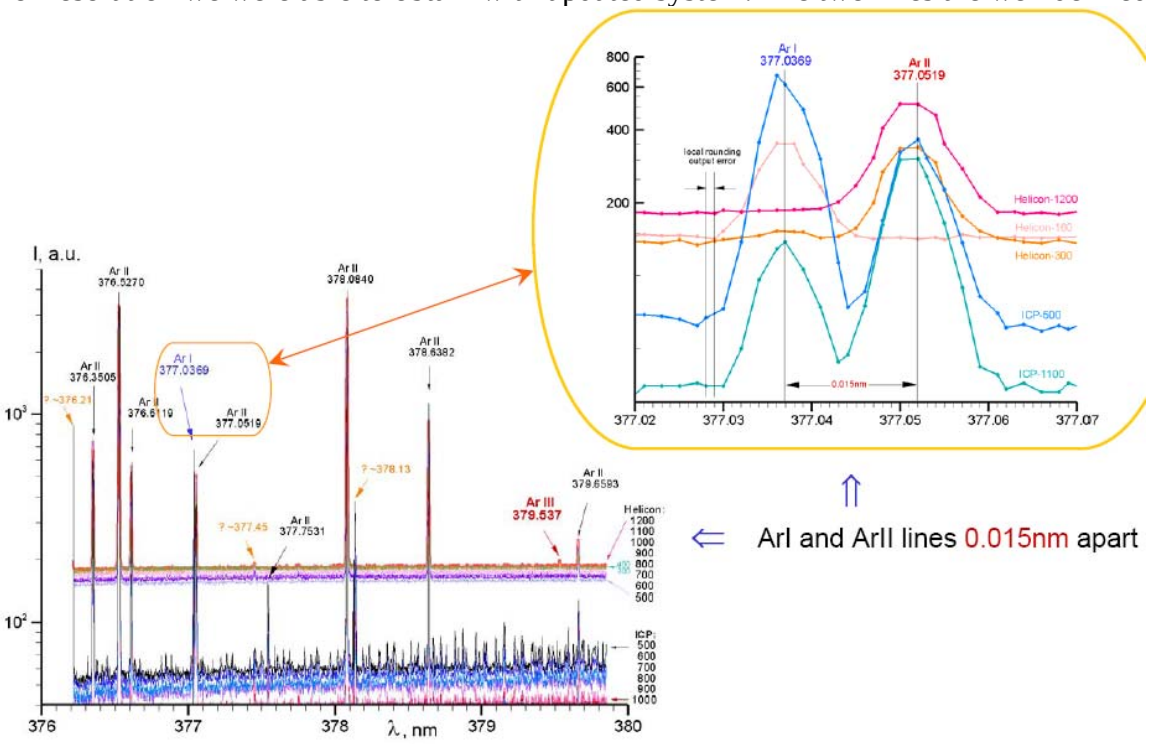

Fig. 62: 1800g/mm spectrum of the 376-380nm region. Zoomed insert shows part with the two closest Ar and Ar^+ lines, just 0.015nm apart

The main pane of Fig. 62 presents a dozen of overlapped spectra of Helicon mode with 500-1200W and ICP mode with 500-1000W RF-power delivered to the antenna. A power scan was taken at fixed 20sccm Ar gas flow, and 140A and 0A magnet current, respectively, in the single-magnet configuration.

Bright atomic lines, visible in ICP regime, completely disappear in the Helicon mode, thus, confirming near complete (~99%) gas utilization. Single Ar^{+} and double Ar^{2+} ionic lines appear in the high-power ICP, and grow in the helicon mode in a concert with applied RF power.

11.3 Boron spectroscopic diagnostics

One can attempt seeding light atomic weight impurity to facilitate Doppler shift and other optical diagnostics. It may also be used for electrical potential profiling, in particular to measure a potential drop across a double-layer.

The lightest impurity is B, element #5. It has A~10.8, easy to ionize I_1~8.3eV, the second ionization potential is I_2~25.2eV. Comparing to Ar (15.8eV & 27.6eV) and other noble gases it has much lower ionization potential, which means that it will be probably ionized within gas discharge. Also boron emits very little ~ a few % of noble gases, and has no health issues at all. It is readily available in different chemically pure forms. We use 98.6% powder or 99.9% pure crystalline lump. We placed small amount inside the quartz tube (Fig. 63). Initially we tried placing BN ceramic pieces, but emission was too low.

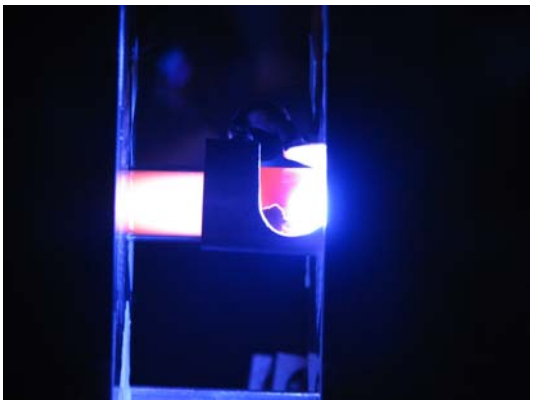

Fig. 63: Boron powder spot inside the discharge volume

For B^{+} emission we looked into the most prominent 345.13030nm line. It was detected in high-power ICP and all Helicon mode discharges as shown in Fig.64. In the 245-349nm region we detected strong single ion line and double Ar^{++} line, but only in helicon mode, which in addition had no atomic line (see. Fig.64).

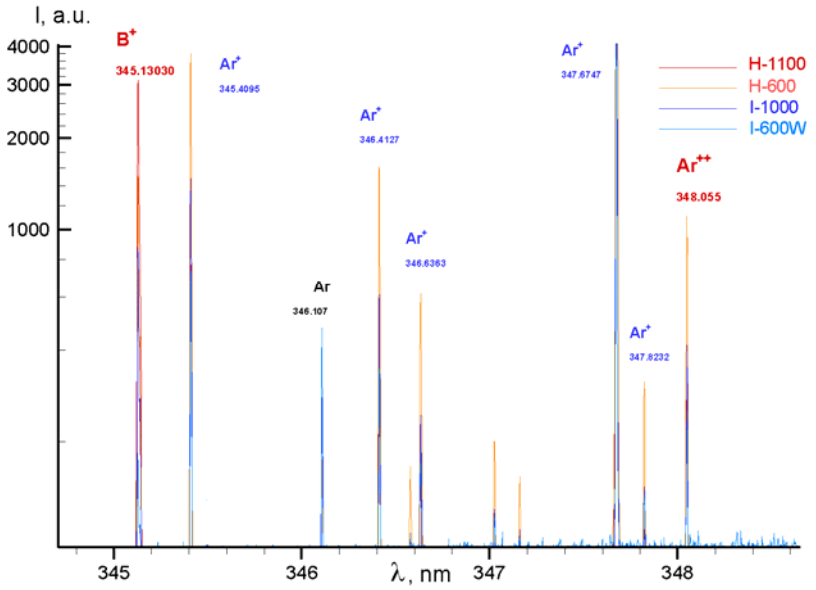

Fig. 64: Prominent BII line surrounded with ArI, ArII and ArIII lines

Ar^{++} and B^{+} were detected in high-resolution, indicating high electron temperature (>10eV). Accurate UV-VIS spectra of the 345nm region for ICP and Helicon discharges were taken for B varied in the 0÷0.15T interval.

When the 345.1nm boron ion line was examined with the highest available holographic 3600g/mm grating it appeared to be broad with two peaks. As it turned out the 0.1A separation very closely matches theoretical calculations for the isotopic shift of the spectral line.

Natural boron consists of roughly 80:20% mix of ^{11}B and ^{10}B isotopes, giving mean A=10.8. Line intensity ratios in Fig. 65 correspond to the typical isotope abundance.

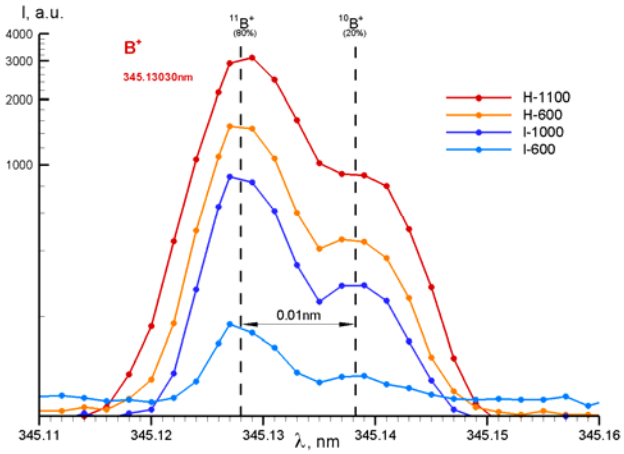

Fig. 65: BII 345.1nm line isotopic shift

Despite several attempts we were unable to detect any other ionic B lines, possibly a very weak signal at ~412.19nm. As to atomic B lines, the only detected lines were two strong doublet lines 249.6771 and 249.7723nm, as shown in Fig. 66. They appear in all regimes. Isotope broadening per theoretical studies is an order of magnitude less than for B^{+} 345nm line, and is undetectable with the best resolution of 0.01A/pixel.

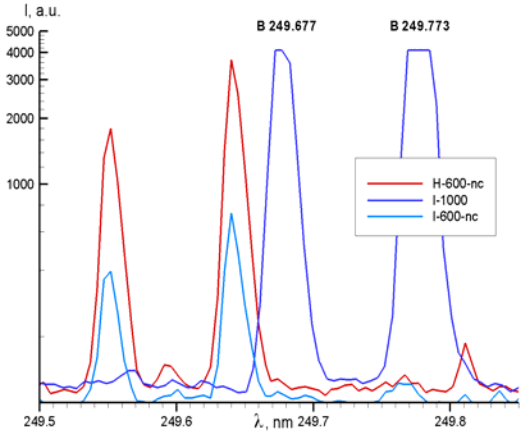

.

Fig. 66: Prominent BI 249nm doublet lines

11.4 Measurement of ionic lines Doppler shift

Doppler shift for expected V~10km/sec correspond to ~10 pixels displacement, and should be detectable. First we did series of studies by looking through the back window port, and later by installing vacuum optical fiber looking into the plume. We have detected sizable line broadening, as shown in Fig. 67, but never resolved double peaked lines. In part this is due to the fact that plasma emission is proportional to its density. Dense stagnant plasma in the ionization region dominates the week radiation from the accelerated plasma. The higher the speed the less is plasma density due to mass flow conservation nV=const once the gas is fully ionized.

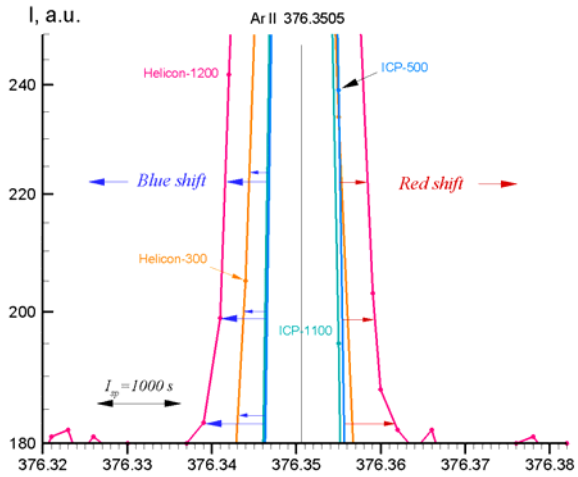

Fig. 67: Ionic Ar+ line broadening due to Doppler shift

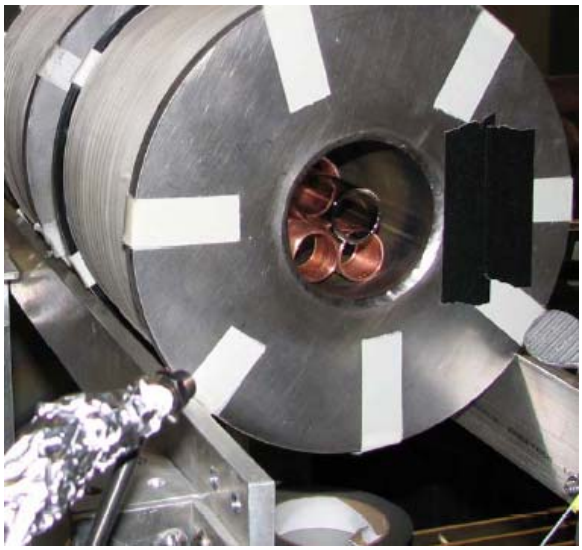

Fig. 68: Vacuum optical setup for ionic Doppler shift measurements

Next a light collecting assembly was placed at a side to look across the beam onto very low-reflecting optical tape as could be seen from Fig. 68. The reason was to minimize reflected light that finds ways from the bright ionization area. The plume itself is visible, though looks dim in the brightly lit vacuum tank. The angle between collector axis and the beam was ~50 degrees, which gives a coefficient of ~0.7 for Doppler shift reduction. Optical fiber was shielded with metal foil to avoid damage by plasma. The field of collection was marked and aligned with the quartz tube orifice by shining laser pointer from the opposite end of the fiber. The spot was ~1cm across centered at the dark tape. Quartz tube was flat with the electromagnet bobbin side.

For these measurements we moved closer to the 3600g/mm grating highest mechanically possible wavelength of ~460nm. For this reason and to minimize required exposure time (10s of seconds) we looked onto prominent 434.8064nm Ar^+ ionic line region. This line with a narrow neighborhood is presented in Fig. 69a. As one can see there are also two other lines in this view – one is atomic Ar and the second is another Ar^+ ionic line. There are a dozen of spectra overlapped in this plot that correspond to the ICP and Helicon modes with magnet current varied in the 50-140A range. Interestingly, the neutral-atomic line remains within instrumental broadening range width-wise, while both charged-ionic show similar broadening. This pattern is true for all other (~20) ArI and ArII lines we looked at using the same optical setup.

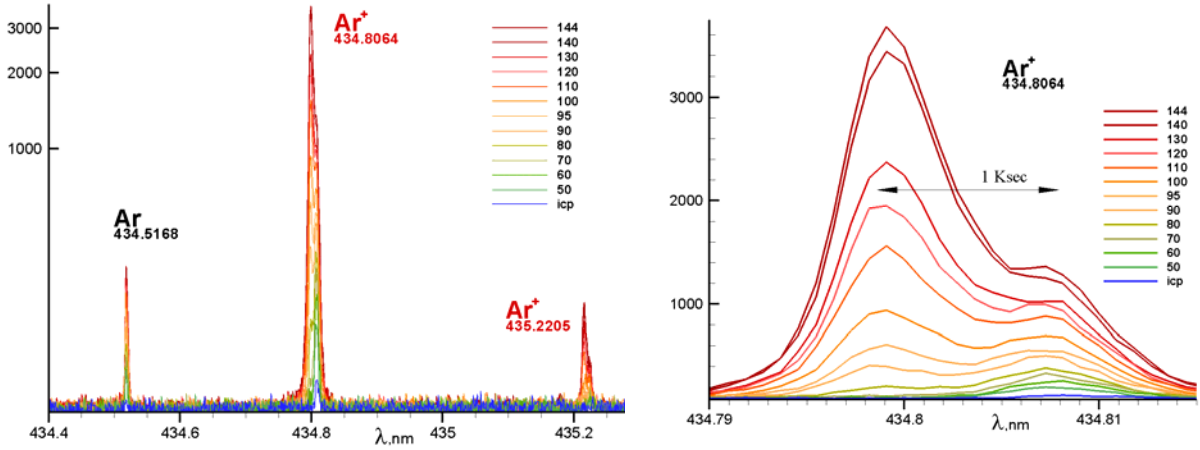

(a) (b)

Fig. 69: (a) – prominent Ar^+ surrounded by atomic and ionic lines,
(b) – zoomed 434.8nm line shows distinct double-peaked profile

If we zoom into the 434.8nm region, the line's shape becomes apparent, see Fig. 69b. It obviously composed of two populations, shifted by ~0.01nm. Our system has roughly 0.01A/pixel resolution, so this shift corresponds to ~10 pixels and therefore is easily detectable. The left (blue-shifted) peak disappears as we go towards ICP discharge with stagnant plasma. Therefore, the second peak should be the stationary populations, and the left one – moving towards the observer.

In Fig. 69b the same scale is used, which hides the two-peak nature of the line, which can be approximated with two Gaussians and plotted to an individual scale, as given in Fig. 70 below.

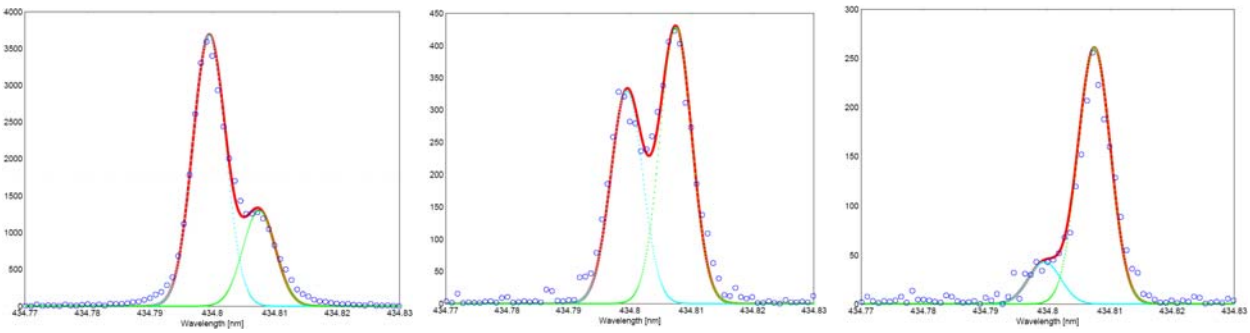

(a) (b) (c)

Fig. 70: (left-to-right) double-Gaussian fit of the measured 434.8nm ionic line shape for I=140A, I=90A and I=70A electromagnet current, respectively

The two-Maxwellian fit was done by visual inspection. Lines have broader wings, which are not fitted well. However the peaks are well matched. Judging by peaks, and taking into account angles between collector and the plume, measured Doppler shift corresponds to V~10km/sec.

11.5 Mach probe measurements

Mach probe is being used to quantify plasma in the plume: flow velocity, plasma density and electron temperature. The first mount was ~1cm in front of quartz tube orifice, as shown in Fig. 71a, with I-V probe characteristic plotted in linear and log scales in the following charts.

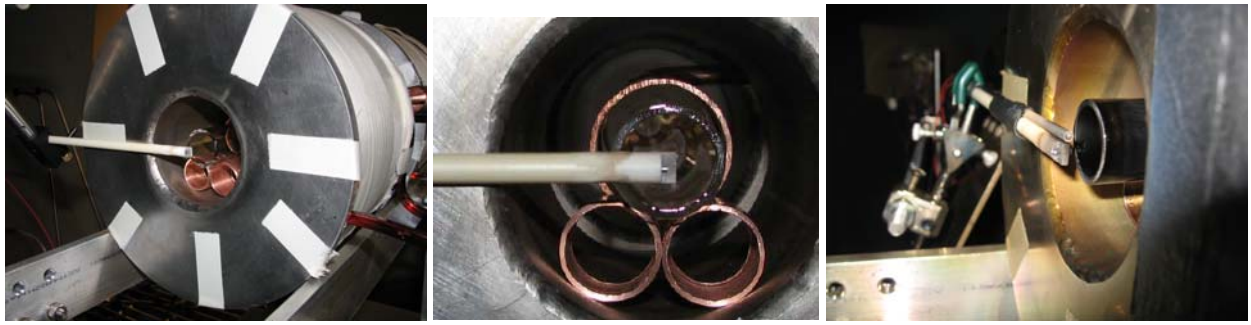

(a) (b) (c)

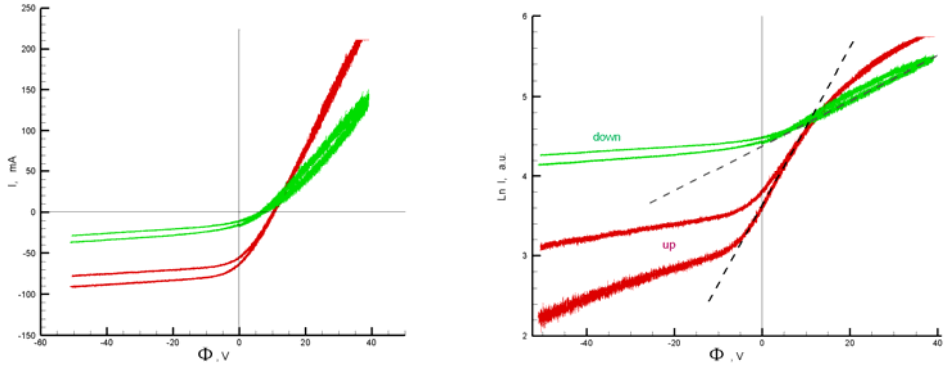

(d) (e)

Fig. 71: (a-c) different views of Mach probe as installed in front of quartz tube's orifice, sometimes used in parallel with flat Langmuir probe; plots of I-V curves in (d) lin-lin and (e) shifted log-lin scales showing an exponential segment

By using i) Hutchinson's [32] and ii) Oksuz's [33] results, and iii) collected current definition:

$$M \approx 0.45 \ln \frac{I_{ion\ sat}^{upstream}}{I_{ion\ sat}^{downstream}} \qquad \ln J_e = \frac{\Phi}{T_e} + C_{RF} \qquad J_i^{sat} \sim en_p U_D A_{probe} \qquad (10)$$

from the known collected current, slope and measured up/downstream current ratios, and also known input RF-power P~300-600W and flow rate, ~20-30sccm of argon gas, we find that the electron temperature is relatively high, T_e ~ 8-12eV, plasma density is relatively high as well n_p ~ 3-5x$10^{12}$$cm^{-3}$, and plasma is leaving tube with Mach number, M ~ 1.

These measured parameters allow us to conclude that thrust force is in the T ~ 6-10 mN range, and energy efficiency is at least ~ 10%.

11.5 RPA energy measurements

Retarding potential analyzer (RPA) was designed, machined and assembeled, electric short-tested and mounted ~30-50cm in front of quartz tube, see Fig. 72.

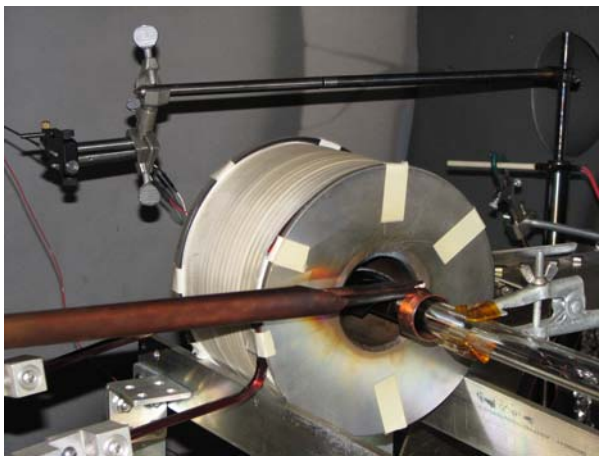

(a)

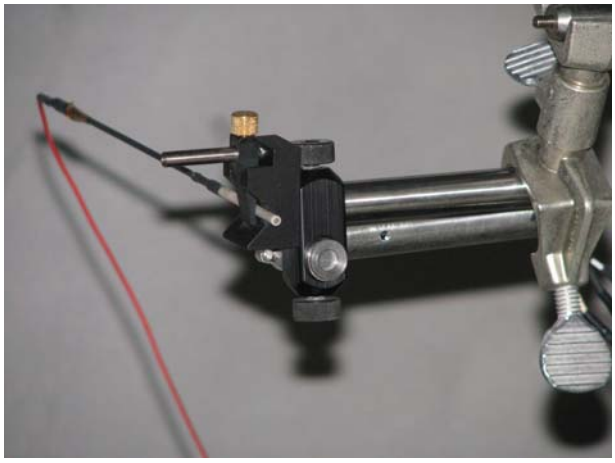

(b)

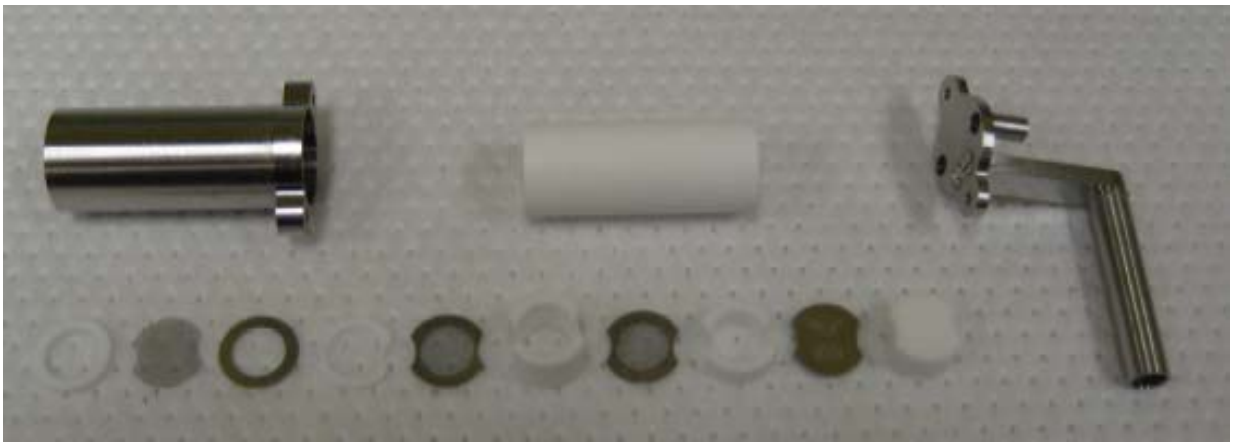

(c)

Fig. 72: (a) – RPA is mounted in the tank; (b) closer view of RPA, smaller flat Langmuir probe with red wire attached; (c) – disassembled RPA showing floating, electron repulsion and ion retarding grids made of ~30μm chemically etched Mo foil, collector and ceramic spacers

11.7 Argon RPA data

The ion distribution function (IDF) data have been collected for both Helicon and ICP modes for comparison. The main focus is power and mass flow scans with high, moderate and removed B field. Typical discharge view with ~10-30sccm Ar flow rate, I~140-160A and ~700-1100W of applied RF power is presented in Fig. 73.

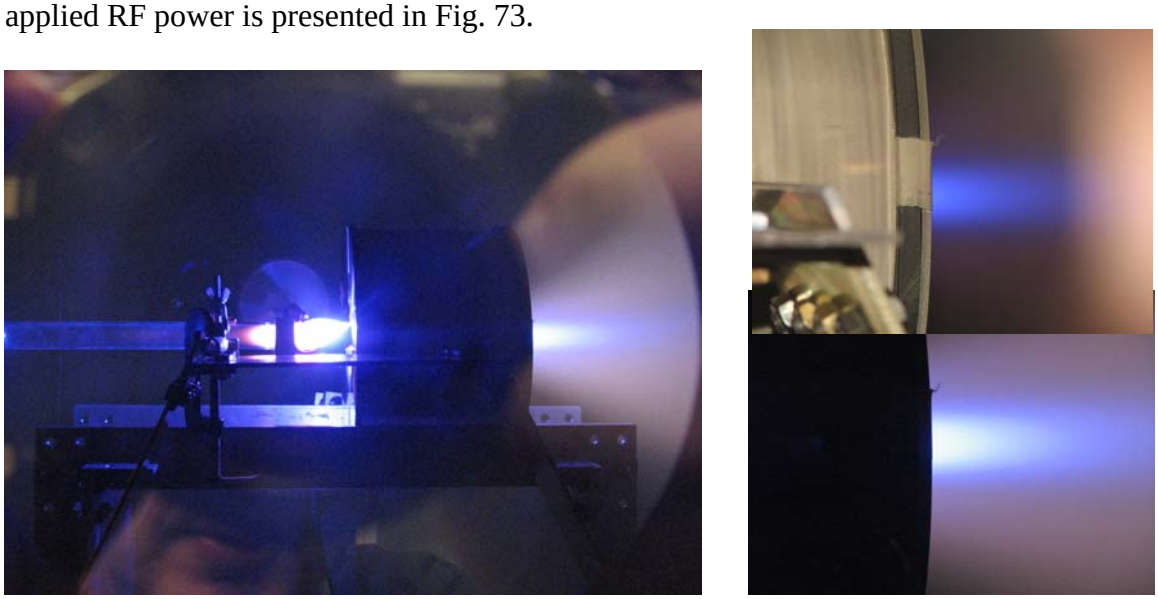

(a) (b)

Fig. 73: (a) - Stable Ar discharge in the high-I single-magnet configuration, (b) – zoomed plume region taken with and without camera flash light

There are several issues with RPA measurements, such as proper biasing of the repelling grids and collector, which could be determined experimentally. Other factors are fluctuations due to plasma and RF interference, which were reduced by multiple sampling. Again, experimentally it was determined that ~0.5sec per point was an optimal interval to balance between time-averaging and rate of each data point acquisition. The increments of 1V were used to scan 0-140V energy interval. Raw I-V curves, and corresponding smoothed by using combination of digital and linear filters, are presented in Fig. 74. These data were taken at ~700W applied RF power and varied flow rate in the 10-50sccm interval. Lower and higher flow rates showed unstable operation due to inability to couple average 700W power to plasma and relatively high, $>10^{-4}$mtorr, background gas pressure, respectively.

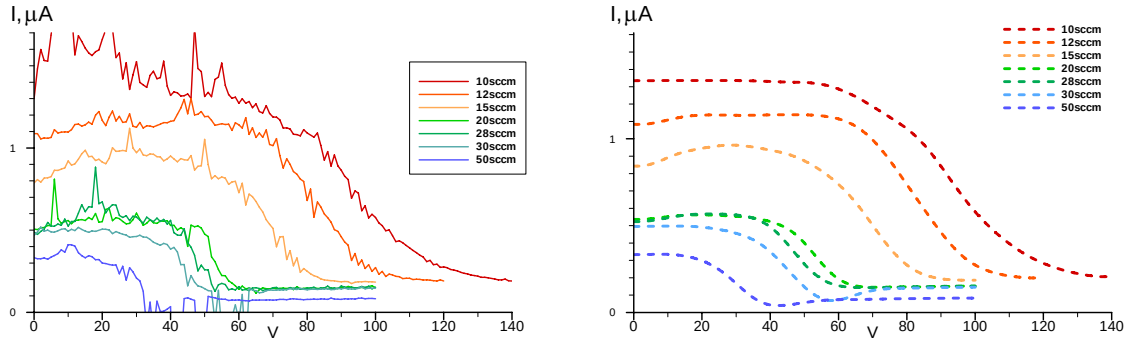

(a) (b)

Fig. 74: (a) – Raw RPA I-V curves for 700W RF power delivered to helicon antenna, (b) – smoothed numerically using filtering

Next, the derivative of the smoothed I-V characteristics was numerically calculated, and negative values were interpreted as ion energy distribution function (IEDF), while positive derivatives have been ignored. This process in illustrated in Fig. 75a, with end result, IEDFs for different flow rates in Fig. 75b.

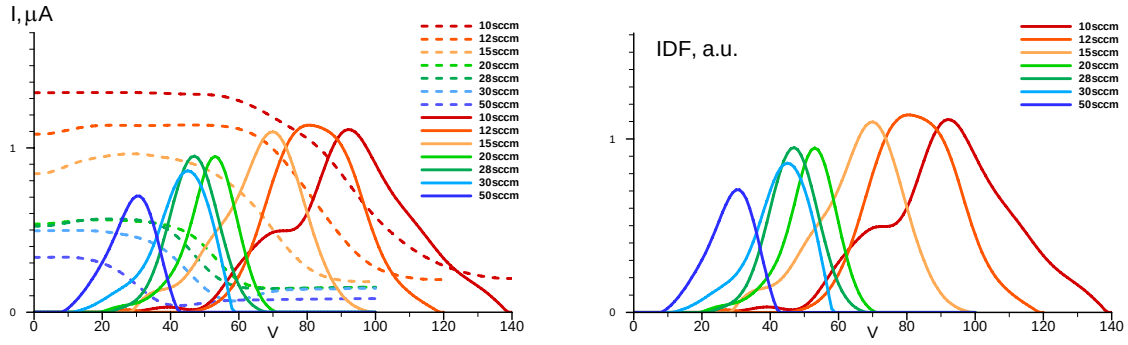

(a) (b)

Fig. 75: (a) – smoothed RPA I-V curves (dashed lines) vs modulus of derivatives (solid curves of the same color), (b) – calculated IEDFs for different volumetric flow rates

Raw and smoothed data for higher, 1100W mean RF power delivered to antenna are presented in Fig. 76. Mass flow scan was taken in the 12-30sccm range. Similarly to the lower power case coupling steadily full power for lower and higher flow rates was impossible.

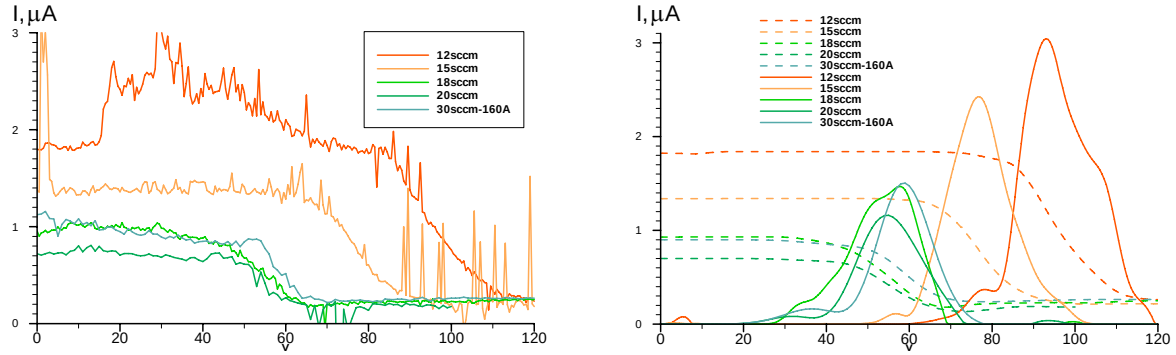

(a) (b)

Fig. 76: (a) – raw RPA I-V curves for 1.1kW RF power and (b) smoothed data (dashed lines) and absolute derivatives (solid curves of the same color) interpreted as IEDFs

From the spectroscopic measurements we know that gas is ~99% ionized for all flow rates. With reduced flow rate kinetic energy of the plume, normalized per particle, increases significantly - from Figs. 75-76 one can see that the specific impulse:

$$I_{sp} \approx 1.4 \times 10^3 \sqrt{\frac{E(eV)}{A}} \qquad (11)$$

goes up steadily from ~1200sec to ~2200sec as the power density per unit mass increases. The IEDF has a pronounced bulk centered on the peak energy E with low dispersion $\Delta E / E < 30\%$ indicating that plasma is created at a localized ionization region. One can see secondary peaks in

the IEDF at energies *~0.5-0.8E* in some cases. But because they carry <5% of the ions it makes absolute contribution insignificant.

From the known flow rates and measured IDF's several major characteristics can be calculated – kinetic energy of the plume, thrust force and thrust efficiency. All these parameters are collected together in chart presented in Fig. 77.

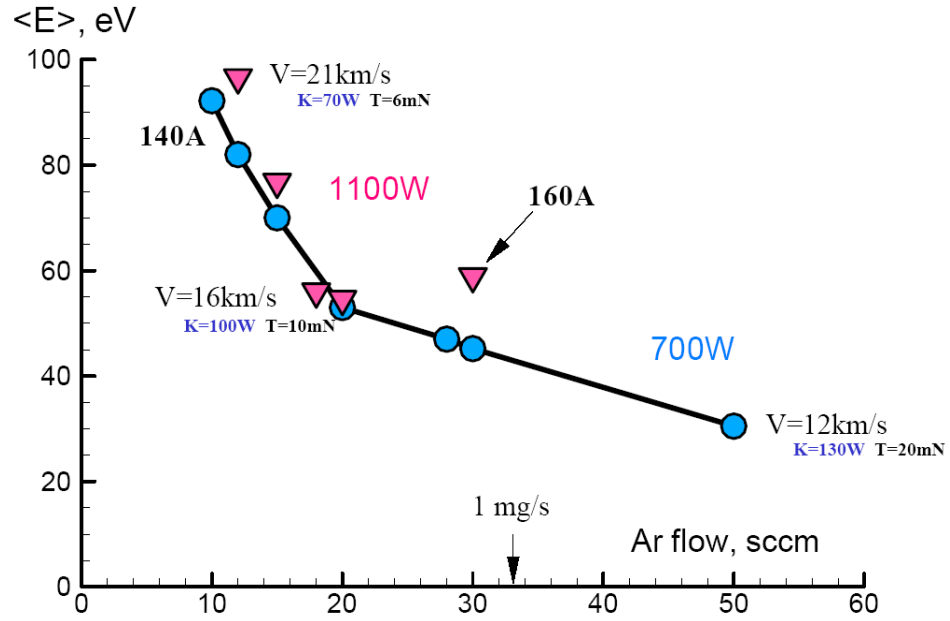

Fig. 77: Plasma plume integral characteristics – exhaust velocity, plume kinetic energy and thrust force - as function of Ar flow rate for different applied RF powers and coil currents

Trust force is in the $T \approx 6-20mN$ interval, in concert with $T \approx 10mN$ estimate made using Doppler shift data. Most importantly, thrust efficiency is in the $\eta_T \approx 10-20\%$ range.

For a comparison, RPA data were taken for ICP mode as well; the discharge is shown in Fig.78.

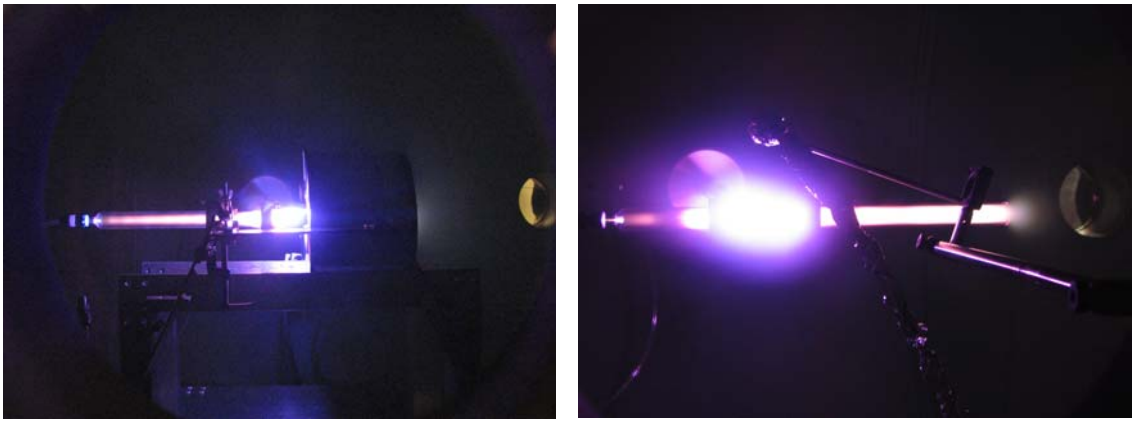

(a) (b)

Fig. 78: (a) - ICP discharge (B=0) in the 2007 mHTX configuration produces a plasma plume measurable by RPA, (b) - a longer quartz tube produces a sizable plume too.

The filtered RPA I-V curves and calculated IEDFs for the ICP mode are presented in Fig. 79 for a power scan. The flow rate was fixed at 20sccm. The current collected by RPA is drastically smaller than in helicon mode. It is not clear why it does not go to zero at high potential with one possibility being a parasitic current to the collector. The distribution function is very similar for different powers, centered at $E \approx 35-38eV$, with higher dispersion than in helicon mode.

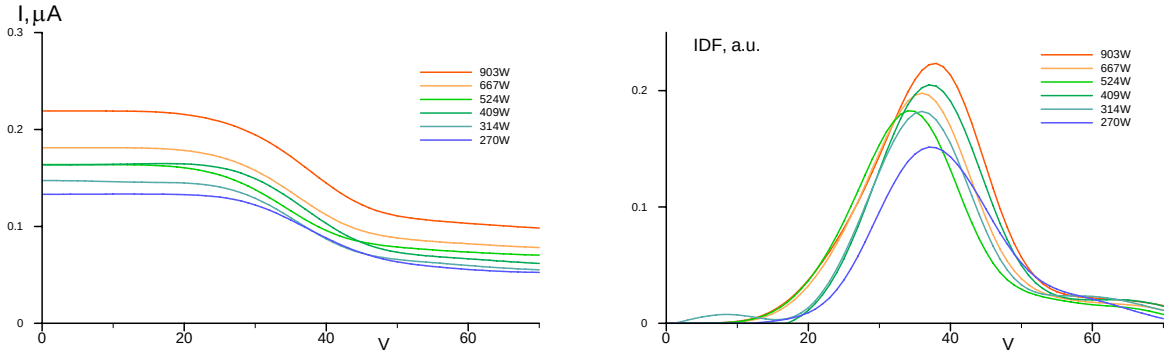

(a) (b)

Fig. 79: Power scan for the ICP discharge, (a) – smoothed RPA I-V curves, (b) – corresponding IEDFs calculated from them

Interestingly, the specific impulse is quite high, ~1300seconds. However, it is still smaller than in the helicon regime with the same gas flow & RF power, ~1.6-2Ksec.

11.8 Nitrogen RPA data

Diatomic propellants are viewed to be less efficient for EP applications. We run stable nitrogen discharge with 500-1000W RF power and ~10sccm flow rate, which atom-wise corresponds to the 20sccm Ar flow rate. The typical helicon mode is presented in Fig. 80. A collimated beam leaving the mHTX is visible, as well as the extended low emission ionization region to the left from helicon antenna. This should be compared to the sharp ionization region boundary observed for all noble gases tried experimentally.

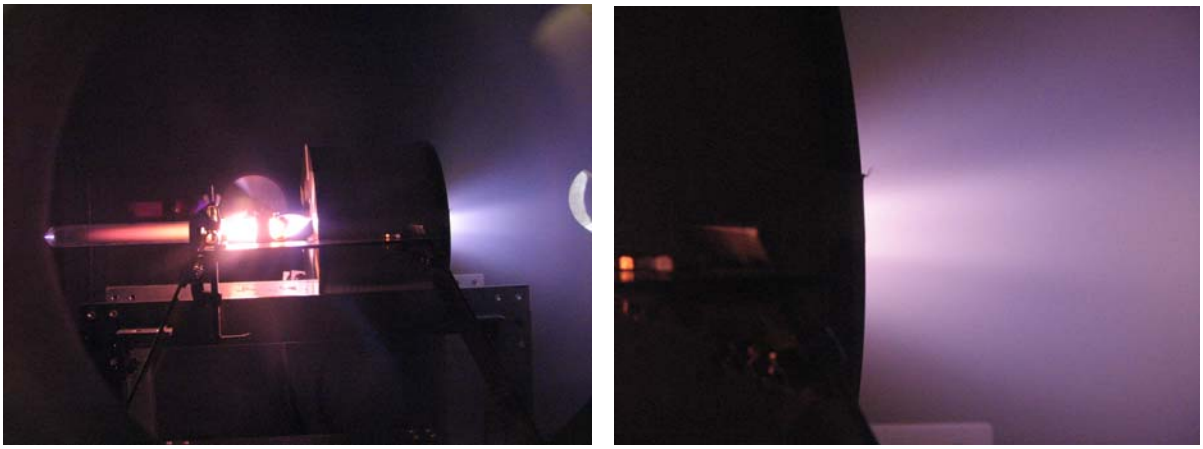

(a) (b)

Fig. 80: H-mode with N_2 operation (a) – discharge view through the side port window, (b) – zoomed plume region with collimated beam in the center

Limited RPA data were taken for mHTH operating on nitrogen. They are presented in Fig. 81 and correspond to the simultaneous power and flow rate scan for three operational points.

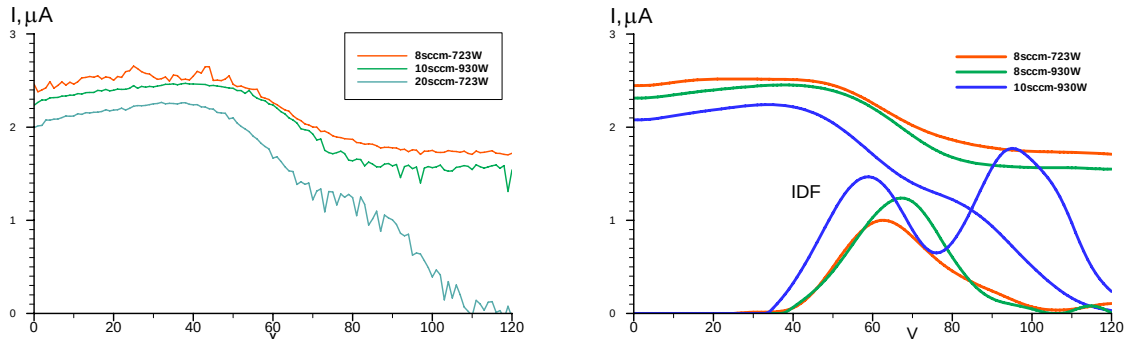

(a) (b)

Fig. 81: (a) – raw RPA I-V curves for RF power / flow rate scan of N_2 discharge; (b) smoothed I-V characteristics and their derivatives = IEDFs

Initial analysis shows that IEDF has two peaks with roughly the same intensity. One possible explanation for this fact is formation and extraction of both atomic and molecular ions.

The first peak of the IEDF in Fig. 81b corresponds to ~28km/sec exhaust velocity (for atomic ions), while the second one for ~36km/sec. For the molecular ions those would correspond to ~20 and ~26km/sec, respectively. Thus, the specific impulse is very high, in excess of 3Ksec. The estimate of thrust efficiency also gives high value $\eta_T \approx 20\%$, with thrust force $T \approx 12mN$.

12. UPGRADED MHTX 2008 DESIGN AND OPERATION

In early 2008 mHTX experiment was upgraded: two new compact electromagnets were built and installed, new tight-fit antenna was constructed and installed as well.

12.1 New electromagnets

The need for new electromagnets became apparent after operating high-I magnets that were built for the 2007 design. Copper is characterized with relatively high thermal resistance drift $\Delta R/R \approx 3.93\times10^{-3}K^{-1}$. Heating by typical for experiment $\Delta T \sim 100°K$ means increase of the coil resistance by ~40%. Coils were designed to allow maximum $I \approx 180A$ current when operating at room temperature at 6V nominal voltage as produced by the high-I power supply. Unfortunately, the maximum voltage that the supplies can maintain is 6.3V, which is quickly reached as the magnet heats up.

The new magnets were designed keeping these limitations in mind, and also with desire to reach stronger magnetic fields >0.2T. The previous design reached $B \approx 1600G$ at $I \approx 150A$. To achieve required parameters the length of the coil was reduced by one third, to ~8cm, and the magnet bore was reduced to ~5cm diameter to allow two additional layers for the same external diameter of the bobbin. The final magnet design contains 132 turns – 11 layers with 12 turns per layer and resistance of around 0.02ohms (previous had ~0.03ohms). New and old magnets are shown in Fig.82 for comparison.

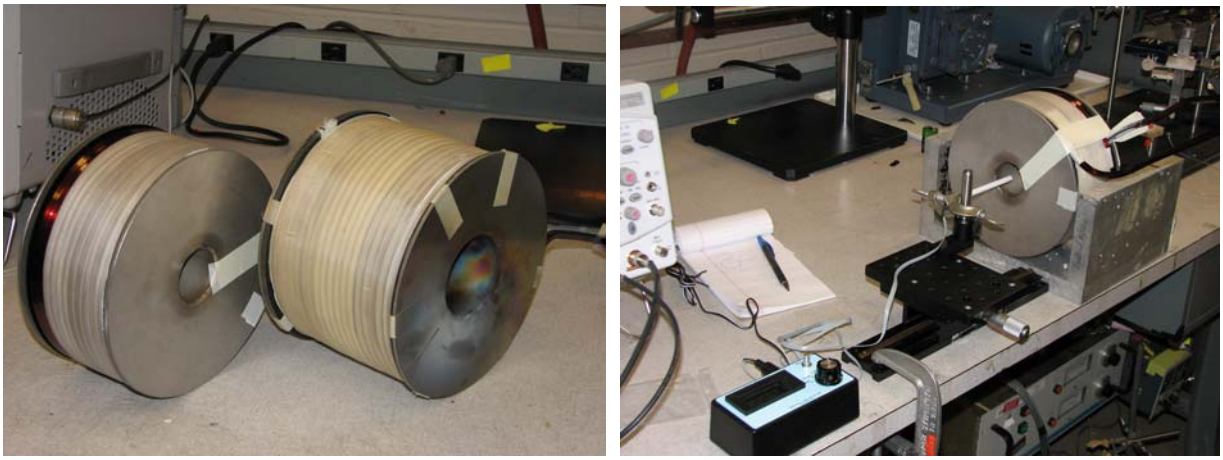

(a) (b)

Fig. 82: (a) - new and old high-I electromagnets showing slimmer design and tighter bore, (b) – setup with translation stage holding the Hall sensor of the gauss-meter to scan B-field strength.

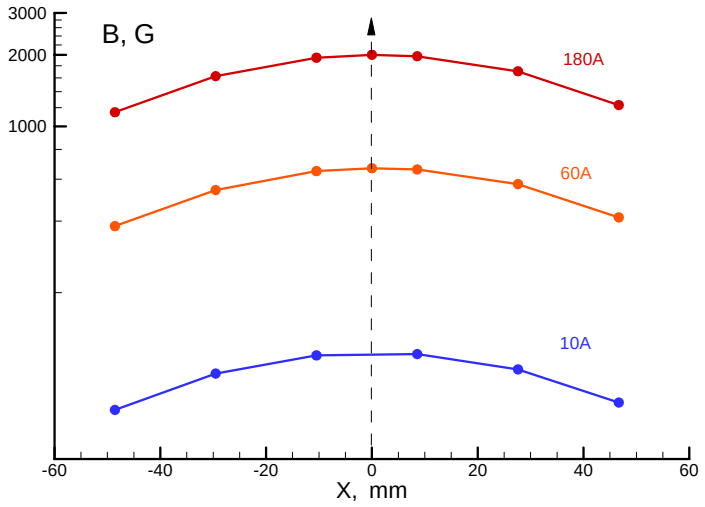

Fig. 83: Measured axial profiles of the magnetic field with high (180A), intermediate (60A) and low (10A) current operations plotted in the linear-log scale with respect to the magnet midplane

Two new electro-magnets were built and tested using setup shown in Fig. 82b. New gauss-meter was acquired; measured B(x) profiles are given in Fig. 83. The magnetic field profile followed driven current in a linear manner. The maximum magnetic field strength of 0.2T was measured.

12.2 New mHTX setup

Upgraded experiment is shown in Fig. 84. It includes new features: a compact magnet and a smaller diameter M=1 antenna that fits into tighter magnet bore.

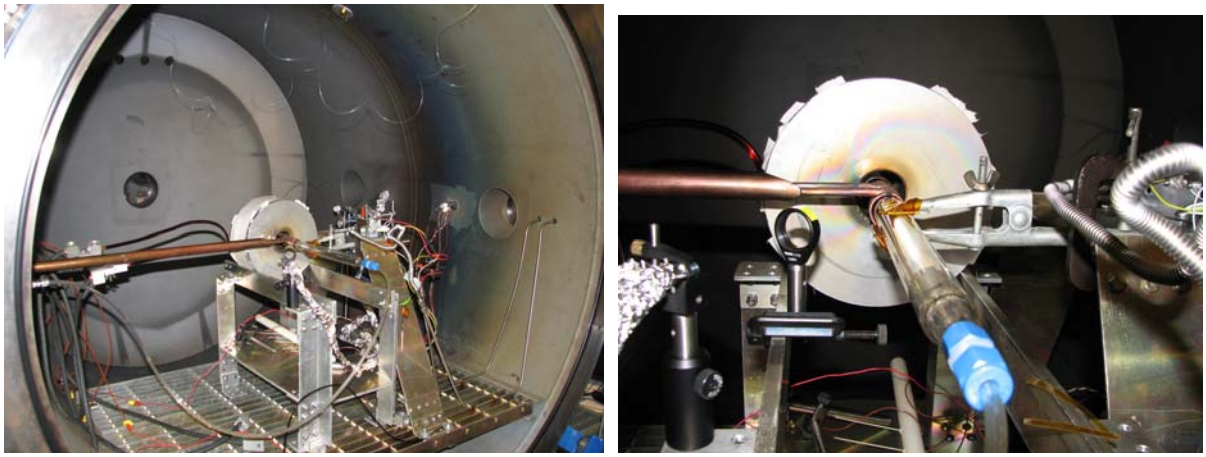

Fig. 84: 2008 mHTX setup

12.3 Ar operation

The new design shows robust operation and easy matching network tuning when operating on argon gas. The following Fig. 85 shows 1.1kW RF power discharge with 20sccm flow rate. The magnetic field was ~0.2T at full 180A current in the coil.

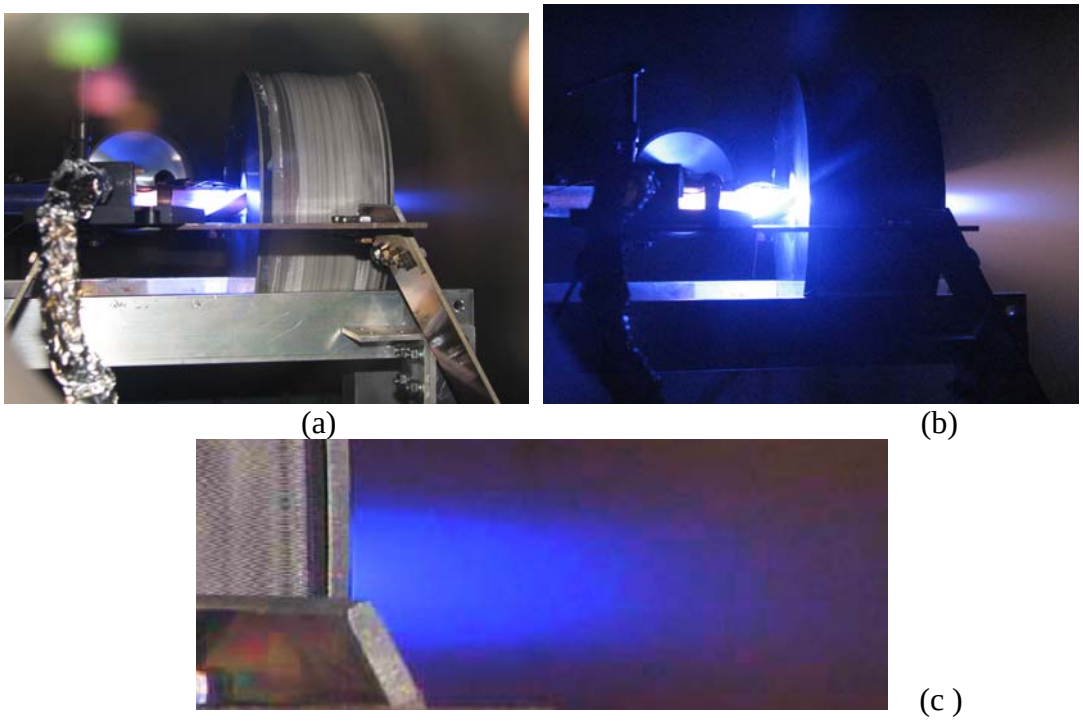

(a) (b)

(c)

Figure 85: full RF power, full magnet current stable helicon mode with 20sccm Ar flow achieved with mHTX 2008 compact configuration, photos were taken with (a) and without (b) camera flash light; (c) – zoomed collimated plume region

For comparison in Fig. 86 we present ICP mode (B=0) and hybrid mode (I=80A).

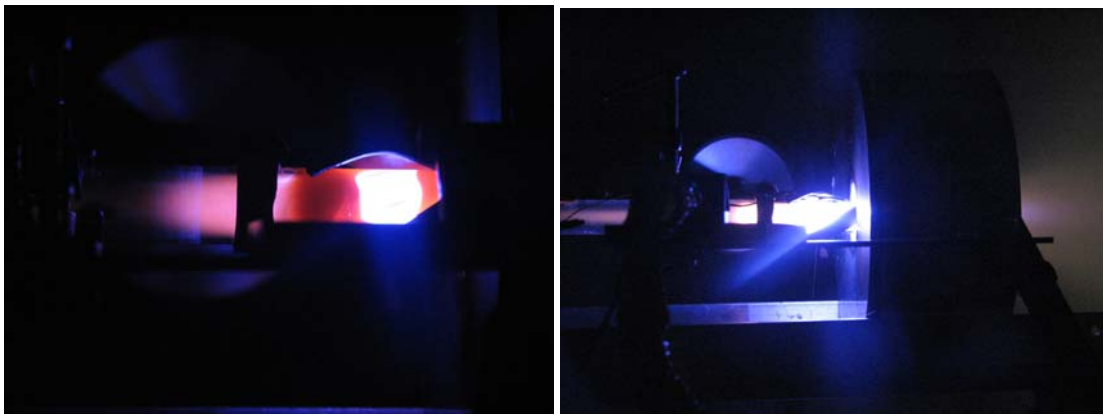

Figure 86: (a) – discharge region in the ICP mode; (b) – side view of the mixed mode with B~880G

Next step efforts will include detailed characterization of the Ar operation using spectroscopic and RPA probing of the discharge in broad range of physical parameters such as applied RF power to the helicon antenna, its position with respect to magnet, current in the magnet, gas flow, etc.

13. COMPACT DESIGN WITH PERMANENT MAGNETS

The magnetic field strength as measured with ring shown in Fig. 87 is up to ~ 4*KGs* for the NdFeB magnet at the left, and ~ 2*KGs* for the Ceramic-5 material ring pair at the right. The operational temperature is equal or higher than one of the present electromagnets ~125^{o}C.

A smaller tube and a different helicon antenna will be used. The system will be compact enough to fit into the bores of the larger electromagnets to additionally control the magnetic field topology if needed.

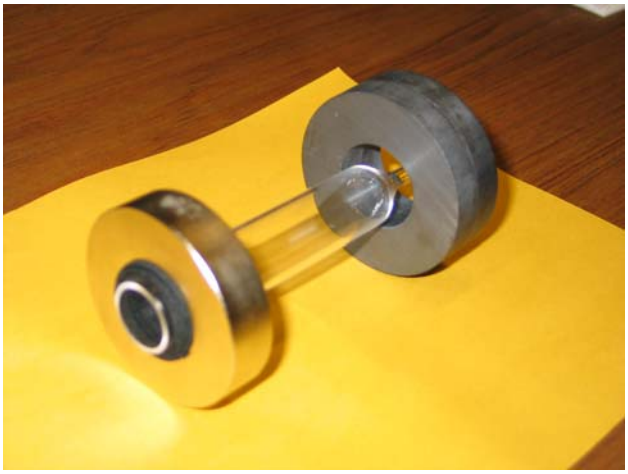

Figure 87: Compact plasma source prototype consisting of a small tube and two strong permanent magnets

14. RESULTS

A mini-helicon (mHTX) was successfully designed, built and thoroughly tested in several configurations with perfect RF-power-to-device coupling (<1W reflected). Following the initial objectives, the following results have been obtained:

i) Helicon modes have been achieved in the 200-1200W power ranges with 99% gas ionization, ~20% thrust efficiency (non-optimized) and ~10-30km/sec flows;

ii) Stable operation with mono-atomic (Ar, Xe, Ne), di-atomic gases (N_2), argon-nitrogen mixtures, and also air was achieved;

iii) Detailed characterization of the operation using spectroscopic measurements – neutral gas, single and double ion spectra, line broadening and Doppler shift was done;

iv) Invasive diagnostics with RPA and plasma probes have indicated generation of a highly accelerated plasma beam with extraordinary low emittance <10 degrees;

v) Specific impulse and thrust are easily variable in a broad range by changing magnetic field strength or gas flow rate and/or applied RF power.

These results clearly show that helicon thruster has many benefits compared to other EP thrusters: high throughput, absence of internal electrodes and external cathodes, potentially long life time, very low divergence of the plasma plume, flexible propellants, variable specific impulse, etc.

In addition, positive data have been collected for all-permanent magnet operation, including magnetic nozzle, showing possibility of a Double Layer formation. Accurate measurements of the super-fine emission line structure of the spectral line due to isotopic shift of the seeded impurity have been performed as well.

Also if importance, the mHTX project provided education and training for 12 MIT students. Three MIT S.M. and one Ph.D. thesis have been completed with direct support from the project, and forwarded to AFRL as the supplemental materials.

15. STUDENTS INVOLVEMENT

The limited annual budget allowed PI to support several students every year with partial financial help from MIT Nuclear Science and Engineering department and from MIT UROP program. So far the project has graduated three [two more are on the way] Science Masters (in Nuclear Engineering, Electrical and in Aerospace Engineering), one Doctoral student with Ph.D. degree in Aerospace Engineering, and one B.S. student. In total a dozen graduate and under-graduate students participated in the mHTX project:

1. Josef Palaia – initial design and construction, M.S.'06 in Nuclear Engineering. Employed by 4Frontiers Corporation focused on planet Mars.

2. Adam Shabshelovitz – electromagnets and machining, B.S. '06 in Aerospace Engineering. Joined U. Michigan Graduate Aerospace Program

3. Justin Pucci - helicon theory and experiment - with project since summer 2005, has graduated with M.S. degree in Aeronautical Engineering from MIT on June 8th, 2007. He joined Aerojet Corporation, Redmond, WA.

4. Murat Celik – spectroscopic experiment and simulations. He has graduated with Ph.D. from MIT Aerospace Engineering in June'07. He is working as a postdoctoral associate at MIT Aero-Astro Department.

5. Nareg Sinenian – principal experiment, plasma flow characterization. He has graduated with Dual M.S. degree in Nuclear Science & Engineering and in Electrical Engineering in February 2008. He is presently employed by the MIT Plasma Science and Fusion Center.

6. Daniel White – power balance and heat loads characterization. His planned graduation with M.S. degree in Aerospace Engineering is June 2008.

7. Taylor Matlock – new principal experiment developer, involved in spectroscopic work and probe measurements. His scheduled graduation with M.S. in Aerospace Engineering is 2009.

8. Stephen Gildea – numerical simulation of plasma transport in Helicon discharge (tentative). He received SMART Foundation fellowship for simulating transport in different EP systems. His scheduled graduation with M.S. in Aerospace Engineering is 2009.

9. Zach LaBRy and Olalekan Abiola are MIT B.S. AAD students assigned to the mHTX through UROP program. They were helping with various parts machining, magnet construction, winding and other immediate needs.

10. Ian Sugel and Dan Stiurca are MIT B.S. students assigned to the mHTX through Summer 2008 UROP program. They will participate is running experiment in the re-designed configuration.

16. PUBLICATIONS/PRESENTATIONS PERTAINING TO THE PROJECT

Several publications, conference presentations and seminar talks have been made so far by the PI and participants. A partial list is:

1. J. M. Pucci, N. Sinenian, J. Palaia, M. Celik, Z. LaBry, A. Shabshelowitz, O. Batishchev, and M. Martinez-Sanchez, Preliminary Characterization of a Helicon Plasma Source for Space Propulsion, AIAA Paper 2006-5255, 42nd AIAA/ASME/SAE/ASEE Joint Propulsion Conference & Exhibit, 9 - 12 Jul 2006, Sacramento, CA, USA
2. Oleg Batishchev, Justin Pucci, Nareg Sinenian, Zachary LaBry, Murat Celik, Manuel Martinez-Sanchez, Mini-Helicon Thruster Experiment at MIT, QO1.4, 48th Annual Meeting of the Division of Plasma Physics, Philadelphia, PA, October 30–November 3, 2006; Bulletin APS, **51** (7) 224, October 2006.
3. Murat Celik, Oleg Batishchev, Manuel Martinez-Sanchez, Application of Spectroscopic Measurements to Electrical Propulsion, VP1.160, 48th APS DPP, Philadelphia PA, 2006; Bulletin APS, **51** (7) 328, October 2006.
4. O. Batishchev, N. Sinenian, M. Celik, M. Martinez-Sanchez, Development of the Mini-Helicon Thruster at MIT, IEPC-2007-355, 30th IEPC, Florence, Italy, September 2007
5. M. Celik, O. Batishchev, M. Martinez-Sanchez, Spectral Measurements of mHTX Helicon Discharge, IEPC-2007-203 paper, 30th IEPC, Florence, Italy, September 2007
6. Murat Celik, Oleg Batishchev, Manuel Martinez-Sanchez, High Resolution Spectral Measurements of Electrical Propulsion Plasma, BO5.6, 49th Annual APS DPP meeting, Orlando FL, Nov. 12-16, 2007; Bulletin APS, **52** (16) 29, November 2007.
7. Nareg Sinenian, Oleg Batishchev, Manuel Martinez-Sanchez, Plasma Flow Characterization of a mini-Helicon Thruster, BO5.8, 49th Annual APS DPP meeting, Orlando FL, Nov. 12-16, 2007; Bulletin APS, **52** (16) 29, November 2007.
8. Oleg Batishchev, Nareg Sinenian, Murat Celik , Manuel Martinez-Sanchez, Results from the mini-Helicon Thruster Experiment, NM5.5, 49th Annual APS DPP meeting, Orlando FL, Nov. 12-16, 2007; Bulletin APS **52** (16) 227, November 2007.
9. Joseph Eugene Palaia, IV, Empirical Aspects of a Mini-Helicon Plasma Thruster Experiment (mHTX@MIT)", MIT M.S. Thesis in Nuclear Science and Engineering, June 2006.

10. Justin Matthew Pucci, An Analysis of Energy Balance in a Helicon, Plasma Source for Space Propulsion, MIT M.S. Thesis in Aeronautics and Astronautics, May 2007.
11. Murat Celik, Experimental and Computational Studies of Electric Thruster Plasma Radiation Emission, MIT Ph.D. Thesis in Aeronautics and Astronautics, May 2007.
12. Nareg Sinenian, Propulsion Mechanisms in a Helicon Plasma Thruster, Dual MIT M.S. Thesis in Nuclear Science & Engineering and in Electrical Engineering, February 2008.

17. CONCLUSION

The mHTX project was extremely intense and fruitful. Basically, it delivered a brand new electro-thermal propulsion concept with compact design and controllable specific impulse, capable of operating with diatomic and noble gases. The concept has favorable scalability to both lower- and high-powers compared to known EP devices.

REFERENCES

1. R.W. Boswell and F.F. Chen, "Helicons, the early years," *IEEE Trans. Plas. Sci*. **25**, 6, Dec 1997, pp.1229-1244.
2. F.F. Chen, "Plasma ionization by helicon waves," *Plasma Phys. Control. Fusion*, **33**, 4, Apr 1991, pp. 339-364.
3. F.F. Chen, "Physics of helicon discharges," *Phys. Plasmas*, **3**,5, May 1996, pp. 1783-1793.
4. Chang Díaz F. R., "The VASIMR Engine," *Scientific American*, **283**, 5, 2000, pp. 72-79.
5. Squire J. P. et al., a) IAC-02-S.4.03, *53rd Intl. Astron. Cong.*, Houston TX, USA, October 10-19, 2002; b) *15th Topical Conference on Radio Frequency Power in Plasmas*, Grand Teton National Park, Moran, Wyoming, USA, May 20, 2003.
6. Carter M. D. et al., "Comparing experiments with modeling for light ion helicon plasma sources," *Phys. Plasmas*, **9**, 12, Dec 2002, pp. 5097-5110.
7. O. Batishchev, K. Molvig, F. Chang-Diaz, J. Squire, "Study of Gas Burn-out Regime in the VASIMR Helicon Plasma Source," paper O-3.3D, *30th EPS CFPP Conference*, St. Petersburg, Russia, July 7-11, 2003.
8. Oleg Batishchev and Kim Molvig, "VASIMR Thruster Operation with Hydrogen and Helium Gas Propellants," *28th IEPC*, paper IEPC03-191, -12p, Toulouse, France, 17-21 March, 2003.
9. R.K. Janev, D.E. Post, W.D. Langer, et al, "Survey of atomic processes in edge plasmas," *J. Nucl. Mater*., **121**, May1984, pp. 10-16.
10. T. Holstein, "Imprisonment of resonance radiation in gases," a) *Phys. Rev*., **72**, 1947, p.1212; b) *Phys. Rev*.**, 83**, 1951, p.1159.
11. A.A.Batishcheva and O.V.Batishchev, "RRC Adaptive Grid Method For Magnetized Plasma," Proceedings of the *17th Int. conference on the Numerical Simulation of Plasmas*, Banff, Canada, May 22–24, 2000, p.29.
12. a) Greg Chevers, NASA Marshall SFC, Private Communication, 2004; b) Christopher Deline, Greg Chavers, and Brian Gilchrist, "Physics of Plasma Detachment in a Magnetic Nozzle," *42nd Joint Propulsion Conference*, paper AIAA 2006-4653, July 2006.

13. J. Gilland, "Small Helicon Plasma experiments," Paper AIAA-2004-3939, *40th Joint Propulsion Conf.*, Ft. Lauderdale, FL, July 2004.
14. S.A. Cohen, et al, "Ion acceleration in plasmas emerging from a helicon-heated magnetic-mirror device," *Phys. of Plasmas*, **10**, 6, 2003, pp. 2593-2598.
15. J.L. Kline, et al., "Ion dynamics in helicon sources," *Phys. of Plasmas*, **10**, 5, 2003, pp. 2127-2135.
16. H. Nassar, et al., "N_2^+/N_2 ratio and temperature measurements based on the first negative N_2^+ and second positive N_2 overlapped molecular emission spectra," *J. of Phys. D*, **37**, 2004, pp.1904-1916.
17. R.F. Boivin, et al., "Electron temperature measurement by a helium line intensity ratio method in helicon plasmas," *Phys. of Plasmas*, **8**, 12, 2001, pp. 5303-5314.
18. Sullivan, Kay, J. Fox, O. Batishchev, and M. Martinez-Sanchez, "Kinetic Study of Wall Effects in SPT Hall Thrusters," *40th AIAA Joint Propulsion Conference*, 2004.
19. J. Palaia, "Empirical Aspects of a Mini-Helicon Plasma Thruster Experiment (mHTX@MIT)," Master of Science Thesis, Massachusetts Institute of Technology, June 2006.
20. J. M. Pucci, N. Sinenian, J. Palaia, M. Celik, Z. LaBry, A. Shabshelowitz, O. Batishchev, and M. Martinez-Sanchez, "Preliminary Characterization of a Helicon Plasma Source for Space Propulsion," *42nd AIAA/ASME/SAE/ASEE Joint Propulsion Conference & Exhibit*, Sacramento, CA, USA, 9 - 12 Jul 2006.
21. Oleg Batishchev, Justin Pucci, Nareg Sinenian, Zachary LaBry, Murat Celik, Manuel Martinez-Sanchez, "Mini-Helicon Thruster Experiment at MIT," QO1.4, *48th Annual Meeting of the Division of Plasma Physics*, Philadelphia, Bulletin APS, **51** (7) 224, October 2006.
22. Murat Celik, Oleg Batishchev, Manuel Martinez-Sanchez, VP1.160, Application of Spectroscopic Measurements to Electrical Propulsion, 48th APS DPP, Philadelphia PA, Bulletin APS, **51** (7) 328, October 2006.
23. M. Celik, "Experimental and Computational Studies of Electric Thruster Plasma Radiation Emission," Ph.D. Thesis in Aerospace Engineering (advisors Prof. M. Martinez-Sanchez and Dr. O. Batishchev), Massachusetts Institute of Technology, Cambridge MA, May 2007.
24. M. Celik, O. Batishchev, M. Martinez-Sanchez, "Spectral Measurements of Helicon Discharge Plasma," *30th International Electric Propulsion Conference*, technical paper IEPC-2007-203, Florence, Italy, September 2007.
25. J. M. Pucci, N. Sinenian, J. Palaia, M. Celik, Z. LaBry, A. Shabshelowitz, O. Batishchev, M. Martinez-Sanchez, "Preliminary Characterization of Helicon Plasma Source for Space Propulsion," *42nd Joint Prop. Conf.*, tech. paper AIAA-2006-5255, Sacramento CA, July 2006.
26. M. Celik, O. Batishchev, M. Martinez-Sanchez, "Optical Diagnostics of BHT-200 Wall Erosion," *Journal of Propulsion & Power*, submitted September 2007.
27. R.W. Boswell, "Plasma production using a standing helicon wave," *Phys. Lett.* **33A**, 7, Dec 1970, pp. 457-458.
28. Justin Matthew Pucci, "An Analysis of Energy Balance in a Helicon, Plasma Source for Space Propulsion", MIT M.S. Thesis in Aeronautics and Astronautics, May 2007.
29. O. Batishchev, J. M. Pucci, N. Sinenian, J. Palaia, Z. LaBry, M. Celik, M. Martinez-Sanchez, "Mini Helicon Thruster Experiment at MIT," QO1.4, *48th Annual Meeting of the Division of Plasma Physics*, Philadelphia, PA, *Bulletin APS* **51**, 7, October 2006, p. 224.

30. C. Charles, R. W. Boswell, "Laboratory evidence of a supersonic ion beam generated by a current-free "helicon" double-layer," *Physics of Plasmas* **11**, 4, April 2004, pp. 1706-1714.
31. ESA DL Helicon Thruster: http://www.esa.int/esaCP/SEM6HSVLWFE_index_0.html
32. I.H. Hutchinson, *Principles of Plasma Diagnostics*, Cambridge University Press, 2002.
33. L.Oksuz, F.Soberon, A.R.Ellingboe, "Analysis of uncompensated Langmuir probe characteristics in radio-frequency discharges revisited", J. Appl. Phys. **99**, 013304, 2006.

AFRL-RZ-ED-TR-2009-0020
Primary Distribution of this Report:

AFRL/RZSA (3 CD + 2 HC)
Dr. Jean-Luc Cambier
10 E. Saturn Blvd.
Edwards AFB CA 93524-7680

AFRL/RZSA (1 HC)
Record Custodian
10 E. Saturn Blvd.
Edwards AFB CA 93524-7680

AFRL/RZSS (1 CD + 1 HC)
Dr. James Haas
1 Ara Road
Edwards AFB CA 93524-7013

Dr. Oleg Batishchev (3 CD + 2 HC)
Massachusetts Institute of Technology
77 Massachusetts Avenue, 37-351
Cambridge, MA 02139

AFRL/RZ Technical Library (2 CD + 1 HC)
6 Draco Drive
Edwards AFB CA 93524-7130

Chemical Propulsion Information Analysis Center
Attn: Tech Lib (Mary Gannaway) (1 CD)
10630 Little Patuxent Parkway, Suite 202
Columbia MD 21044-3200

Defense Technical Information Center
(1 Electronic Submission via STINT)
Attn: DTIC-ACQS
8725 John J. Kingman Road, Suite 94
Ft. Belvoir VA 22060-6218